ALTERED HYDROLOGICAL AND SEDIMENT DYNAMICS IN HIGH-ALPINE AREAS – EXPLORING THE POTENTIAL OF MACHINE-LEARNING FOR ESTIMATING PAST AND FUTURE CHANGES

CUMULATIVE DISSERTATION

submitted in partial fulfilment
of the requirements for the degree of

Doctor rerum Naturalium (Dr. rer. Nat.)

in the research discipline
Geoecology

by
Lena Katharina Schmidt

submitted to
Institute of Environmental Sciences and Geography,
Faculty of Mathematics and Natural Sciences
University of Potsdam

Potsdam, July, 2023

Reviewers
Prof. Dr. Axel Bronstert University of Potsdam
Dr. Theresa Blume German Research Centre for Geosciences, Potsdam
Apl. Prof. Dr. Tobias Heckmann Catholic University of Eichstätt-Ingolstadt

Supervisors
Prof. Dr. Axel Bronstert
Assoz.-Prof. Dr. Stefan Achleitner, University of Innsbruck, Austria

Mentor
Dr. Theresa Blume

Examination Board members
Prof. Dr. Oliver Korup, University of Potsdam
Dr. habil. Wolfgang Schwanghardt, University of Potsdam
Dr. Till Francke, University of Potsdam

Published online on the
Publication Server of the University of Potsdam:
https://doi.org/10.25932/publishup-62330
https://nbn-resolving.org/urn:nbn:de:kobv:517-opus4-623302

DECLARATION OF ORIGINALITY

I, Lena Katharina Schmidt, hereby declare that, to the best of my knowledge, this work does not bear resemblance to any other work in whole or in part and has been completed by myself. I did not use any other sources and means than specified. Furthermore, this work has not been previously submitted to any university. All sources have been referred to and this work gives adequate credit to others for their work. I, in no way, claim to have created this information myself.

_____ _____

Location, Date Signature

ACKNOWLEDGEMENTS

This thesis owes its existence to the support of numerous kind-hearted people. This section serves to express my profound gratitude towards...

… **Axel**, for his unwavering support, guidance, and trust; the freedom to develop my own ideas and the reassurance and encouragement to see them through.

… **Till**, for always being there to discuss my ideas, for developing even more complicated ideas together; for feedback, guidance, help in problem-solving, many hours dedicated to revising manuscripts, and the fun (albeit physically demanding) field work campaigns in Vent and Fendt. Working with you has been a great pleasure.

… **Theresa**, for her guidance, meticulous and quick feedback for the first manuscript and several abstracts, reassurance and walks in the park,

… **Tobias Heckmann** for agreeing to act as an external reviewer of this thesis without a moment's hesitation,

… **Peter** for his remarkable support during my parental leave, and his diligent work in preparing the data and the model, as well as **Marvin** for his contributions.

… **Andi** and **Rene**, for their help and support, and for standing by me during long days of installations in the Ötztal that were as fun as they were demanding,

… **Stefan Achleitner**, **Carolina Kinzel** and the environmental engineering lab at University of Innsbruck for their kind support during my field- and laboratory work,

… The **HyKli working group** for such a positive work environment. I truly felt at home.

… My **colleagues** and **friends**, including Elli, Matthias, Lisa, Joscha and Melli, for sharing this time with me, and being there in fun and difficult times. A special mention goes to **Erwin**, **Amalie** and **Luke**, with whom I have thoroughly enjoyed sharing an office.

… The **NatRiskChange research-training group**, especially **Annegret Thieken**, **Theresia Petrow** and **Karen Lebek** for their unwavering support. I am grateful for the friendships I found in all three cohorts, the enriching discussions and fun retreats, the opportunity to grow together and benefit from each other's experience.

… **Elli**, **Lisa**, **Joscha**, **Matthias**, **Melli** and **Seth** for proofreading,

… **DFG** for funding this work and providing exceptional support for young parents,

… The **Potsdam graduate school** for providing excellent courses that helped me grow,

… The **German Hydrological Society** for a fieldwork scholarship

… To my **co-authors, editors,** and **reviewers**, for their valuable contributions,

… **Daniel Bazant** and for **Martin Schüttig** their assistance with GIS and IT matters, as well as **Sabine** and **Silke**, for their support,

… Stack overflow for helping to solve many R issues; Oriol Pavón Aroca (this document was formatted using a modified version of his thesis template (CC BY 4.0)).

… The wonderful **Baugruppe Gärtnerhof** for taking the load off me and having my back,

… Last but not least: **My family**. **Perry** for having my back and supporting me as best he could though all the ups and downs; **Paul** for a welcome distraction from the challenges of this PhD, and for reminding me what is truly important; **My parents** – I wouldn't be who I am without them. Especially thanks to '**Oma Motte**' and '**Oma Rike**' for taking such good care of Paul during the final sprint.

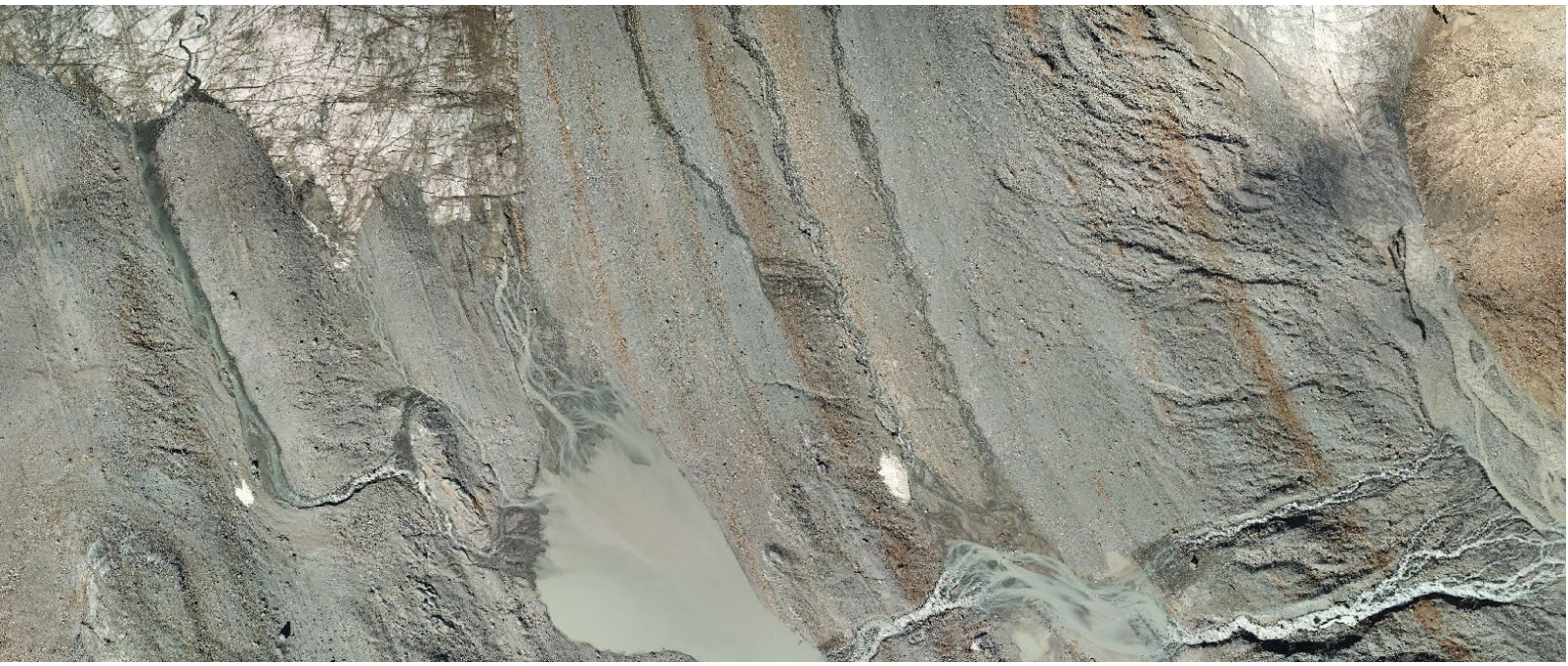

'Mountains are like early warning systems for climate change. The impacts are felt first and most intensely in these fragile environments.'

(Quote associated with Dr. Christina Figueres, former Executive Secretary of the UNFCCC).

ABSTRACT

Climate change fundamentally transforms glaciated high-alpine regions, with well-known cryospheric and hydrological implications, such as accelerating glacier retreat, transiently increased runoff, longer snow-free periods and more frequent and intense summer rainstorms. These changes affect the availability and transport of sediments in high alpine areas by altering the interaction and intensity of different erosion processes and catchment properties.

Gaining insight into the **future alterations in suspended sediment transport by high alpine streams** is crucial, given its wide-ranging implications, e.g. for flood damage potential, flood hazard in downstream river reaches, hydropower production, riverine ecology and water quality. However, the current understanding of how climate change will impact suspended sediment dynamics in these high alpine regions is limited. For one, this is due to the scarcity of measurement time series that are long enough to e.g. infer trends. On the other hand, it is difficult – if not impossible – to develop process-based models, due to the complexity and multitude of processes involved in high alpine sediment dynamics. Therefore, knowledge has so far been confined to conceptual models (which do not facilitate deriving concrete timings or magnitudes for individual catchments) or qualitative estimates ('higher export in warmer years') that may not be able to capture decreases in sediment export. Recently, machine-learning approaches have gained in popularity for modeling sediment dynamics, since their black box nature tailors them to the problem at hand, i.e. relatively well-understood input and output data, linked by very complex processes.

Therefore, the **overarching aim** of this thesis is to estimate sediment export from the high alpine Ötztal valley in Tyrol, Austria, over decadal timescales in the past and future – i.e. timescales relevant to anthropogenic climate change. This is achieved by informing, extending, evaluating and applying a **quantile regression forest (QRF)** approach, i.e. a nonparametric, multivariate machine-learning technique based on random forest.

The first study included in this thesis aimed to understand present sediment dynamics, i.e. in the period with available measurements (up to 15 years). To inform the modeling setup for the two subsequent studies, this study identified the most important predictors, areas within the catchments and time periods. To that end, water and sediment yields from three nested gauges in the upper Ötztal, Vent, Sölden and Tumpen (98 to almost 800 km² catchment area, 930 to 3772 m a.s.l.) were analyzed for their distribution in space, their seasonality and spatial differences therein, and the relative importance of short-term events. **The findings** suggest that the areas situated above 2500 m a.s.l., containing glacier tongues and recently deglaciated areas, play a pivotal role in sediment generation across all sub-catchments. In contrast, precipitation events were relatively unimportant (on average, 21 % of annual sediment yield was associated to precipitation events). Thus, the second and third study focused on the Vent catchment and its sub-catchment above gauge Vernagt (11.4 and 98 km², 1891 to 3772 m a.s.l.), due to their higher share of areas above 2500 m. Additionally, they included discharge, precipitation and air temperature (as well as their antecedent conditions) as predictors.

The second study aimed to estimate sediment export since the 1960s/70s at gauges Vent and Vernagt. This was facilitated by the availability of long records of the predictors, discharge, precipitation and air temperature, and shorter records (four and 15 years) of turbidity-derived sediment concentrations at the two gauges. **The third study** aimed to estimate future sediment export until 2100, by applying the QRF models developed in the second study to pre-existing precipitation and temperature projections (EURO-CORDEX) and discharge projections (physically-based hydroclimatological and snow model AMUNDSEN) for the three representative concentration pathways RCP2.6, RCP4.5 and RCP8.5.

The **combined results of the second and third study** show overall increasing sediment export in the past and decreasing export in the future. This suggests that peak sediment is underway or has already passed – unless precipitation changes unfold differently than represented in the projections or changes in the catchment erodibility prevail and override these trends. Despite the overall future decrease, very high sediment export is possible in response to precipitation events. This two-fold development has important implications for managing sediment, flood hazard and riverine ecology.

This thesis shows that **QRF can be a very useful tool** to model sediment export in high-alpine areas. Several validations in the second study showed good performance of QRF and its superiority to traditional sediment rating curves – especially in periods that contained high sediment export events, which points to its ability to deal with threshold effects. A technical limitation of QRF is the inability to extrapolate beyond the range of values represented in the training data. We assessed the number and severity of such out-of-observation-range (OOOR) days in both studies, which showed that there were few OOOR days in the second study and that uncertainties associated with OOOR days were small before 2070 in the third study. As the pre-processed data and model code have been made publically available, **future studies** can easily test further approaches or apply QRF to further catchments.

ZUSAMMENFASSUNG

Der Klimawandel verändert vergletscherte Hochgebirgsregionen grundlegend, mit wohlbekannten Auswirkungen auf Kryosphäre und Hydrologie, wie beschleunigtem Gletscherrückgang, vorübergehend erhöhtem Abfluss, längeren schneefreien Perioden und häufigeren und intensiveren sommerlichen Starkniederschlägen. Diese Veränderungen wirken sich auf die Verfügbarkeit und den Transport von Sedimenten in hochalpinen Gebieten aus, indem sie die Interaktion und Intensität verschiedener Erosionsprozesse und Einzugsgebietseigenschaften verändern.

Eine Abschätzung der **zukünftigen Veränderungen des Schwebstofftransports in hochalpinen Bächen** ist von entscheidender Bedeutung, da sie weitreichende Auswirkungen haben, z. B. auf das Hochwasserschadenspotenzial, die Hochwassergefahr in den Unterläufen, sowie Wasserkraftproduktion, aquatische Ökosysteme und Wasserqualität. Das derzeitige Verständnis der Auswirkungen des Klimawandels auf die Schwebstoffdynamik in diesen hochalpinen Regionen ist jedoch begrenzt. Dies liegt zum einen daran, dass es kaum ausreichend lange Messzeitreihen gibt, um z.B. Trends ableiten zu können. Zum anderen ist es aufgrund der Komplexität und der Vielzahl der Prozesse, die an der hochalpinen Sedimentdynamik beteiligt sind, schwierig - wenn nicht gar unmöglich - prozessbasierte Modelle zu entwickeln. Daher beschränkte sich das Wissen bisher auf konzeptionelle Modelle (die es nicht ermöglichen, konkrete Zeitpunkte oder Größenordnungen für einzelne Einzugsgebiete abzuleiten) oder qualitative Schätzungen ("höherer Sedimentaustrag in wärmeren Jahren"), die möglicherweise nicht in der Lage sind, Rückgänge im Sedimentaustrag abzubilden. In jüngster Zeit haben Ansätze des maschinellen Lernens für die Modellierung der Sedimentdynamik an Popularität gewonnen, da sie aufgrund ihres Black-Box-Charakters auf das vorliegende Problem zugeschnitten sind, d. h. auf relativ gut verstandene Eingangs- und Ausgangsdaten, die durch sehr komplexe Prozesse verknüpft sind.

Das **übergeordnete Ziel** dieser Arbeit ist daher die Abschätzung des Sedimentaustrags am Beispiel des hochalpinen Ötztals in Tirol, Österreich, auf dekadischen Zeitskalen in der Vergangenheit und Zukunft – also Zeitskalen, die für den anthropogenen Klimawandel relevant sind. Dazu wird ein **Quantile Regression Forest (QRF)**-Ansatz, d.h. ein nichtparametrisches, multivariates maschinelles Lernverfahren auf der Basis von Random Forest, erweitert, evaluiert und angewendet.

Die erste Studie im Rahmen dieser Arbeit zielte darauf ab, die "gegenwärtige" Sedimentdynamik zu verstehen, d. h. in dem Zeitraum, für den Messungen vorliegen (bis zu 15 Jahre). Um die Modellierung für die beiden folgenden Studien zu ermöglichen, wurden in dieser Studie die wichtigsten Prädiktoren, Teilgebiete des Untersuchungsgebiets und Zeiträume ermittelt. Zu diesem Zweck wurden die Wasser- und Sedimenterträge von drei verschachtelten Pegeln im oberen Ötztal, Vent, Sölden und Tumpen (98 bis fast 800 km² Einzugsgebiet, 930 bis 3772 m ü.d.M.), auf ihre räumliche Verteilung, ihre Saisonalität und deren räumlichen Unterschiede, sowie die relative Bedeutung von Niederschlagsereignissen hin untersucht. Die Ergebnisse deuten darauf hin, dass die Gebiete oberhalb von 2500 m ü.

M., in denen sich Gletscherzungen und kürzlich entgletscherte Gebiete befinden, eine zentrale Rolle in der Sedimentdynamik in allen Teileinzugsgebieten spielen. Im Gegensatz dazu waren Niederschlagsereignisse relativ unbedeutend (im Durchschnitt wurden 21 % des jährlichen Austrags mit Niederschlagsereignissen in Verbindung gebracht). Daher konzentrierten sich die zweite und dritte Studie auf das Vent-Einzugsgebiet und sein Teileinzugsgebiet oberhalb des Pegels Vernagt (11,4 und 98 km², 1891 bis 3772 m ü. M.), da sie einen höheren Anteil an Gebieten oberhalb von 2500 m aufweisen. Außerdem wurden Abfluss, Niederschlag und Lufttemperatur (sowie deren Vorbedingungen) als Prädiktoren einbezogen.

Die **zweite Studie** zielte darauf ab, den Sedimentexport seit den 1960er/70er Jahren an den Pegeln Vent und Vernagt abzuschätzen. Dies wurde durch die Verfügbarkeit langer Aufzeichnungen der Prädiktoren Abfluss, Niederschlag und Lufttemperatur sowie kürzerer Aufzeichnungen (vier und 15 Jahre) von aus Trübungsmessungen abgeleiteten Sedimentkonzentrationen an den beiden Pegeln ermöglicht. Die **dritte Studie** zielte darauf ab, den zukünftigen Sedimentexport bis zum Jahr 2100 abzuschätzen, indem die in der zweiten Studie entwickelten QRF-Modelle auf bereits existierende Niederschlags- und Temperaturprojektionen (EURO-CORDEX) und Abflussprojektionen (des physikalisch basierten hydroklimatologischen und Schneemodells AMUNDSEN) in den drei repräsentativen Konzentrationspfaden RCP2.6, RCP4.5 und RCP8.5 angewendet wurden.

Die **kombinierten Ergebnisse der zweiten und dritten Studie** legen nahe, dass der Sedimentexport in der Vergangenheit insgesamt zugenommen hat und in der Zukunft abnehmen wird. Dies deutet darauf hin, dass der Höhepunkt des Sedimenteintrags erreicht ist oder bereits überschritten wurde - es sei denn, die Niederschlagsveränderungen entwickeln sich anders, als es in den Projektionen dargestellt ist, oder Veränderungen in der Erodierbarkeit des Einzugsgebiets setzen sich durch. Trotz des allgemeinen Rückgangs in der Zukunft sind sehr hohe Sedimentausträge als Reaktion auf Niederschlagsereignisse möglich. Diese zweifältige Entwicklung hat wichtige Auswirkungen auf das Sedimentmanagement, die Hochwassergefahr und die Flussökologie.

Diese Arbeit zeigt, dass **QRF ein sehr nützliches Instrument zur Modellierung des Sedimentexports in hochalpinen Gebieten sein kann**. Mehrere Validierungen in der zweiten Studie zeigten eine gute Modell-Performance und die Überlegenheit gegenüber traditionellen Sediment-Abfluss-Beziehungen – insbesondere in Zeiträumen, in denen es zu einem hohen Sedimentexport kam, was auf die Fähigkeit von QRF hinweist, mit Schwelleneffekten umzugehen. Eine technische Einschränkung von QRF ist die Unfähigkeit, über den Bereich der in den Trainingsdaten dargestellten Werte hinaus zu extrapolieren. Die Anzahl und den Schweregrad an solchen Tagen, in denen der Wertebereich der Trainingsdaten überschritten wurde, wurde in beiden Studien untersucht. Dabei zeigte sich, dass es in der zweiten Studie nur wenige solcher Tage gab und dass die mit den Überschreitungen verbundenen Unsicherheiten in der dritten Studie vor 2070 gering waren. Da die vorverarbeiteten Daten und der Modellcode öffentlich zugänglich gemacht wurden, können künftige Studien darauf aufbauend weitere Ansätze testen oder QRF auf weitere Einzugsgebiete anwenden.

CONTENTS

LIST OF FIGURES

LIST OF TABLES

ABBREVIATIONS

BE	benchmark efficiency
CART	classification and regression trees
CP	change point
DEM	digital elevation model
DOY	day of year
DTM	digital terrain model
GCM	global climate model
GLM	generalized linear model
HD	Hydrographiscer Dienst Tirol
HEF	Hintereisferner
ML	machine learning
NSE	Nash-Sutcliffe efficiency
OOB	out-of-bag
OOOR	out of observation range
P	precipitation
Q	discharge
QRF	quantile regression forest
Qsed	sediment discharge
RCM	regional climate model
RCP	representative cocentration pathway
RF	random forest
RQ	research question
S	Sölden
SD	standard deviation
sQ	specific discharge
SRC	sediment rating curve
SS	Sen's slope
SSC	suspended sediment concentration
SSCg	gravimetric suspended sediment concentration
sSSY	specific suspended sediment yield
SSY	suspended sediment yield
T	Tumpen (Chapter 2); air temperature (Chapter 3 and 4)
TiWAG	Tiroler Wasserkraft AG
V	Vent
VF	Vernagtferner
WOY	week of year
WY	water yield

1 INTRODUCTION

1.1 BACKGROUND: CLIMATE CHANGE IN THE EUROPEAN ALPS AND SUSPENDED SEDIMENT EXPORT

In the European Alps, observations within the past century reveal a **temperature increase** that was about twice as high as the northern-hemispheric average, with especially pronounced warming after 1980, and projections suggest a further acceleration of temperature increase in the 21st century (Brunetti et al., 2009; Gobiet et al., 2014). High-alpine areas are particularly sensitive to this warming due to their **cryospheric landscape elements**, i.e., glaciers, snow cover and permafrost (Beniston et al., 2018). As a result, widespread and accelerating **glacier retreat** and thinning have been observed in the past and projected for the future (Escher-Vetter, 2007; Abermann et al., 2009; Hanzer et al., 2018), alongside increases in ablation season length (Di Mauro and Fugazza, 2022), reduced **snow cover duration** and extent (Hanzer et al., 2018; Kormann et al., 2016; Rottler et al., 2021), and **permafrost thaw** (Klug et al., 2017) (see influence of temperature on cryosphere in Figure 1.1). In addition to this, **precipitation** changes, as more (liquid) precipitation occurs in summer and less in winter, concurring with an increase in **heavy summer precipitation** (Giorgi et al., 2016; Scherrer et al., 2016).

These changes in climatic drivers translate to substantial changes in the **hydrological** processes of high-alpine catchments, as **discharge** from ice melt, snowmelt and firn melt is – or has so far been – by far the most important contributor to runoff (Kormann et al., 2016) (dark blue element in Figure 1.1). On decadal scales, runoff volumes transiently increase (e.g. from ca. 1500 mm of annual runoff at the high-alpine gauge 'Vernagt' in the 1980s to ca. 2300 mm in 2007, ibid.) before a decrease after *peak water*, i.e. the maximum runoff from long-term glacier storage (Hanzer et al., 2018; Sommer et al., 2020; Farinotti et al., 2012). Regarding the seasonal distribution, projections indicate potential changes in hydrograph timing, including earlier occurrences of annual peak flows and prolonged flood seasons, particularly in catchments at higher elevations (Hanus et al., 2021).

These climatological and hydrological changes alter the **properties of high-alpine catchments** (see green elements in Figure 1.1) as well as **erosion** processes (yellow elements in Figure 1.1), and the combination of all of these changes alters **sediment dynamics** and consequentially the concentration of **sediments transported in suspension** by high-alpine streams (brown elements in Figure 1.1). In the following, I will give a brief overview of the processes and their potential directions of change – which will also illustrate that the interaction and relative importance of the different processes can vary distinctly between catchments.

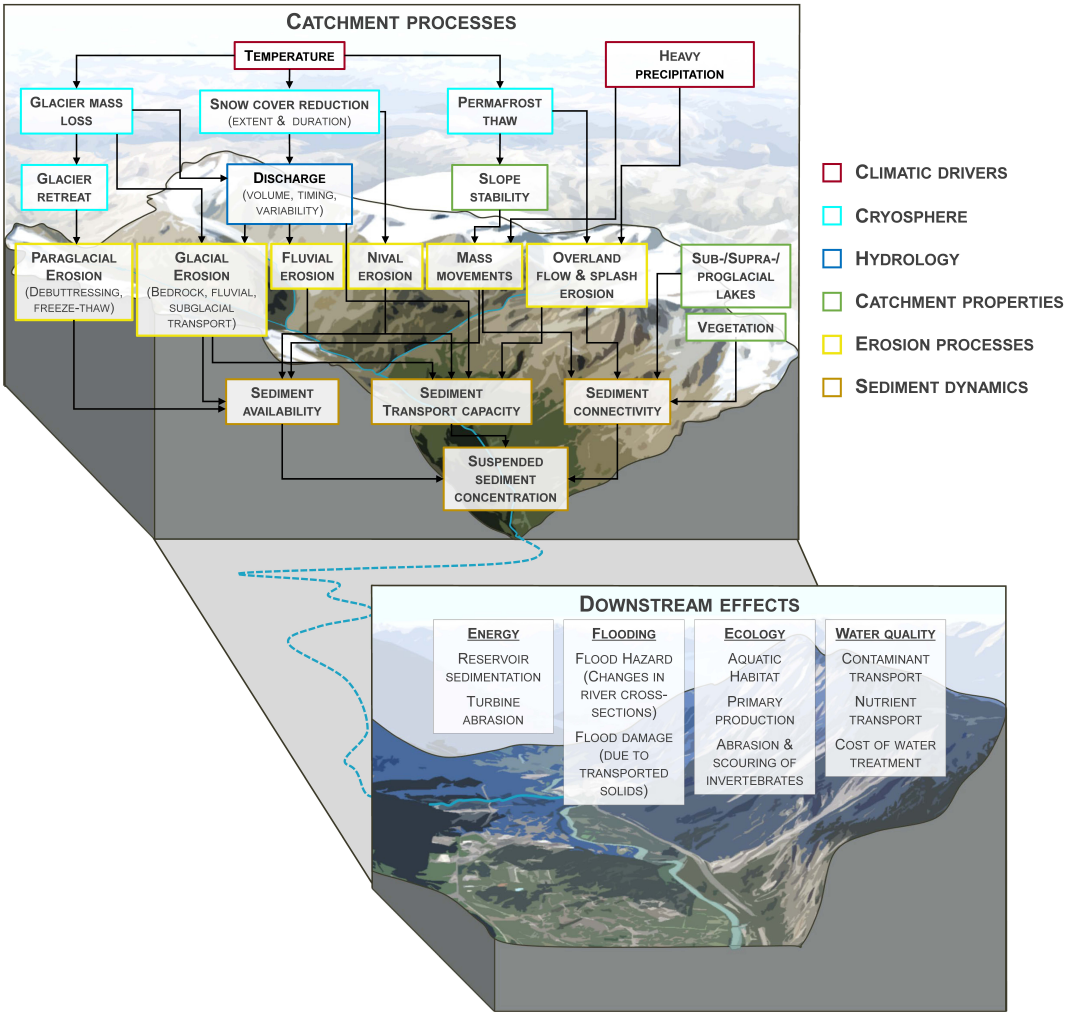

Figure 1.1. *Complex interactions of the drivers and processes within high-alpine catchments that determine suspended sediment concentrations at the catchment outlet (top), and overview of downstream effects (bottom). Some arrows are omitted for clarity. Own representation based on Bilotta and Brazier (2008), Delaney and Adhikari (2020), Li et al. (2020), Nones (2019), Vercruysse et al. (2017), and Zhang et al. (2022). Image basis: Google earth V 7.3.2.5491.*

Altered **catchment properties**, such as decreased **slope stability** as a consequence of permafrost degradation, rapid thaw during prolonged warm periods, or more intense or frequent rainstorm events (Huggel et al., 2010), have been found to result in increases in **mass movements**, such as rockfalls or debris flows, for example in the Sulden catchment in the Italian Alps, not far from the study area of this thesis (Savi et al., 2020). On the other hand, decreases in frost-weathering can also lead to decreases in debris flow occurrence, as has been projected for the (non-glaciated) Illgraben catchment in Switzerland (Hirschberg et al., 2021). At the same time, temperature and precipitation changes impact land cover development, which can either decrease sediment availability as the **vegetation cover** expands, or lead to increased sediment export if erosion is predominant (Altmann et al., 2023). In turn, **(pro-) glacial lakes**, which have formed at increasing numbers since the last ice age due to glacier retreat, can trap suspended sediments and thus interrupt the transport to the catchment outlet – but can also be the source of glacier lake outburst floods, which can transport substantial

amounts of sediment downstream (Buckel et al., 2018; Carrivick and Heckmann, 2017; Veh et al., 2022).

As a consequence of the changes in climatic drivers, hydrology and catchment properties, erosion processes and their interactions are changing substantially. **Paraglacial erosion** impacts deglaciated areas, and leads to increased instability of slopes in response to decreased glacial support (**debuttressing**) or increased susceptibility of oversteepened moraines to (freeze-thaw weathering-induced) rockfalls or landslides (Huggel et al., 2012; Hartmeyer et al., 2020; Chiarle et al., 2021; Zhang et al., 2022).

Beneath the glaciers, sediment is produced by **glacial erosion**, i.e. through abrasion, plucking or quarrying of the underlying bedrock by the ice and debris frozen therein, and subglacial fluvial activity can then transport sediments from below the glacier (Delaney et al., 2019). While these subglacial sediment sources contributed a substantial part to the sediment export from glacierized catchments in the past decades (e.g. up to 70 % at the Grießgletscher, Switzerland; Delaney et al., 2018a), it is expected that the erosive capacity of the thinning glaciers will diminish (Herman et al., 2021) and subglacial fluvial sediment transport will decrease. Yet, a modeling study also suggested that, sediment export could continue to increase after peak water, as melt affects higher regions of the glaciers where transport was limited prior to glacier retreat, depending on the amount of sediment stored subglacially (Delaney and Adhikari, 2020).

Fluvial erosion and sediment transport in proglacial areas are also subject to change, as transient changes in runoff coincide with potentially large supplies of recently uncovered glacigenic sediment, which is now easily accessible by proglacial rivers (Ballantyne, 2002; Carrivick and Heckmann, 2017). Erosion rates in the proglacial area can be much higher than from the remaining catchment (Delaney et al., 2018a), while in other catchments, sediment from non-glacial sources dominates (Beylich et al., 2017). Thus, the balance between erosion and deposition depends on the conditions in the individual catchment, such as topography and river morphology. This is closely linked to **sediment connectivity**, describing the effectiveness of sediment transfer in the catchment, i.e. from hillslopes to the channels and along the channels to the catchment outlet (Carrivick and Heckmann, 2017; Lane et al., 2017; Cavalli et al., 2019). Essentially, sediment connectivity determines whether proglacial areas act as sediment sources or sinks, which can also change as glaciers retreat (e.g. due to the formation of proglacial lakes, see above) (ibid.). The changes in snow cover duration and extent may translate to changes in **nival erosion** i.e. by snow gliding or avalanches (Geitner et al., 2021), and snowmelt-driven overland flow (Costa et al., 2018a) and as snow cover duration decreases, erosive precipitation has a higher chance of affecting uncovered material.

Essentially, the geomorphological functioning of high-alpine catchments, that in the past were shaped by glaciers, held together by permafrost and accustomed to certain amounts of discharge and precipitation, are now in a transient, paraglacial state, adjusting from glacial to non-glacial conditions (Ballantyne, 2002). This affects the concentration of sediments transported in suspension by high-alpine streams. For one, **sediment availability** changes, as

more recently deglaciated areas expand and leave behind loose sediments that are susceptible to erosion (Heckmann et al., 2016; Carrivick and Heckmann, 2017). At the same time, **sediment connectivity** (see above) and **transport capacity** change, as more or less water is available to transport the sediments (Micheletti and Lane, 2016).

Measuring suspended sediment concentrations (SSCs) in high-alpine streams is relatively straightforward and commonly done using the relatively close correlation with turbidity, which can be continuously monitored. In this, SSCs at a catchments outlet are similar to the heart rate in the human body, which can easily be felt, e.g. at the wrist, but changes therein are determined by the interplay of various interacting internal (bodyweight, fitness, pre-existing conditions) and external factors (medication, air temperature, stressors). However, given the sheer amount of influencing variables and their complex interactions (as illustrated by the tangled knot of arrows in Figure 1.1), it is not at all straightforward to understand and explain the very high variability in SSC – let alone deducing future changes – especially as opposing future trajectories are possible for many involved processes.

1.2 MOTIVATION: WHY STUDY SUSPENDED SEDIMENTS IN A NATURAL HAZARDS CONTEXT?

At first glance, a bit of sand and silt transported within alpine streams may seem harmless and comparatively unspectacular when compared to typical natural hazards. Yet, these sediments are linked to hazards both within high-alpine catchments and beyond the catchment boundaries. **Within-catchment hazards**, those that pose a direct threat to humans or infrastructure inside the catchment, include hillslope instabilities and associated rockfalls, debris flows or other forms of mass movement, as well as lake outburst given the presence of (pro-)glacial lakes (Heckmann et al., 2016; Savi et al., 2020).

However, there are also sediment-related **offsite consequences**, and as sediment export (per unit area) is much higher than from lower lying areas, high-alpine areas have disproportionate influence on downstream areas (Beniston et al., 2018; Hinderer et al., 2013) (bottom part of Figure 1.1). For example, if **too much sediment** is transported to downstream areas, it can lead to river bed aggradation (i.e. filling of river channels with sediments) and promote or exacerbate flooding, since reductions in channel capacity can amplify flood hazards even if the frequency of high discharge events does not change (Slater et al., 2015; Nones, 2019). This can increase the amount of water running outside of the channel, and cause severe damage (Rickenmann et al., 2016), where sediment related processes can be responsible for a considerable part of the incurred costs (Rickenmann et al., 2016; Badoux et al., 2014). Another consequence of too much sediment is reservoir sedimentation. This is primarily a problem for (the cost efficiency of) hydropower production, complemented by abrasion of turbines and other equipment (Hinderer et al., 2013), but can also reduce the ability of reservoirs to handle

high discharge events and thus to serve for flood protection (Hinderer et al., 2013; Guillén-Ludeña et al., 2018).

On the other hand, **too little sediment** can e.g. cause riverbank erosion and river profile degradation, which can alter flow velocities if the bed sediment texture or in-channel vegetation changes (Brils, 2008; Nones, 2019). Either way, not considering sediment transport and morphological changes can lead to false estimates of the impacts of floods in rivers with high sediment transport (Nones, 2019). Nevertheless, sediments have so far been only marginally considered in the European Floods Directive (ibid.)

Further sediment-related problems relate to **water quality**, **ecotoxicology** and the cost of water treatment, because fine sediment particles are a key factor in transporting **nutrients** and **contaminants** along rivers (Naden, 2010). This includes the legacy of historical contaminations that are stored within sediment deposits and can lead to secondary pollution in case of erosion (Walling, 2005; Brils, 2008; Milner et al., 2017; Vercruysse et al., 2017). With respect to ecological consequences, too much sediment can lead to a reduction of primary production (i.e. food availability higher up the food chain), abrasion and scouring of invertebrates (Bilotta and Brazier, 2008; Milner et al., 2009). Especially, the settling of fine sediments into gaps between gravel particles hinders the flow of water within the hyporheic zone, which leads to reduced oxygen levels and negatively impacts benthic organisms and the suitable conditions for fish spawning grounds (Naden, 2010). Conversely, the provision of 'enough' sediment is vital for the preservation of habitats, e.g. on floodplains, mud flats and deltas (Naden, 2010).

This illustrates the importance of working towards understanding sediment dynamics in high-alpine areas and estimating future changes in sediment export. However, as of yet, knowledge on future changes is limited (Zhang et al., 2022; Carrivick and Tweed, 2021), and in the following, I will elucidate the two major reasons for this knowledge gap.

1.3 CHALLENGE #1: SHORT MEASUREMENT TIME SERIES

As briefly mentioned above, SSCs are commonly determined indirectly, via turbidity, once the relationship between SSCs and turbidity for a specific location has been established based on SSCs in water samples. Beyond that, insights can be gained from flushings of hydropower intakes (which mainly targets coarse material, i.e. bedload) (Kammerlander et al., 2017), lake stratigraphy analyses (Lane et al., 2019) or differences between consecutive digital elevation models that can e.g. be inferred from photogrammetry (e.g. Micheletti and Lane, 2016; Delaney et al., 2018a; Clapuyt et al., 2019; both with coarser temporal resolutions and targeted at longer timescales).

Yet, long turbidity measurement time series, i.e. spanning several decades and therefore long enough to e.g. deduce trends or assess the response to climate change, are very rare (see also Zhang et al., 2022). There are a few long time series in Switzerland, e.g. from the upper Rhône river basin in Switzerland, where SSC has measured twice per week since the 1970s (Costa et al., 2018b; Hinderer et al., 2013) and for the Gornergletscher catchment in the Swiss Alps, where a series of studies exists between 1970 and 1990, complemented by measurements in 2016/17 (Delaney et al., 2018b). In Austria, turbidity measurements have been implemented at a total of 28 gauges between 2006 and 2008 (Lalk et al., 2014). Yet given the very high intra- and interannual variability in SSCs (Vercruysse et al., 2017), these time series are still relatively short, so that it is not straightforward (or even possible) to deduce meaningful trends. As a result, there is little information on timescales relevant to anthropogenic climate change, i.e. decadal timescales as opposed to longer ones (for which information can be derived e.g. from lake stratigraphy) (Huss et al., 2017). Thus, as the lack of measurement data precludes deriving meaningful trends and analysing the response to climatic changes at the relevant timescales, we have to employ models.

1.4 CHALLENGE #2: LACK OF PROCESS-BASED MODELS

Ideally, we would use a fully distributed physically-based model, that can take into account all processes relevant to sediment dynamics in high-alpine catchments, and pluvial as well as thermal drivers of sediment mobilization and transport (Zhang et al., 2022). Unfortunately, such models do not yet exist (ibid.) – and given the number and complexity of the involved processes (see Figure 1.1) it is questionable whether their implementation is feasible.

Thus, up until now, studies that attempted to project future suspended sediment export relied on rather qualitative analyses. For example, they compared observations of warmer and colder ablation seasons (Stott and Mount, 2007; Bogen, 2008), determined the response of suspended sediment export to past changes in the meteorological or hydrological drivers and applied them to projected changes in these drivers (Li et al., 2021b) or fitted a multiple regression model to short time series and only altered the temperature input (Stott and Convey, 2021) (see also section 4.1). Yet all these approaches cannot account for interactions between variables and may not be able to model decreases in sediment export (see 'qualitative approaches' in Figure 1.2). In the following paragraphs, I will give a brief overview of the state of current conceptual, process-based and data-based models for sediment dynamics in high-alpine areas.

CONCEPTUAL MODELS

The current understanding of the processes governing sediment export from deglaciating drainage basins can be illustrated using conceptual models. Such conceptual models expect an initial increase as deglaciation begins to accelerate, and an eventual decrease (long) after the glaciers have disappeared and the landscape stabilizes (upper panel of Figure 1.2) (Embleton-hamann and Slaymaker, 2012; Antoniazza and Lane, 2021; Carrivick and Tweed, 2021; Zhang et al., 2022). In between lies *peak sediment*, the timing of which is presumed to depend on erosive precipitation, so that it may occur simultaneous with or even before peak water or simultaneous with the completion of deglaciation or at some point in between (Zhang et al., 2022) (see also section 4.1). While this is informative at a generalized, overarching level of knowledge, it is not necessarily helpful to infer specific points in time or quantitative estimates of future sediment yields, especially for individual catchments.

PROCESS-BASED MODELS

Physics-based or process-based models that can take into account all relevant processes at the catchment scale do not (yet) exist, owing to the complexity and large number of interacting processes involved in sediment dynamics in high-alpine areas (Figure 1.1) (see also review by Zhang et al., 2022). There are numerous process-based models for individual processes, such as soil erosion, for example within the well-known and often-applied Soil Water Assessment Tool (SWAT) (e.g. Vigiak et al., 2017) (for in-depth reviews, see: Pandey et al., 2016; Schäuble, 2006). SWAT, however, is "weak in glaciated catchments" even for discharge (Adnan et al., 2019), and glacier erosion processes, landslides or gully erosion cannot be considered (Vigiak et al., 2017) (and machine-learning techniques have shown to be more accurate; Jimeno-Sáez et al., 2022; Rahman et al., 2022).

Some process-based models can even approximate glacier impact, i.e. WBMsed (Cohen et al., 2013) and HydroTrend (Kettner and Syvitski, 2008) (which are both based on BQART; Syvitski and Milliman, 2007), by using the glacier covered fraction of the analyzed catchments. HydroTrend even uses changes in the equilibrium line altitude (which divides the glacier into accumulation and ablation area; Braithwaite and Raper, 2009) to model short-term changes in glaciers. However, both WBMsed and HydroTrend are designed for very large spatial scales, such as sediment export to the oceans from large river basins, and temporal scales, such as changes in sediment export since the last glacial maximum, and cannot consider processes that can be important in high-alpine areas, such as hysteresis effects, landslides, mass movements, changes in hillslope stability or permafrost (de Vente et al., 2013). Thus, in recent years, data-based approaches have increasingly been applied to modeling sediment dynamics.

DATA-BASED APPROACHES

In the following section, I will outline the most common data-based approaches to model SSCs in increasing complexity. They all share the core principle of estimating the relationship between input data (e.g. discharge, precipitation) and output data (SSCs) – without applying any knowledge of the underlying physical processes.

At the lowest level of complexity, univariate linear regression is applied to discharge, also known as sediment rating curves (SRC) (Vercruysse et al., 2017; Francke et al., 2008a) (section 3.3.1). While being simple to implement and interpret, this approach rarely captures much of the variability in SSC, making it the method of choice for preliminary estimates or if data availability is poor.

Multivariate regression techniques, such as generalized linear models (GLMs) (Francke et al., 2008a), the 'hydroclimatic multivariate sediment rating curve' (HMRC) (Costa et al., 2018a) or the 'sediment-availability-transport model' (SAT) (Zhang et al., 2021) have the advantage of being interpretable and still relatively easy to fit. However, their being bound to linear or monotonous relationships predestines them to struggle with threshold effects (e.g. activation of mass movements). Additionally, it will be difficult to consider all relevant processes, and GLMs proved not to be robust (Francke et al., 2008a).

Machine-learning tools have become a popular approach to model sediment concentrations. While there are many different techniques (see review by Gupta et al., 2021), most are variants or special cases of support vector machines or artificial neural networks (e.g. combined with fuzzy logic = 'neuro-fuzzy'). These more complex machine-learning tools generally perform better in modeling SSC than simpler models (Francke et al., 2008a; Lantz, 2019) – as "the nature of their complexity often allows them to naturally capture complex interactions" (Boehmke and Greenwell, 2019). Yet, this is at the expense of interpretability, since they all constitute black box approaches. However, black box methods tend to perform well for black box problems such as high-alpine sediment dynamics, 'where the input data and output data are well-understood or at least fairly simple, yet the process that relates the input to output is extremely complex' (Lantz, 2019).

One group that can also be attributed to machine learning is tree-based ensembles, i.e. random forests (RF) and quantile regression forests (QRF). These have so far not been applied to modeling sediment export to the same extent as other machine-learning approaches, but outperformed generalized linear models and sediment rating curves (Francke et al., 2008a) as well as support vector machines and artificial neural networks (Al-Mukhtar, 2019) in modeling sediment concentrations. As an additional benefit, RF and QRF allow to quantify model uncertainty due to their inherent ensemble characteristics, and it is (at least theoretically) possible to peek into the black box to some extent, by quantifying variable importance (which is complicated by interactions between the predictors as I will discuss in section 5.2).

1.5 OVERALL AIM AND RESEARCH QUESTIONS

To sum up the above: as a result of short measurement time series and a lack of adequate models, future changes in sediment export from deglaciating high-alpine areas are poorly understood. Measurement time series are often too short to deduce trends, qualitative approaches can likely not model decreases and conceptual models are not suitable to deduce specific timings or magnitudes of sediment export for individual catchments (upper panel of Figure 1.2). This leaves us – in a metaphorical sense – short-sighted, as only blurred or coarse outlines of the past and future can be identified, and a perception of (temporal) distance is hardly possible.

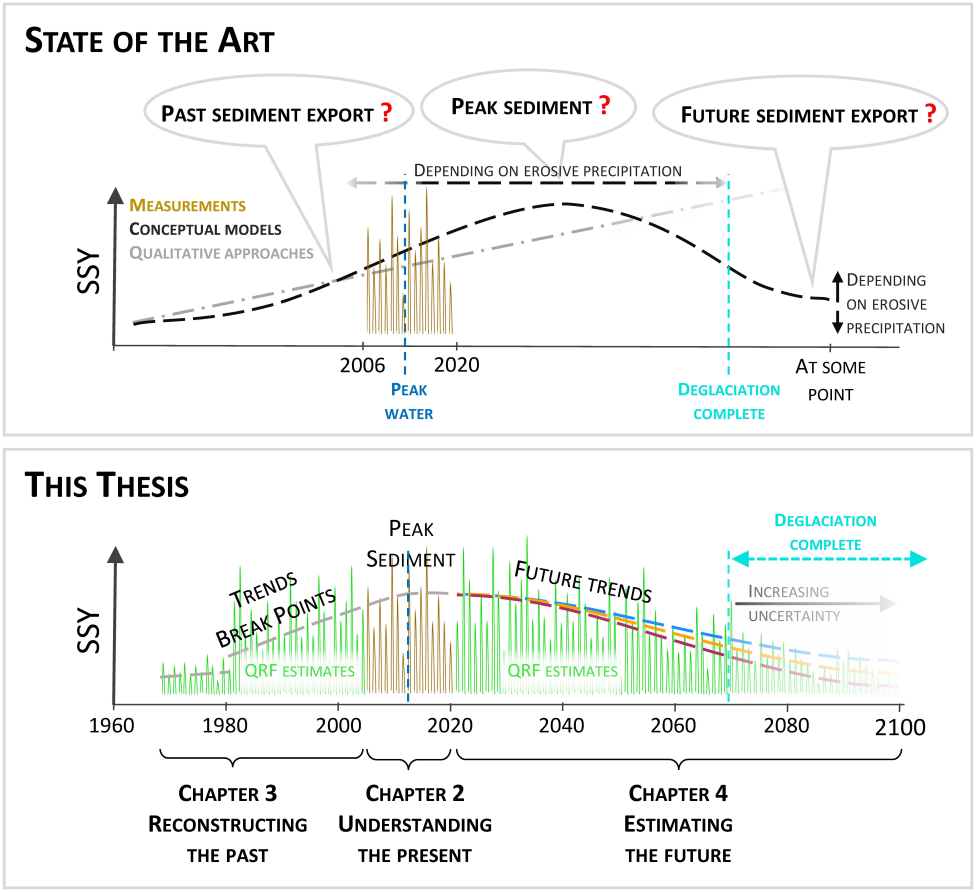

Figure 1.2. *Schematic representation of the aims of this thesis. Top: short measurement time series preclude robust trend analyses, qualitative approaches may not be able to capture decreases and conceptual models cannot necessarily serve to deduce e.g. the timing of peak sediment for specific catchments. Bottom: This thesis aims to explore a machine-learning based modeling approach (QRF) informed by analyses of existing measurements (chapter 2) in order to provide estimates of past (chapter 3) and future (chapter 4) suspended sediment yields (SSY), which can then be analysed for trends, step-like changes ('break points') and future changes in different emission scenarios.*

Therefore, the overarching aim of this thesis is to facilitate estimating changes in sediment export from high-alpine catchments on decadal scales (relevant to anthropogenic climate change), in the past and future, by informing, extending and testing a data-driven quantile

regression forest approach. This approach will be trained on the available short time series of SSC and applied to long measurement time series and projections of the predictors. To stick with the analogy of short-sightedness, the resulting picture will certainly still be blurry (i.e. associated with uncertainty), but will hopefully provide a better sense of (temporal) distance and prevent us from running into unexpected obstacles. From this overarching aim, the main research questions (RQs) of this thesis derive as follows:

RQ1: Which are the most important predictors, areas and time periods for sediment export in the study area?

RQ2: Is quantile regression forest a suitable approach to estimate past and future sediment export?

RQ3: How did the suspended sediment export from the study area change in the past, how may it change in the future – and why?

Thus, chapter 2 aims to learn from 'the present' (i.e. the period with available measurement data) in order to understand suspended sediment dynamics in the study area (lower panel of Figure 1.2). The gained insights will be used to inform the model setup (e.g. choice of predictors) and prioritize study areas for chapters 3 and 4, and to have a background against which past and future changes can be interpreted.

Chapters 3 and 4 assess whether quantile regression forest (QRF) is a suitable approach to model sediment export in the past (chapter 3) and the future (chapter 4) by assessing advantages and limitations, considering sensitivities and comparing the performance to sediment rating curves (chapter 3).

Finally, this will enable investigating changes in sediment export (and their reasons) in the past five decades (chapter 3) and for different emission scenarios until the end of the 21st century (chapter 4), by analysing the resulting SSY estimates (and the predictors) for trends and the consequential location of peak sediment, step-like changes and shifts in seasonality (Figure 1.2).

1.6 METHODS

1.6.1 STUDY AREA

To answer the research questions and test the proposed modeling approach, the upper Ötztal region in Tyrol, Austria, offers unique opportunities. Here, the abundance of pre-

existing knowledge and measurement timeseries is outstanding, especially in the Rofental, a subcatchment of the Ötztal upstream gauge Vent (Strasser et al., 2018) (for a map see e.g. Figure 2.1). For example, discharge time series are available for the gauges Vent and Vernagt since 1967 and 1974, respectively, alongside previous studies on hydrological modeling (Kuhn et al., 2016; Kormann et al., 2016; Tecklenburg et al., 2012), especially of future hydrological changes (Hanzer et al., 2018). The gauges Vernagt, Vent, Sölden and Tumpen along the Rofenache and Ötzaler Ache form a series of nested catchments, which enables investigations on several spatial scales of both discharge and suspended sediments. At gauge Vent, SSC measurements are available since 2006, and at gauge Vernagt, SSC measurements from 2000 and 2001 (Naeser, 2002) provide a unique opportunity for model validation (section 3.3.1).

Moreover, the two largest glaciers in the Rofental catchment above gauge Vent, the Vernagtferner and the Hintereisferner have been monitored since 1964/65 and 1952, respectively. Additionally, the VF is one of the very few alpine glaciers where summer and winter mass balances have been determined separately (Escher-Vetter, 2007), which allows for more detailed analyses (see section 3.5.2).

Additionally, long observations of precipitation and temperature (Strasser et al., 2018) and previous water balance and meteorological analyses (Kuhn et al., 1982; Braun et al., 2007) are available. This is complemented by knowledge on permafrost (Sailer et al., 2014; Klug et al., 2017) and a more general permafrost distribution map for the European Alps (Boeckli et al., 2012), on the hydrological functioning of the Vent catchment via isotope-based hydrograph separation (Schmieder et al., 2016, 2018a), the availability of digital elevation models (Land Tirol, 2016), glacier inventories (e.g., Fischer et al., 2015; Buckel and Otto, 2018) and MODIS-derived snow cover data (Matiu et al., 2020). Finally, the absence of reservoirs or (significant) influence of hydropower (see also section 2.2.1) allows studying sediment dynamics in a relatively undisturbed area.

1.6.1 QUANTILE REGRESSION FOREST

QRF is based on (classification and) regression trees (Breiman et al., 1984). These are constructed by recursively splitting the data according to rules to obtain groups with similar values of the response variable. (An oversimplified splitting rule example would be: if air temperature is ≤ 0°C, all SSC are close to zero, whereas if air temperature is > 0°C, most SSC will be (much) larger than 0.)

QRF repeatedly draws random subsets of the original dataset (bootstrap samples), and constructs decision trees for each bootstrap sample, resulting in a forest of decision trees (Figure 1.3). This is identical to random forest techniques, which QRF is based on, with the difference that random forest only keeps the mean of all single-tree predictions, whereas QRF keeps the entire distribution, which enables assessments of prediction uncertainty. At each node, the predictors used to make the split are chosen randomly, which (theoretically) allows to assess predictor importance (section 5.2). Predictive performance can be analysed through

out-of-bag data, i.e. how well the model predicts SSC in the data that are not included in the bootstrap sample.

The advantages of QRF include that it is a multivariate approach that can handle non-normal distributions (as is the case for SSC for example) as well as interactions between variables (as e.g. between temperature and discharge), and that it is not bound to linear or monotonous relationships.

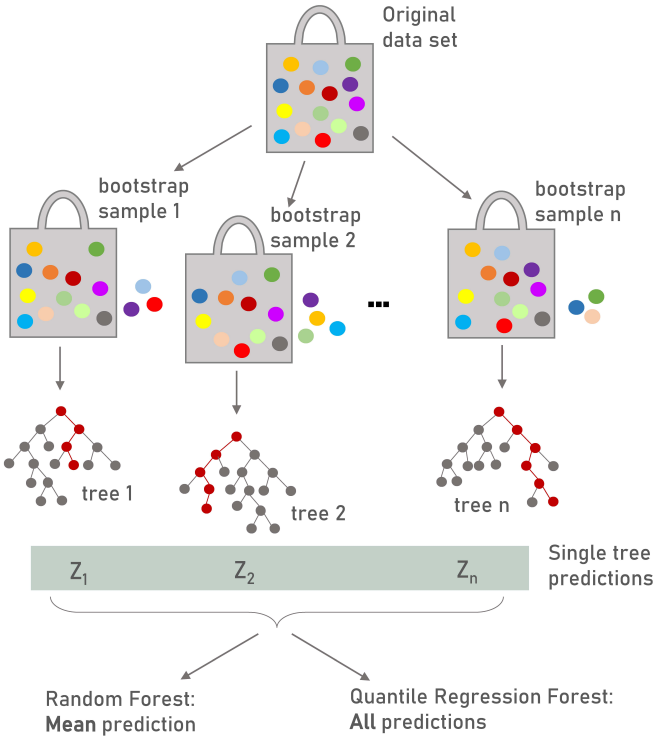

Figure 1.3. *Schematic representation of the quantile regression forest approach (modified after Carranza et al., 2021).*

1.7 AUTHOR CONTRIBUTIONS

This cumulative dissertation includes three manuscripts that are published or under review for publication in peer-reviewed journals. The text and figures remain as published (or submitted), while the layout has been adjusted to the formatting of this thesis and the key points at the beginning of chapters two to four were added. While the author of this thesis is the main author of all three manuscripts, several co-authors contributed to these studies in various ways. Their contributions are as follows:

Chapter 2: LKS planned the sampling and conceptualized the study together with the supervisors TF and AB. TB and JS mentored and reviewed. **LKS** conducted the statistical analyses with support and supervision by TF and AB. **LKS** conducted the GIS analysis. ER developed the code and performed the calculations for the snow cover analysis. **LKS** prepared the original draft including all figures and all authors contributed to the writing of this manuscript.

Chapter 3: LKS developed the general idea and conceptualized the study with TF and PG, with mentoring and reviewing by AB. **LKS** gathered the raw data. **LKS**, PG and TF installed and maintained the automatic water sampler for gauge Vernagt heavily supported by the installations run by CM, who also supplied past data. PG prepared the input data, adapted and extended the model code and performed modeling experiments with the support and supervision of TF and **LKS**. **LKS** conducted the statistical analyses with support by TF. CM reviewed and evaluated the results in the glaciological context. **LKS** prepared the original draft, including all the figures, and all the authors contributed to the writing of this paper.

Chapter 4: LKS developed the general idea and conceptualized the study with TF and PG, with mentoring and reviewing of AB. **LKS** requested the necessary input data, PG adapted and extended the model code under supervision of TF and **LKS**, and PG and **LKS** performed the model runs. **LKS** developed and conducted the analysis of model limitations and conducted the statistical analyses with support and supervision by TF. **LKS** prepared the original draft of the manuscript including all figures, and all authors contributed to writing this paper.

LKS = Lena Katharina Schmidt
TF = Till Francke
AB = Axel Bronstert
TB = Theresa Blume
JS = Johannes Schöber
ER = Erwin Rottler
PG = Peter Martin Grosse
CM = Christoph Mayer

2 UNDERSTANDING THE PRESENT

Published as: ***Schmidt, L. K.****, Francke, T., Rottler, E., Blume, T., Schöber, J., and Bronstert, A.: Suspended sediment and discharge dynamics in a glaciated alpine environment: identifying crucial areas and time periods on several spatial and temporal scales in the Ötztal, Austria Earth Surf. Dynam., 10, 653–669, https://doi.org/10.5194/esurf-10-653-2022, 2022*

KEY POINTS

- Analyzing 15 years of discharge and suspended sediment concentration at three nested gauges
- Complemented by snow cover maps, precipitation data, glacier inventories and glacier mass balances
- Spring onset of sediment transport coincides with snowmelt above 2500 m a.s.l. (recently deglacierized areas, glacier forefields, little vegetation)
- Precipitation events are less important than expected (ca. ¼ of annual sediment export)
- Thermally induced sediment export (glacier and snow melt) is dominant

ABSTRACT

Glaciated high-alpine areas are fundamentally altered by climate change, with well-known implications for hydrology, e.g. due to glacier retreat, longer snow-free periods and more frequent and intense summer rainstorms. While knowledge on how these hydrological changes will propagate to suspended sediment dynamics is still scarce, it is needed to inform mitigation and adaptation strategies. To understand the processes and source areas most relevant to sediment dynamics, we analyzed discharge and sediment dynamics in high temporal resolution as well as their patterns on several spatial scales, which to date few studies have done.

We used a nested catchment setup in the Upper Ötztal in Tyrol, Austria, where high-resolution (15-minute) time series of discharge and suspended sediment concentrations are available for up to 15 years (2006 – 2020). The catchments of the gauges Vent, Sölden and Tumpen range from 100 to almost 800 km² with 10 to 30 % glacier cover and span an elevation range of 930 to 3772 m a.s.l.. We analyzed discharge and suspended sediment yields (SSY), their distribution in space, their seasonality and spatial

differences therein and the relative importance of short-term events. We complemented our analysis by linking the observations to satellite-based snow cover maps, glacier inventories, mass balances and precipitation data.

Our results indicate that the areas above 2500 m a.s.l., characterized by glacier tongues and the most recently deglaciated areas, are crucial for sediment generation in all sub-catchments. This notion is supported by the synchronous spring onset of sediment export at the three gauges, which coincides with snowmelt above 2500 m but lags behind spring discharge onsets. This points at a limitation of suspended sediment supply as long as the areas above 2500 m are snow-covered. The positive correlation of annual SSY with glacier cover (among catchments) and glacier mass balances (within a catchment) further supports the importance of the glacier-dominated areas. The analysis of short-term events showed that summer precipitation events were associated with peak sediment concentrations and yields, but on average accounted for only 21 % of the annual SSY in the headwaters. These results indicate that under current conditions, thermally induced sediment export (through snow and glacier melt) is dominant in the study area.

Our results extend the scientific knowledge on current hydro-sedimentological conditions in glaciated high-alpine areas and provide a baseline for studies on projected future changes in hydro-sedimentological system dynamics.

2.1 INTRODUCTION

Glaciated high-alpine areas are central for discharge and sediment dynamics even beyond their catchment boundaries because the discharge and sediment fluxes from these areas are typically much higher (per unit area) than from lower-lying areas (Beniston et al., 2018; Hallet et al., 1996; Hinderer et al., 2013; Milliman and Syvitski, 1992). As a consequence, glaciated high-alpine areas have disproportionate influence on downstream water quality and quantity, flood hazard, hydropower generation and ecological habitats (Huss et al., 2017; Vercruysse et al., 2017).

However, glaciated high-alpine areas are also particularly sensitive to climatic change and climate warming is especially pronounced here (Gobiet et al., 2014). As a result of the rising temperatures, widespread and accelerating glacier retreat has been observed for several decades (e.g. Abermann et al., 2009; Sommer et al., 2020). Hydrological consequences include changes in water quantities (such as a transient increase in runoff) (Vormoor et al., 2015; Wijngaard et al., 2016), streamflow variability (van Tiel et al., 2019) and hydrograph timing e.g. due to earlier snowmelt onset and a prolonged glacier melt period (Hanus et al., 2021; Kormann et al., 2016; Rottler et al., 2021, 2020).

Possible climate change impacts on sediment dynamics are manifold, as all of the hydrological changes can affect sediment dynamics by changing the magnitude and timing of transport capacities. At the same time, sediment supply may change as glacier retreat uncovers vast amounts of sediment previously inaccessible to pluvial and fluvial erosion (Carrivick and Heckmann, 2017; Leggat et al., 2015) and as subglacial sediment discharge transiently increases (Delaney and Adhikari, 2020). Intense precipitation events, which are projected to increase in intensity and occur more frequently (Bürger et al., 2019; Giorgi et al., 2016; Scherrer et al., 2016), have a higher chance of affecting unfrozen material during prolonged snow-free periods (Kormann et al., 2016; Rottler et al., 2021; Wijngaard et al., 2016) and may thereby lead to a shift in the relative importance of sediment sources. Adding to this, permafrost thaw can destabilize hillslopes and facilitate mass movements (Chiarle et al., 2021; Huggel et al., 2010; Savi et al., 2020). On the other hand, changes in catchment-scale connectivity can provide new pathways or close off old pathways for loose material to the receiving waters waters (Cavalli et al., 2013; Lane et al., 2017), depending on local preconditions, for example due to the formation of a proglacial lake.

Balanced sediment management to address future changes is not only required in the context of hydropower production and reservoir sedimentation (Schöber and Hofer, 2018). It is also needed to prevent disturbances of the natural sediment regimes that may lead to decreasing species diversity and loss of habitat in aquatic environments (Gabbud and Lane, 2016), changing flood hazard (Nones, 2019) or changes in water quality (Bilotta and Brazier, 2008). In order to inform these management strategies, it is crucial to understand how changes in influencing factors and their complex interactions propagate to sediment dynamics, yet to date our understanding is still very limited (Huss et al., 2017).

A first step towards facilitating the assessment of future changes is to understand discharge and sediment dynamics in the recent past and present. Studies that have embarked on this journey to date have either compared (mean) annual sediment yields across a number of sites (e.g. Delaney et al., 2018b; Hinderer et al., 2013; Lalk et al., 2014; Micheletti and Lane, 2016; Schöber and Hofer, 2018; Tschada and Hofer, 1990) or investigated dynamics in daily or even finer temporal resolution but only at one or two locations (Beylich et al., 2017; Collins, 1996, 1990; Costa et al., 2018a; Guillon et al., 2018; Leggat et al., 2015; Orwin and Smart, 2004; Swift et al., 2005; Tsyplenkov et al., 2020). However, it is crucial to consider discharge and sediment dynamics in high temporal resolution as well as their spatial patterns in order to understand the dominant processes and thereby help inform modeling approaches that can put into perspective the effects of future changes.

In the present study, we aim to pinpoint the areas and processes most relevant to sediment dynamics in combination with discharge dynamics on several spatial and temporal scales. Our approach builds on three combined discharge and sediment gauges in a nested catchment setup in the Ötztal Alpine region, where discharge data and

relatively long suspended sediment time series of up to 15 years are available in high temporal resolution for catchments of 100 to almost 800 km² in size. To improve the existing sediment concentration data set, we improved the relationship between turbidity and suspended sediment concentrations at the gauge in Sölden by operating an automatic water sampler. To complement our analysis, we investigate glacier inventories and mass balances, precipitation data, satellite-based snow cover maps and land cover characteristics.

More specifically, we (1) explore changes in discharge and suspended sediment yield magnitudes across spatial scales, (2) analyze the seasonal distribution of both fluxes as well as the relative importance of (precipitation) events as compared to snow and glacier melt and (3) examine the importance of different elevation bands for sediment export in spring using a synoptic view of snow cover evolution and sediment seasonality.

2.2 METHODS

2.2.1 STUDY AREA

The study area is a nested catchment setup within the Ötztal valley in Tyrol, Austria (Figure 2.1). The Ötztal Alps are part of the Ötztal–Stubai massif within the crystalline central Eastern Alps and biotite–plagioclase, biotite and muscovite gneisses, variable mica schists and gneissic schists dominate (Strasser et al., 2018). The entire catchment of 783 km² stretches from 931 m a.s.l. at the gauge in Tumpen (T) to 3772 m a.s.l. at the Wildspitze, the highest summit of Tyrol. Nested within are the 441 km² catchment of the gauge in Sölden (S) at 1343 m a.s.l. and the 98 km² catchment of the gauge in Vent (V) at 1891 m a.s.l. (Table 2.1). The areas between the gauges in Vent and Sölden (i.e., the area downstream of Vent and upstream of Sölden) and between Sölden and Tumpen have been termed S-V and T-S, respectively.

The climate in the catchment is comparatively dry since it is located in the inner Alpine region and is shielded from precipitation arriving from both the north and the south (Kuhn et al., 1982). Annual precipitation recorded at valley stations such as Vent (687 mm) and Längenfeld (see Figure 2.1, 730 mm) (Hydrographic Yearbook of Austria, 2016) is much lower than recordings by accumulating rain gauges in altitudes >3000 m, where annual precipitation can exceed 1500 mm (Kuhn et al., 2016; Strasser et al., 2018). The precipitation gradient with elevation has been estimated at about 5 % per 100 m (Schöber et al., 2014). Mean annual temperature at the gauge in Vent is 2.5 °C (Strasser et al., 2018) and increases to 6.3 °C at Umhausen (see Figure 2.1), 5 km upstream of the Tumpen gauge (Zentralanstalt für Meteorologie und Geodynamik (ZAMG), 2013).

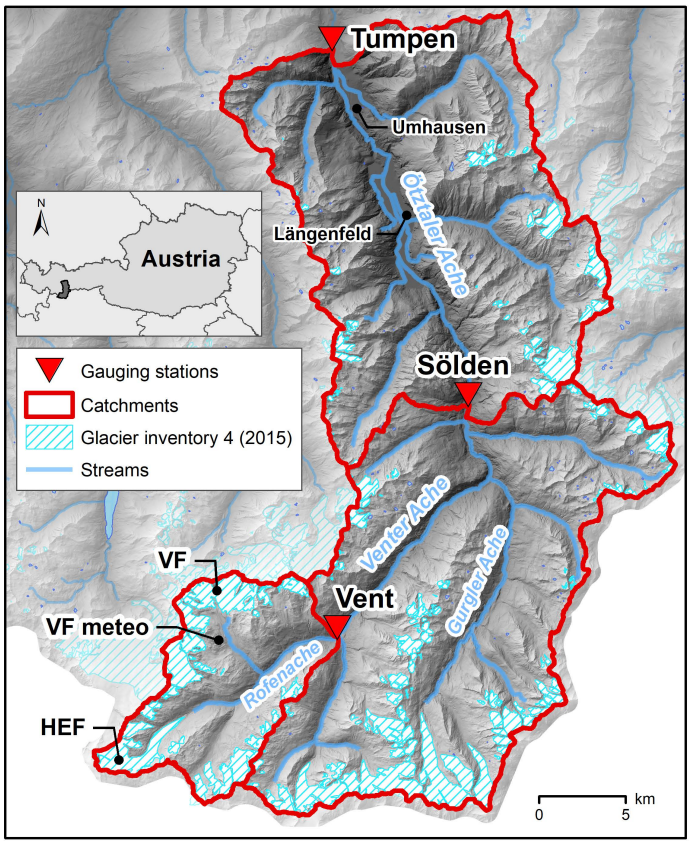

Figure 2.1. *Nested catchment areas of the three gauging stations Vent, Sölden and Tumpen within the Upper Ötztal, Tyrol, Austria. The locations of the Hintereisferner and Vernagtferner glaciers are marked by HEF and VF, respectively. 'VF meteo' shows the location of the Vernagtferner meteorological station (Bavarian Academy of Sciences and Humanities), providing precipitation and air temperature data for the event analysis. Sources: 10 m DTM of Tyrol (Land Tirol, 2016), glacier inventory 4, 2015 (Buckel and Otto, 2018), rivers and water bodies by tiris open government data (Land Tirol, 2021).*

The Ötztaler Ache is one of the largest tributaries of the Inn River and is fed by the Venter Ache and Gurgler Ache (Gattermayr, 2013). Upstream of Tumpen, the Ötztaler Ache is largely uninfluenced by hydropower, with a few small hydroelectric plants upstream of the gauges in Sölden and Tumpen that do not retain water and temporarily store coarse sediment fractions in sand traps. The Ötztaler Ache shows a strong seasonality with a snow- and ice-melt-dominated peak in summer (e.g., Strasser et al., 2018) and low-flow conditions in winter.

All sub-catchments are partially glaciated, ranging from almost 28 % glacier cover in the Vent catchment to 10 % glacier cover in the Tumpen catchment (Table 2.1). Glaciers in the area are subject to accelerating glacier reftreat, as can be seen in the difference between the two glacier inventories (3 and 4) from 2006 and 2015 (Buckel and Otto, 2018; Fischer et al., 2015). The magnitude of this glacier retreat is illustrated in the reduction in glacier cover from almost 35 % in 2006 to 28 % in 2015 in the Vent catchment. With respect to land cover, high elevations are dominated by glaciers and

bare rock or sparsely vegetated terrain while lower altitudes are characterized by mountain pastures and coniferous forests as well as agriculture in the valley floors.

Table 2.1*. Characteristics of the sub-catchments. Calculations based on: [1]DTM of Tyrol, 10m resolution (Umweltbundesamt, 2018), [2]Glacier inventory 3 (Fischer et al., 2015) and [3]Glacier inventory 4 (Buckel and Otto, 2018) using ArcGIS Version 10.6.1.*

Catchment	Vent (V)	S-V	Sölden (S)	T-S	Tumpen (T)
Catchment size [km²] [1]	98.1	342.7	440.8	342.0	782.8
Mean elevation (min - max) [m.a.s.l.] [1]	2891 (1891-3772)	2607 (1343-3619)	2670 (1343-3772)	2250 (931-3496)	2487 (931-3772)
Mean slope (min – max) [°][1]	25 (0 - 76)	29 (0 - 83)	28 (0 - 83)	32 (0 - 83)	30 (0 - 83)
Glacier cover GI 3 (2006) [%] [2]	34.4	14.8	19.2	4.9	12.9
Glacier cover GI 4 (2015) [%] [3]	28.1	11.9	15.6	3.6	10.3
Glacier cover GI 3 (2006) [km²] [2]	33.7	50.8	84.5	16.8	101.3
Glacier cover GI 4 (2015) [km²] [3]	27.6	41.0	68.6	12.4	81.0

2.2.2 DATA AND ANALYSES

2.2.2.1 DISCHARGE AND SEDIMENT CONCENTRATION DATA

For our analyses, we used discharge and turbidity-based suspended sediment concentration data from the three gauging stations in Vent (Rofenache), Sölden and Tumpen as depicted in Figure 2.1 (Table 2.2).

Although discharge data have been recorded by the Hydrographic Service of Tyrol since 1967 and 1976 in Vent and Tumpen, respectively, we only considered the period of time when concomitant turbidity measurements are available, i.e., since 2006. This was to focus on analyzing the present and recent past and to exclude long-term trends, e.g., due to increased glacier ablation since the 1980s (Hock, 2020), as much as possible.

Sediment concentration data at all stations are acquired by continuous turbidity measurements using optical infrared turbidity sensors (Solitax sensors by Hach, yielding tentative concentrations in mg L^{-1}). At the gauges in Vent and Tumpen, we used the data as received by the Hydrographic Service of Tyrol. These data result from a calibration of turbidity data to sediment concentrations based on water samples that

were taken by hand close to the turbidity probes in the stream and at several points spanning the width of the gauge (for details see Lalk et al., 2014). These data have been quality-checked by the Hydrographic Service except for the years 2019 and 2020.

*Table 2.2. Characteristics and sources of investigated data. (HD: Hydrographic Service of Tyrol, Austria; TiWAG: Tiroler Wasserkraft AG/hydropower company of Tyrol). *Turbidity measurements in Vent and Sölden are interrupted during the winter months to prevent damage to the equipment by ice.*

Station	Variable	Temporal resolution	Spatial resolution	Time period	Source
Vent (Rofenache)	Discharge	15 min	Gauge measurement	2006 - 2020	HD
	Suspended sediment concentrations*	15 min	Gauge measurement	2006 - 2020	HD
Sölden	Discharge	15 min	Gauge measurement	2012 - 2020	TiWAG
	Suspended sediment concentrations*	15 min	Gauge measurement	2012 – 2020 (2018 missing)	TiWAG
Tumpen	Discharge	15 min	Gauge measurement	2006 - 2020	HD
	Suspended sediment concentrations	15 min	Gauge measurement	2006 - 2020	HD
All catchments	Snow cover	daily	250 m	2002 - 2018	Matiu et al. (2020)

Similarly, at the gauge in Sölden, the TiWAG used water samples taken close to the turbidity sensor to translate turbidity measurements into a continuous sedigraph from 2012 to 2017 (see Schöber and Hofer, 2018, for details). We took additional water samples in 2019 and 2020 using automatic samplers (MAXX P6 L Vacuum) in order to improve the data situation especially at rarely sampled high concentrations and to continue observations as measurements by the TiWAG had been discontinued after 2017. For this purpose, the turbidity values recorded by the turbidity probe were recorded by a logger programmed to initiate sampling if one of three criteria was met: (i) regular sampling to ensure one sample at least every 4 d, (ii) threshold-based sampling to obtain samples across the whole range of possible turbidity values and (iii) event-based sampling. For the latter, a sample was initiated if the turbidity increase was steeper than a predetermined empirical threshold and if the absolute turbidity level exceeded the moving average of the past 10 d. The suction tube of the automatic sampler in Sölden was attached to the turbidity sensor's case, which was immersed at the side of the channel. The collection of one sample takes ca. 1.5 minutes, and we specified that two samples had to be at least 30 min apart. Gravimetric sediment concentrations SSC_g [$g\ L^{-1}$] were then determined in the laboratory by filtering the water samples onto glass fiber filters with a pore size of 0.45 µm and drying the filters at 60 °C until the weight was constant (see e.g. Delaney et al., 2018b).

In total, we took 99 samples in Sölden between April 2019 and October 2020. To verify whether these can be combined with the 268 samples taken by the TiWAG between 2012 and 2017, we tested for significant differences between linear models estimated for the two groups by means of an ANCOVA (analysis of covariance). This showed no significant differences between the two linear models. However, strictly speaking, the assumptions for an ANCOVA are violated because the residuals of the TiWAG data are not normally distributed (Shapiro–Wilk test, $p < 0.001$). By contrast, the residuals of our data are normally distributed (Shapiro–Wilk test, $p = 0.03$), which allows for the computation of confidence and prediction intervals around the linear model (Figure 2.2). Since all data points of the TiWAG samples are located within the prediction interval and the linear model based on TiWAG data lies within the confidence interval of the linear model based on our data, we conclude that there is good enough agreement to estimate one linear model using all 367 available samples. The resulting model ($SSC[\mathrm{g\,L^{-1}}] = 1.8487 \cdot turbidity\ [\mathrm{g\,L^{-1}}] + 0.0079$, $R^2 = 0.84$) is applied to the complete turbidity time series.

The variance observed in the SSC–turbidity relationship does not appear to be unusually high compared to other studies reporting similar coefficients of determination (Delaney et al., 2018b; Felix et al., 2018) and can be attributed to changes in particle size, shape or color (Merten et al., 2014).

From the discharge and SSC data, we calculated sediment discharge Q_{sed} [t/s] (for the analysis of events), water yield WY [m³/time], suspended sediment yield SSY [t/time] (to assess the magnitude of water and sediment export) and annual specific discharge sQ [mm a^{-1}], annual specific suspended sediment yield sSSY [t km^{-2} a^{-1}] (for comparison among gauges) as follows:

$Q_{sed}(t) = SSC(t) \cdot Q(t)$, where Q is discharge [m^3 s^{-1}]

$WY = \Delta t \cdot \sum Q$ and $SSY = \Delta t \cdot \sum Qsed$, where Δt is the corresponding temporal resolution [s], and

$sQ = \frac{WY}{A}$ and $sSSY = \frac{SSY}{A}$, where A [km^2] is the catchment area.

In order to assess discharge and sediment flux seasonality, we calculated the percentage of annual water yield $p_w(WOY)$ and annual suspended sediment yield $p_{sed}(WOY)$ exported in a given week of year (WOY) as

$\mathrm{p}_w(\mathrm{WOY}) = \frac{WY(WOY)}{WY(year)}$ and $\mathrm{p}_{sed}(\mathrm{WOY}) = \frac{SSY(WOY)}{SSY(year)}$.

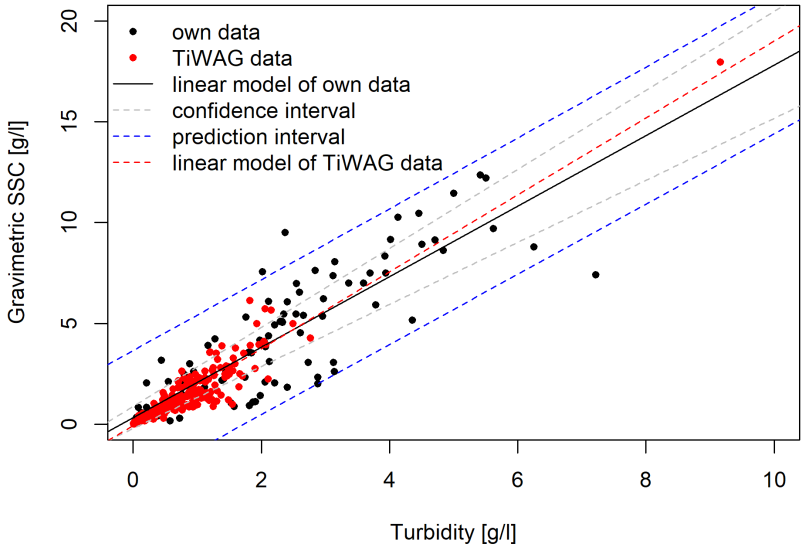

Figure 2.2. *Gravimetric suspended sediment concentrations SSC_g in samples vs. turbidity measured at the gauge in Sölden. TiWAG samples taken between 2012 and 2017 are all located within the prediction interval of the linear regression based on our samples and the linear model based on TiWAG data is located within the confidence interval.*

2.2.2.2 SEDIMENT EVENT ANALYSIS

To assess the relative importance of sediment events in time and space, we analyzed the largest Q_{sed} events of each year in Vent and Tumpen. We excluded Sölden from the analysis, as comparability would be limited since data are missing before 2012 and in 2018.

For the Vent catchment, we analyzed the events with respect to the antecedent air temperature and precipitation conditions. Since availability of high-quality (i.e. gap-free) data in high temporal resolution is limited, we confined this analysis to the years 2011 to 2020. We based our analysis on Q_{sed} calculated from discharge and sediment concentrations at the gauge in Vent and precipitation and air temperature data from the Vernagtferner station (2640 m a.s.l., located 6.25 km west of the gauge in Vent within the catchment) provided by the Bavarian Academy of Sciences. We visually identified Q_{sed} peaks that were clearly higher than the characteristic daily amplitude of the respective season. Since automatic event detection is not straightforward and thresholds are unsuitable due to the intense interannual and seasonal variability in Q_{sed}, we used expert knowledge to visually identify the events based on the beginning of the rising limb and the return to the before-event Q_{sed} or the point of inflection before the next event or daily fluctuation.

In order to be classified as a precipitation event, precipitation had to be > 3 mm in the 24 hours before of the end of the Q_{sed} event. We chose this low threshold, since the

point-like measurements often represent an underestimate of catchment precipitation due to the high spatial variability of precipitation within the almost 100 km² catchment and topographic effects. Additionally, we considered the hydrograph shape at the gauge in Vent as complementary indication, which typically shows a sharp increase in the case of a precipitation event. For classification as a melt-induced event, liquid precipitation had to be smaller than 3 mm within 24 h and the mean absolute temperature had to be above 1.5 °C. Additionally, we used the temporal development in daily snow cover data (Sect. 2.2.2.3) for the verification of snowmelt events.

For the Tumpen catchment, we visually identified Q_{sed} peaks as described above for the years 2011 to 2020 to ensure comparability. However, given the almost 800 km² area of the Tumpen catchment with considerable topography, there are only a few stations measuring precipitation for the whole time and in sufficient temporal (i.e., sub-daily and preferably sub-hourly) resolution. Therefore, we did not classify the events with respect to precipitation events.

2.2.2.3 GIS ANALYSIS, SNOW COVER DATA AND STATISTICAL ANALYSES

To derive the catchment areas for the three gauges, we used ArcGIS (version 10.6.1; Environmental Systems Research Institute, 2018) and the 10 m Digital Terrain Model of Tyrol (Land Tirol, 2016) to calculate the flow direction (D8) and flow accumulation, and finally we used the watershed tool. We then clipped the glacier areas of the glacier inventories 3 (Fischer et al., 2015) and 4 (Buckel and Otto, 2018) with the resulting catchment areas to obtain the respective glacier areas within the catchment (Table 2.1) and erased the areas of glacier inventory 4 of 2015 from the inventory 3 of 2006 to assess recently deglaciated areas.

In order to analyze land cover classes within the different elevation bands, we first calculated 250 m elevation bands for the whole catchment area upstream the gauge in Tumpen using the contour tool. Subsequently, we clipped glacier inventories and CORINE land cover data (Umweltbundesamt, 2018) to the elevation band areas.

We calculated average weekly snow-free areas based on data provided by Matiu et al. (2020), who used MODIS remote sensing products and derived daily nearly cloud-free snow cover data for the European Alps using temporal and spatial filters. We used these gridded data and intersected them with the areas of the 250 m elevation bands to gain the daily percentages of snow-free area for each elevation band and averaged these for each week of the year. In this, our basic idea is similar to the active contributing drainage area (ACDA) as proposed by Li et al. (2021), which uses the freezing line altitude to quantify the percentage of the catchment where the ground is unfrozen and thus susceptible to erosion. However, as an advantage over the ACDA, which yields the percentage of unfrozen area for the whole catchment, we are able to differentiate

between different areas within the catchment. We consider the resulting snow-free fraction of the respective elevation bands to be potentially erodible under the assumption that the ground no longer covered by snow is largely unfrozen and thus susceptible to erosion.

All statistical analyses were conducted in R version 3.5.1 (R Core Team, 2018).

2.3 RESULTS

2.3.1 SPATIAL DIFFERENCES IN MEAN ANNUAL DISCHARGE AND SUSPENDED SEDIMENT YIELDS

Mean annual specific discharge (sQ) is highest in the Vent catchment with 1543 mm a^{-1}, and gradually decreases to 885 mm a^{-1} in the T-S catchment, i.e. the area between the lowest gauge in Tumpen and the gauge in Sölden. Specific suspended sediment yield (sSSY) is markedly higher in the Vent catchment (1532 t km^{-2} a^{-1} on average) as compared to Sölden and Tumpen (1071 and 954 t km^{-2} a^{-1} on average) and the intermediate catchments. Adding to this, sSSY shows much higher interannual variability than sQ and the variability is highest at the gauge in Vent.

Absolute mean annual discharge and sediment yield increases with increasing catchment size (Table 2.3). The distributions of both fluxes are severely right-skewed (as the location of mean to maximum values show) since low values are much more frequent than high values. Maximum sediment concentrations decrease slightly with increasing catchment size, which points to a dampening along the flow-path.

Table 2.3. *Mean (min–max) observed values of discharge (Q), suspended sediment concentration (SSC) and suspended sediment yield (SSY) at the three gauges. For better comparability between the stations, SSCs recorded during the winter months from November to April were set to zero if there were NA values.*

Station	Q [m^3 s^{-1}] mean (min-max)	SSC [g L^{-1}] mean (min-max)	SSY [10^3 t a^{-1}] mean (min-max)
Vent (2006 – 2020)	4.8 (0.1 – 76.3)	0.54 (0 – 59.2)	150.3 (72.0 – 238.0)
Sölden (2012 – 2020)	19.2 (0.9 – 247.6)	0.59 (0 – 49.2)	472.3 (291.3–797.0)
Tumpen (2006 – 2020)	27.2 (2.7 – 266.2)	0.60 (0 – 50.7)	747.6 (339.8–1167.8)

To investigate whether the spatial differences of mean sQ and sSSY are equally distributed across the seasons, we subdivided the year into seasons that match

governing hydrological processes, so that 'spring' from April to June corresponds to the time dominated by snowmelt and 'summer' from July to September corresponds to the bulk of glacier melt (Figure 2.3).

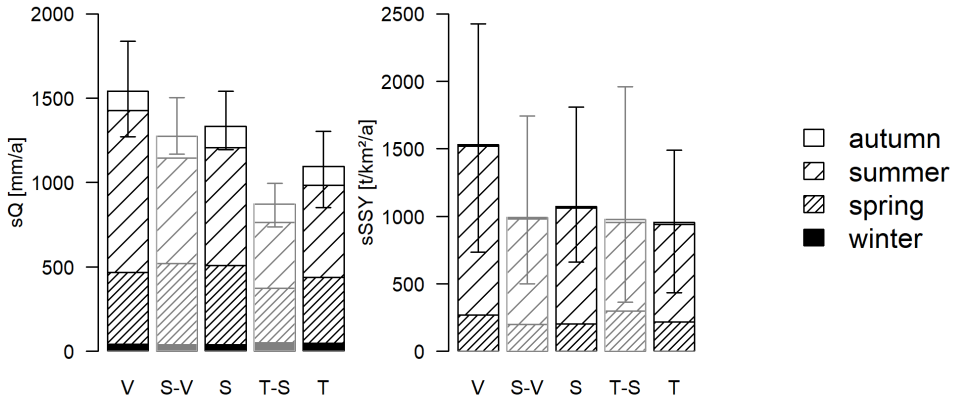

Figure 2.3. *Mean annual specific discharge (sQ) and suspended sediment yields (sSSY) at the gauges Vent, Sölden and Tumpen as well as the intermediate catchments between gauges in Vent and Sölden (S-V) and between gauges in Sölden and Tumpen (T-S). Bars are divided into seasons: winter (Jan – Mar), spring (Apr – Jun), summer (Jul – Sep), autumn (Oct – Dec). Whiskers depict minimum and maximum annual values.*

Both discharge and suspended sediment export are not equally distributed throughout the year. The discharge regimes at all gauges are clearly dominated by spring and summer streamflow (April – September), whereas autumn and winter discharge contributions (October – March) are small and almost equal across all sub-catchments. The most striking differences between the sub-catchments occur during the glacier melt period in summer, when sQ in the Vent catchment is markedly higher than in the downstream catchments.

Sediment yield is even more seasonal than discharge, with almost no export during autumn and winter (October – March). Mean summer sSSY values are markedly higher in Vent (1250 t km^{-2} a^{-1}) than in the other catchments (660 – 860 t km^{-2} a^{-1}), and differences between the sub-catchments are less pronounced in spring (ranging from 200 t km^{-2} a^{-1} in the S-V to 300 t km^{-2} a^{-1} in the T-S sub-catchment).

2.3.2 DISCHARGE AND SUSPENDED SEDIMENT YIELDS IN RELATION TO GLACIER COVER AND GLACIER MASS BALANCES

Annual specific discharge (sQ) and suspended sediment yields (sSSY) show significant positive correlations (significance level $\alpha = 0.01$) with increasing glacier cover among the respective catchments, although the high inter-annual variation in sSSY leads to a much weaker relationship and lower R^2 than for sQ (Figure 2.4).

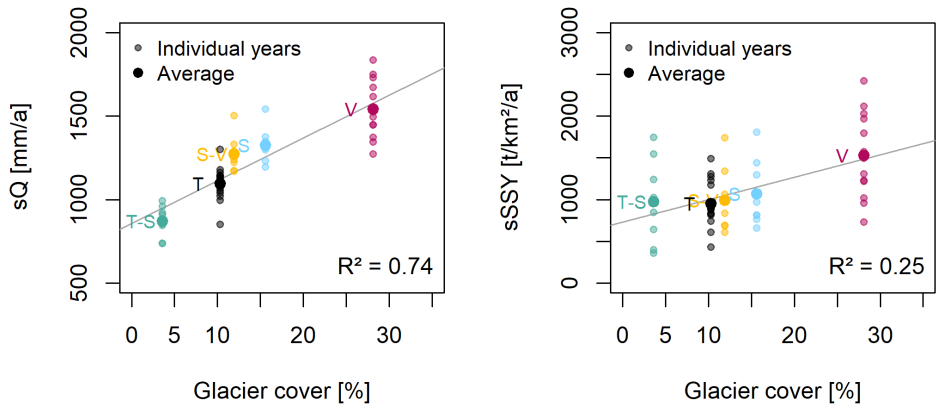

Figure 2.4. *Annual specific discharge (left) and annual specific suspended sediment yields (right) vs. glacier cover (glacier inventory 4, 2015; Buckel and Otto, 2018) in the sub-catchments.*

Minimum and maximum annual water yields at the three gauges differed by a factor of 1.3 to 1.5 in the years 2006 to 2020, while annual sediment yields varied by a factor of 3.3 to 5.4 (see also whiskers in Figure 2.3 or the range of values at each gauge in Figure 2.4 and Figure 2.5). For both variables, the interannual variability was most pronounced at the highest gauge in Vent.

In order to examine this, we considered the relationship between annual water yield and annual suspended sediment yield as well as the relationship of both to annual glacier balances. Unfortunately, we had to limit the latter analysis to the Vent catchment as mass balance data for glaciers within the other sub-catchments are lacking.

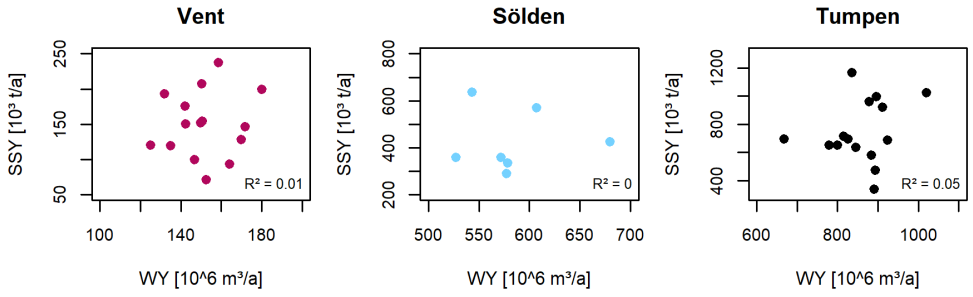

Figure 2.5. *Annual water and suspended sediment yield at the gauges in Vent, Sölden and Tumpen.*

We did not find a clear relationship of annual water yield and annual sediment yield at any of the gauges (Figure 2.5). However, the interannual variability can be at least partly attributed to differences in glacier mass balances: both sQ and sSSY in Vent correlate positively with the cumulative annual mass balances of Vernagt- and Hintereisferner (Figure 2.6), the two largest glaciers within the Vent catchment. Although the correlation for the entire available sQ and mass balance time series since 1976 (grey line in left panel of Figure 2.6) is significant ($\alpha = 0.01$), the correlation for the years since 2006 (i.e., the period of time investigated in this paper) is not significant and has a very

low R^2. The correlation between sSSY and annual balances is significant at a level of $\alpha = 0.05$.

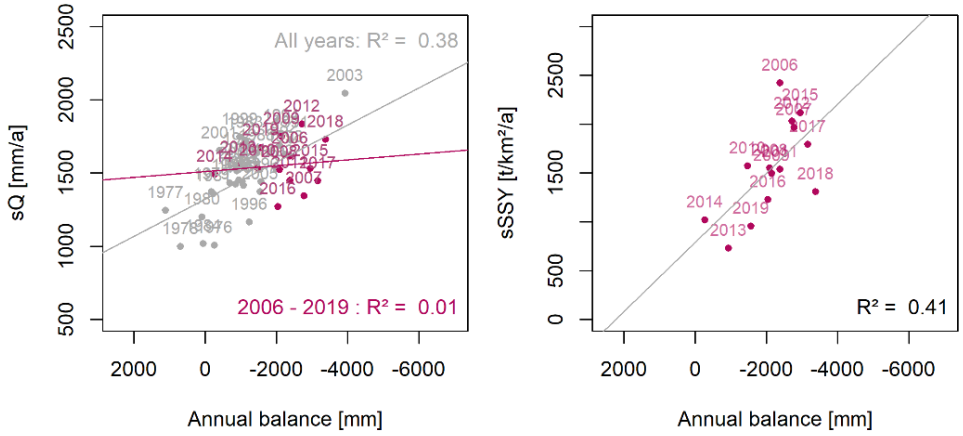

Figure 2.6. *Correlation of annual specific discharge and annual specific suspended sediment yields at the gauge in Vent with the sum of annual mass balances of the two largest glaciers within the Vent catchment (in millimeters), Vernagtferner and Hintereisferner (World Glacier Monitoring Service, 2021), corresponding to the respective glacier areas. The grey points, line and R^2 in the left panel refer to the entire available sQ and mass balance time series starting in 1976.*

2.3.3 SEASONALITY OF DISCHARGE AND SUSPENDED SEDIMENT YIELDS AND SPATIAL DIFFERENCES THEREIN

In order to assess discharge and suspended sediment seasonality for different spatial scales, we calculated the percentages of annual water yield p_w(WOY) and annual suspended sediment yield p_{sed}(WOY) that are transported in a given week of year WOY (Figure 2.7).

Water yield is very low between October and March at all gauges due to temperatures below the freezing point. As temperatures start to rise in spring, snowmelt usually starts around March in low elevations and mid-May in high elevations (see also Figure 2.8) causing the initial increases in water yield. In Sölden and Tumpen, peak p_w(WOY) values are recorded in early June, whereas the highest p_w(WOY) values in Vent are not achieved until the end of June or early July. Water yield at all gauges recedes as temperatures start to drop in September.

Suspended sediment seasonality is even more pronounced than discharge seasonality, as sediment yields start to increase later in the year and decrease earlier, and they are thus constrained to a smaller time window at all gauges (Figure 2.7). The highest p_{sed}(WOY) values occur during the ice-melt-dominated period after mid-July, coinciding

with the highest weekly p_w(WOY) at the gauge in Vent but delayed with respect to peak p_w(WOY) at the lower-lying gauges (Figure 2.7).

Discharge seasonality becomes more pronounced with elevation (Figure 2.7): of the annual water yield, 62 %, 52 % and 50 % are generated in summer in Vent, Sölden and Tumpen, and 11%, 13% and 14% in winter and autumn, respectively. An analysis of the individual years showed that the timing of the water yield increase in early spring is very similar at the three gauges. However, initially specific discharge is lower in Vent compared to Sölden and Tumpen, as snowmelt starts roughly at the same time in spring in all sub-catchments, but at a much lower rate upstream compared to downstream as temperatures above the freezing point occur earlier in lower areas. Later in summer, specific discharge is higher in Vent as compared to Sölden and Tumpen.

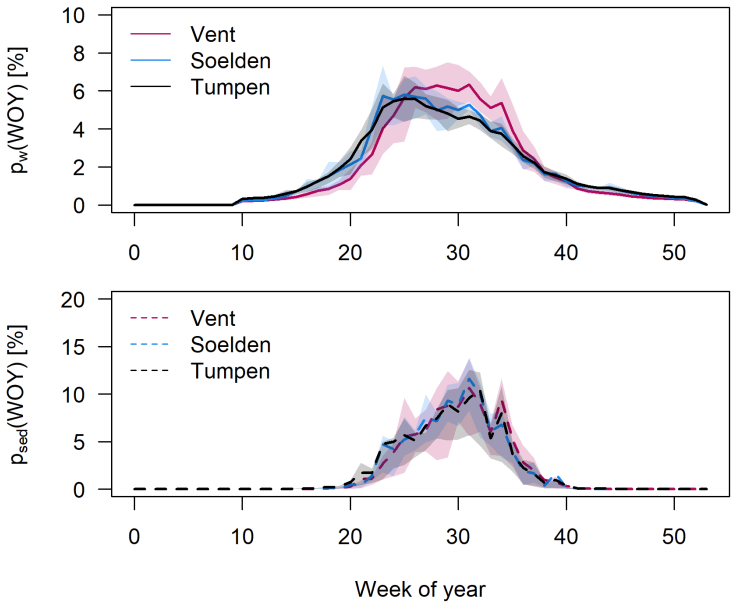

Figure 2.7. *Seasonality illustrated by mean percentages of annual water yield (p_w(WOY)) and suspended sediment yield (p_{sed}(WOY)) per week of year at the three gauges. Lightly colored areas show interquartile ranges (i.e. 25 % and 75 % quantiles).*

Interestingly, the timing and seasonal distribution of specific sediment yield are very similar at the three gauges (Figure 2.7), although absolute sediment yield is higher at the downstream gauges. This was also confirmed by an analysis of individual years: only in 4 of the 15 years of data (2007, 2009, 2018 and 2019) were very small portions of the annual SSY in Tumpen transported starting 2 weeks before the initial rise in Vent, but the first sharp increase in SSY was always simultaneous at the three gauges. Thus, suspended sediment seasonality changes only slightly with elevation: 81 %, 80 % and 76 % of the annual SSY are transported in summer in Vent, Sölden and Tumpen and 18 %, 19 % and 23 % in spring, respectively. The striking decrease in p_{sed}(WOY) at all stations in week 33 (i.e. around mid-August) is due to the coincidental absence of large events in the observed period in this week compared to the weeks before and after.

2.3.4 SPATIOTEMPORAL DYNAMICS OF SNOW COVER AND SUSPENDED SEDIMENT SEASONALITY

To explore the simultaneous onset of sediment export at all sites and the delay compared to the initial rises in water yield, we used a synoptic view of the mean spatiotemporal snow cover evolution with sediment seasonality.

The spatial snow cover evolution shows that in March (ca. week 10), the entire area above 2000 m is usually covered by snow (Figure 2.8). Until the end of April (ca. week 18), the area above 2500 m is still entirely snow-covered while about 20 % and 60 % of the two elevation bands below 2500 m are already snow-free. Starting in May, snow melts in areas above 2750m.

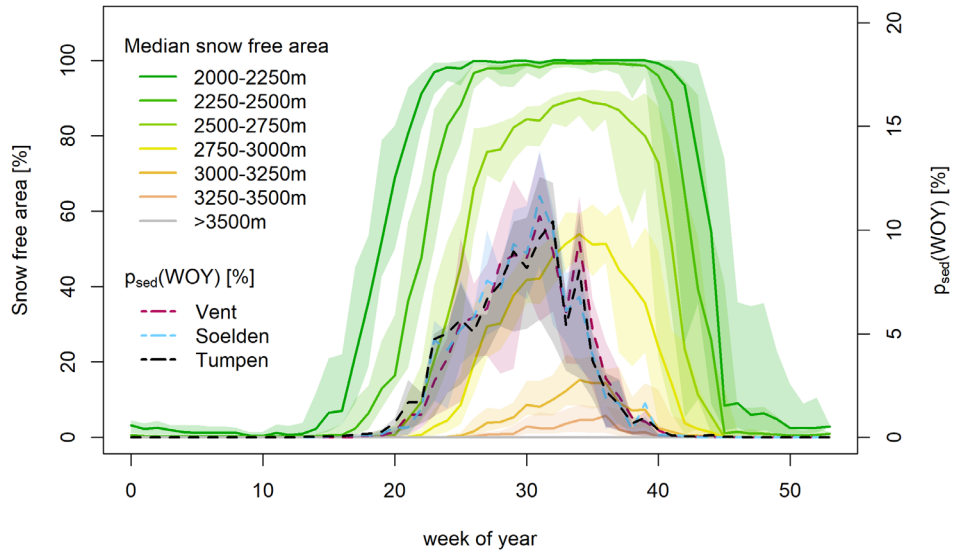

Figure 2.8. *Mean weekly percentage of annual SSY p_{sed}(WOY) and median snow free fraction resolved to selected elevation bands (above 2000 m a.s.l.) within the Tumpen catchment. Lightly colored areas depict interquartile ranges (i.e. 25 % and 75 % percentiles).*

The initial rise in p_{sed}(WOY) at all gauges coincides with the onset of snowmelt above 2500 m. Further differentiation between the elevation bands above 2500 m is difficult: firstly, an analysis of the individual years showed that snowmelt often started simultaneously in all elevation bands above 2500 m (although with different intensities). Furthermore, Matiu et al. (2020) warn against analyses of short periods of time that are too detailed due to uncertainties in the snow cover data and advise to average over weeks to months. Yet what was clear from the analysis of individual years as well as from Figure 2.7 is that the onset of snowpack removal in the areas below 2500 m always preceded the initial rise in suspended sediment p_{sed}(WOY) at the three gauges.

In autumn, sediment export declines as soon as the first snow cover starts to build up, which happens simultaneously at all elevations above 2000 m but to variable extents.

2.3.5 CHARACTERISTICS OF AREAS ABOVE 2500 M A.S.L.

To investigate whether the co-occurrence of snowmelt above 2500 m with spring increases in sediment export is linked to changes in land cover, we analyzed CORINE land cover data for the individual elevation bands (Figure 2.9). The most striking differences between the areas below and above 2500 m a.s.l. are the decrease in natural grasslands and the increase in bare rock surfaces. Moreover, the first glacier areas can be found above 2500 m and for most glaciers in the area, the (tip of the) glacier tongue is located here. In the elevation band below, between 2250 and 2500 m a.s.l., 93 % of the 0.5 km² glacier area that had remained in this elevation band during the glacier inventory of 2006 had melted by 2015. Thus the most recently deglaciated proglacial zones – with a much larger area of 3.2 km² glacier retreat between 2006 and 2015 – are located between 2500 and 2750 m.

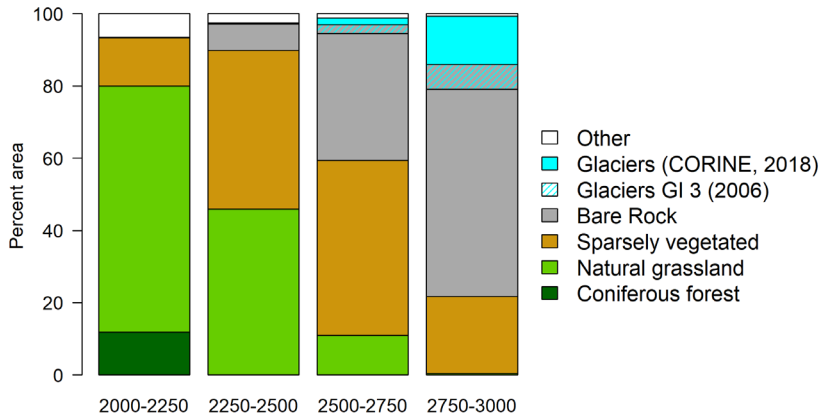

Figure 2.9. *Land cover in the elevation bands between 2000 and 3000 m a.s.l., based on CORINE land cover data (Umweltbundesamt, 2018).*

2.3.6 EVENT-BASED ASSESSMENT OF SUSPENDED SEDIMENT DYNAMICS

For Vent, we identified between 6 and 16 Q_{sed} events per year and a total of 100 events. Of the counted events, 95 % were shorter than 24 hours and the periods classified as events correspond to 0.5 to 1.5 % of the year. All events combined transported on average 7 % of the annual water yield (min. 4 % - max. 9 %, i.e., 6×10^6

to 13 × 10^6 m^3) and 25 % of the annual sediment yield in Vent (min. 12 % – max. 40 %, i.e., 8.5 × 10^3 to 57 × 10^3 t).

In Tumpen, we identified between 7 and 13 events per year and a total of 84 events. Compared to the 100 events identified in Vent, this means that some of the events detected in Vent did not stand out against the diurnal amplitude in Tumpen. The events in Tumpen were slightly longer than the events in Vent, as only 83 % were shorter than 24 hours. All events combined on average accounted for 6 % of the annual water yield (min. 4 % and max. 9 %, i.e. 35 × 10^6 and 80 × 10^6 m^3) and 26 % of the annual SSY in Tumpen (min. 16 % to max. 38 %, i.e., 102 × 10^3 t to 372 × 10^3 t). Similar to Vent, the periods classified as events correspond to 1 to 2 % of the year.

Although we only examined the events of the last 10 years, these proportions seem to be representative for the whole time series since 2006, as indicated by the grey area in Figure 2.10, which shows that up to almost 40 % of the cumulated yield is transported within 2 % of the time.

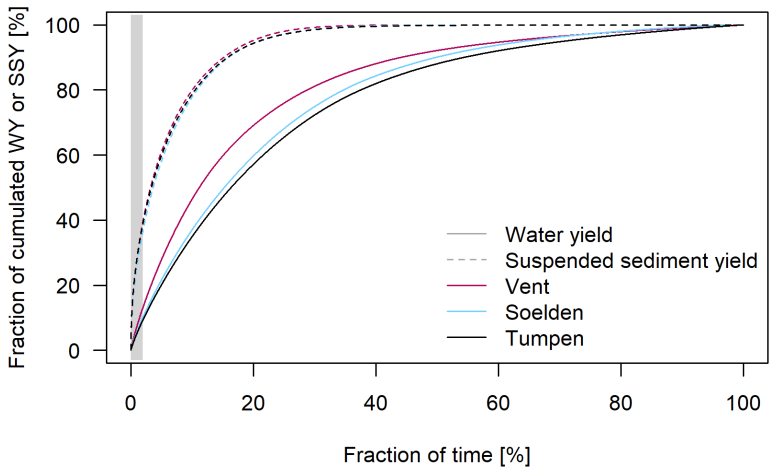

Figure 2.10. *Duration curves of water and suspended sediment yield based on 15-min data. The grey area represents the percentage of time classified as events. Note that the three lines for suspended sediment are very similar and might appear as only one line.*

Of the identified events, 84 % were associated with precipitation, while the remaining events were associated with the melting of snow or ice. The events associated with precipitation transported on average 21 % (min. 7 % - max. 40 %) of the annual SSY and 5 % (min. 2 % - max. 9 %) of the annual water yield. The most extreme event was observed in August 2014, when 26 % of the annual SSY (ca. 26 000 t) and 2.2 % of the annual water yield were transported in only 25 h. We hypothesize that this was associated with mass movements, as the event was preceded by a prolonged precipitation period (67 mm within 7 d and 30 mm within 24 h before the event), but do not have field observations from this time.

However, we did observe an event on 28 August 2020, when an extreme precipitation event of about 100 mm within 3 d led to a mass-wasting event onto the Hintereisferner, one of the largest glaciers within the Vent catchment. A total of 13 % of the annual SSY at the gauge in Vent (about 15 000 t) was exported within the first 30 h and 20 % within 4 d. The starting zone of the observed mass movement is located in an area with a high probability of permafrost occurrence (Boeckli et al., 2012).

2.4 DISCUSSION

2.4.1 MAGNITUDES OF WATER AND SUSPENDED SEDIMENT YIELD

We determined the order of magnitude of mean specific discharge (sQ) and specific suspended sediment yields (sSSY) on several spatial scales of 900 to 1500 mm a^{-1} for discharge and 1000 to 1500 t km^{-2} a^{-1} for sSSY, which generally correspond well to values reported for other catchments in the Ötztal and Stubai Alps (Schöber and Hofer, 2018). Our estimates of sSSY fall at the high end compared to the extensive collection of studies compiled by Hinderer et al. (2013) for the European Alps: only three catchments (the Haut Glacier D'Arolla and, the Tsidjiore Nouve and the Vispa with higher or similar glacier cover compared to Vent) showed higher annual sSSY than at the gauge Vent. Remarkably, the specific discharge of the order of 1500 mm at the gauge in Vent appears high compared to areal precipitation estimates for the Vent catchment between 1200 and 1500 (Hanzer et al., 2018; Kuhn et al., 2016; Stoll et al., 2020), leaving almost no room for evapotranspiration. This phenomenon can be explained by the contribution of non-equilibrium glacier melt and thus release of water from long-term glacier storage (Hock et al., 2005).

2.4.2 SPATIAL DIFFERENCES IN DISCHARGE AND SSY AS WELL AS RELATIONS TO GLACIER COVER AND MASS BALANCES

We found that mean annual values for both sQ and sSSY were highest at the gauge in Vent and thus correlate positively with glacier cover among the analyzed catchments. Similar correlations have been reported across the European Alps for spatially distinct catchments (Hinderer et al., 2013; Lalk et al., 2014; Schöber and Hofer, 2018) as opposed to the situation of nested catchments in our study.

The increase in specific discharge with glacier cover among catchments is reasonable given its correlation with high-altitude, non-equilibrium glacier storage and higher

contribution of glacier meltwater in Vent compared to lower elevations, where snowmelt gains in relative importance (Kormann et al., 2016; Kuhn et al., 2016; Weber and Prasch, 2016a). However, precipitation also increases with elevation: mean annual precipitation at the gauge in Vent of 666 mm is much lower than the 1200 to 1500 mm estimated for the Vent catchment, and even 1525 to 1900 mm is reported for the 11.4 km² Vernagtferner sub-catchment (2600 – 3600 m elevation) (Braun et al., 2007; Kuhn et al., 2016; Hanzer et al., 2018; Stoll et al., 2020). Further contributing factors are lower temperatures and vegetation cover leading to lower evapotranspiration in higher elevations.

Looking at interannual differences within the Vent catchment, annual sQ of the period 2006 to 2020 did not show a significant correlation with glacier mass balances and a very low R^2, as opposed to the entire available time series since 1976 (Figure 2.6). We attribute this to the leverage of individual years such as 2014, when a ca. 10-year flood occurred in the Ötztaler Ache on August 13th and the percentage of the annual water yield during precipitation events was 9 % (the highest percentage of the 10 years examined) while, unusually, the annual glacier mass balance was close to zero.

The increase in mean sSSY with glacier cover is in line with the current understanding that glaciers act as important sediment sources, especially during the transitional, paraglacial state of deglaciation (Ballantyne, 2002), through glacial erosion, the provision of proglacial sediments following their retreat and the transport of subglacial sediments by meltwaters (Beylich et al., 2017; Delaney et al., 2018a; Schöber and Hofer, 2018). This is further supported by the negative correlation between annual glacier mass balance and annual sSSY (i.e., positive correlation between glacier ablation and sediment export) as well as our finding that differences in mean annual sQ and sSSY were mainly due to differences during the glacier melt period. Interestingly, specific discharge volumes show much lower interannual variability than sSSY, which we attribute to the compensating effect of glaciers for interannual streamflow variability (Hock et al., 2005). We did not find a clear relationship between annual water yield and annual sediment yield at any of the gauges and conclude that annual water yield does not seem to explain much of the interannual variability in SSY.

2.4.3 SEASONALITY OF DISCHARGE AND SUSPENDED SEDIMENT YIELDS AS WELL AS SPATIAL DIFFERENCES THEREIN

We further assessed the spatiotemporal distribution by analyzing the seasonality of discharge and SSY at the three gauges. This showed that discharge seasonality is scale-dependent, as water yield increases earlier at the lower gauges due to earlier onsets of snowmelt, as well as lower relative contributions of glacier melt and higher relative contributions of precipitation in lower elevations (see also Kormann et al., 2016, Weber

and Prasch, 2016). Accordingly, the highest weekly percentages of annual water yield p_w(WOY) are observed during the snowmelt phase at the gauges in Sölden and Tumpen but during the glacier melt phase in Vent. This can be attributed to the higher percentage of glacier cover further upstream and associated higher daily discharge maxima during summer (Gattermayr, 2013). In contrast, SSY seasonality is synchronous at the three gauges. The mean annual cycle suggests that sediment discharge is negligible in winter. It has to be noted, that there are no direct SSC measurements at the Vent and Sölden gauges during late autumn and winter, as the respective monitoring is routinely paused to avoid damages to the equipment by ice and reinstalled before the initial rise in concentrations in spring. However, turbidity recordings at the gauge in Tumpen show that the total sSSY of roughly 0.5 t km^{-2} in January to March accounts for less than 1 % of the annual sSSY. Sediment supply seems to be limited in spring as the initial rise in water yield precedes the beginning of sediment export and similar discharge volumes transport higher amounts of sediment in late summer compared to spring

2.4.4 SPATIOTEMPORAL DYNAMICS OF SNOW-COVER AND SUSPENDED SEDIMENT SEASONALITY

To explore the reasons behind the simultaneous onset of suspended sediment export at the three gauges, we investigated the temporal evolution of snow-free area in different elevation bands. The snowmelt timing as derived from the MODIS product (Matiu et al., 2020) is well in accordance with the timing as reported by Kuhn et al. (2016).

As the spring increase in sediment export at all gauges coincides with snowmelt above 2500 m a.s.l., we conclude that the areas above 2500 m are crucial source areas, where the determining processes are activated as the snow melts. These processes include the initiation of ice melt and export of sediment from subglacial and proglacial areas as well as increased susceptibility of snow-free and possibly unfrozen hillslopes to pluvial erosion. The suitability of snow-free area as a proxy for these processes is also supported by the coinciding decline in sediment transport and build-up of first snow cover in autumn.

The areas above 2500 m contain landscape elements such as glacier tongues and proglacial areas, which have been identified as very significant for sediment dynamics in other catchments (Delaney et al., 2018a; Orwin and Smart, 2004; Schöber and Hofer, 2018). For example, Delaney et al. (2018a) found that although far more sediment originated subglacially, erosion rates in proglacial areas were over 50 times greater than in the rest of the Griesgletscher catchment in the Swiss Alps. As another characteristic of the areas above 2500 m, permafrost is likely to occur in favorable or cold conditions according to the permafrost distribution map provided by Boeckli et al. (2012) and as demonstrated by Klug et al. (2017). Thus, erosion processes associated with permafrost

thawing could also play a role, for example as the active layer becomes susceptible to pluvial erosion once it has thawed (Li et al., 2021a).

We conclude that sediment export in all three catchments is limited as long as the areas above 2500 m are frozen or snow-covered and subglacial sediment sources are still inactive. This has implications for the future, since these areas will likely be snow-free for longer periods in summer (Hanus et al., 2021; Hanzer et al., 2018) during which sediments from these areas can be mobilized. At the same time, the crucial areas might increase in size as glaciers retreat and recently deglaciated areas increase. Additionally, assuming that permafrost degradation is an ongoing and largely irreversible process, the increase in erodible surfaces due to permafrost melt seems very likely.

2.4.5 EVENT-BASED ASSESSMENT OF SUSPENDED SEDIMENT DYNAMICS

All Q_{sed} events combined (up to 2 % of the total time span) on average accounted for 25 % and 26 % of the annual sediment yield but only 7 % and 6 % of annual water yield in Vent and Tumpen, respectively. In combination with the more pronounced seasonality of SSY, this explains the much 'flashier' behavior compared to discharge (Figure 2.10). Similar proportions have been reported for other glaciated catchments (Leggat et al., 2015; Wulf et al., 2012), which suggests greater availability and/or easier mobilization of sediments compared to fluvial systems wherein up to 90 % of sediment is transported during short, high-discharge events (Delaney et al., 2018b).

In Vent, 84 % of the events were associated with precipitation. While this implies that, so far, thermally induced sediment export through snow and glacier melt yields the biggest share of SSY in Vent, we also showed that individual summer rainstorm events can account for up to 26 % of the annual yield (ca. 26 000 t) within just over 24 hours if mass movements are involved. Since we had to limit this analysis to the Vent catchment, we cannot assess spatial variation in the importance of precipitation events.

We suggest that hydro-sedimentological events such as the one observed in August 2020 – involving mass movements that were triggered by heavy precipitation and are probably associated with increased hydro-sedimentological connectivity and/or permafrost thaw – are likely to occur more frequently in the future: in view of expected future developments, such as more frequent high-intensity summer rainstorms (Giorgi et al., 2016), prolonged snow-free periods in summer during which these rainstorms can become erosive (Hanus et al., 2021; Hanzer et al., 2018), the exposure of vast amounts of sediment due to glacier retreat (Carrivick and Heckmann, 2017; Lane et al., 2017) and accelerating permafrost thaw, which facilitates more frequent slope-failure events (Savi et al., 2020), heavy precipitation events have the potential to drastically gain in importance with regard to sediment export.

2.4.6 OUTLOOK

To our knowledge, this study represents the first extensive analysis of discharge and suspended sediment dynamics on multiple spatial and temporal scales in a glaciated, high-alpine setting. The employed approach can bridge the gap between detailed, small-scale investigations of individual (pro-)glacial areas and wide-area comparisons of numerous gauges in low temporal resolution. Our results extend the knowledge on hydro-sedimentological dynamics in glaciated high-alpine areas and can therefore serve as a basis for future studies and management strategies. For example, studies attempting to model sediment dynamics in high-alpine areas might consider focusing more attention on the areas above 2500 m compared to other parts of the study area. Likewise, studies on future changes in high-alpine sediment dynamics need to consider the potentially changing role of precipitation and mass movements relative to the currently dominating thermal processes.

2.5 CONCLUSION

Discharge dynamics in glaciated high-alpine areas are expected to change fundamentally due to climate change, yet little is known about how exactly these changes propagate to sediment dynamics. To provide the basis for future studies investigating these future changes, we analyzed discharge and suspended sediment concentration data from the recent past in a nested catchment setup in the Ötztal in Tyrol, Austria, and aimed to identify the areas, time periods and processes that are crucial for suspended sediment and discharge dynamics.

We showed that mean annual discharge and suspended sediment export were highest in the smallest, highest, most glaciated sub-catchment above the gauge in Vent and that annual water and sediment yields correlated significantly with annual glacier mass balances. This demonstrates that glaciated areas are important sediment sources and glacier meltwater contribution is high.

Discharge seasonality is more pronounced at higher elevations due to a later onset of snowmelt, higher glacier melt contributions and a considerable positive precipitation gradient with elevation.

However, the onset of suspended sediment export in spring occurs almost synchronously at the three gauges and the time lag compared to the spring increase in discharge points towards a limitation of sediment supply during this time. We analyzed sediment seasonality in synopsis with snowmelt timing in different elevation bands, which suggests that the areas above 2500 m a.s.l., including glacier tongues, bare rock surfaces and recently deglaciated areas, are crucial for suspended sediment dynamics.

Our analysis showed that sediment dynamics are largely dominated by melt-driven processes, as precipitation events play a subordinate role compared to thermally induced discharge and suspended sediment export. However, single large rainfall events can significantly contribute to the annual sediment budget, which we attribute to the activation of additional sediment supply by mass-wasting processes and increased hydro-sedimentological connectivity during phases of excessive overland flow. We discuss the fact that these events are likely to occur more frequently in the future, which may result in a shift in the relative importance of precipitation events for sediment dynamics.

Our study extends the scientific knowledge on current hydro-sedimentological dynamics in glaciated high-alpine areas and provides a baseline for investigations on projected future changes in hydro-sedimentological system dynamics. Such future investigations should focus on the areas above 2500 m and the role of precipitation events when addressing future changes in suspended sediment and discharge dynamics, e.g., in modeling studies.

2.6 DATA AVAILABILITY

Discharge and suspended sediment concentration data from the gauges at Vent and Tumpen recorded by the Hydrographic Service of Tyrol, Austria, as well as sediment concentrations from our samples taken in Sölden are published under https://doi.org/10.23728/b2share. be13f43ce9bb46d8a7eedb7b56df3140 (Schmidt and Hydrographic Service of Tyrol, Austria, 2021).

Discharge and turbidity time series recorded by the TiWAG at the gauge in Sölden along with suspended sediment concentration data in TiWAG samples can be requested via info-ausbau.kw.kaunertal@tiwag.at.

Precipitation and air temperature data recorded at the Vernagtferner hydro-meteorological station by the Bavarian Academy of Sciences and Humanities are successively made available on PANGEA and data until 2012 are already available at https://doi.pangaea.de/10.1594/PANGAEA.829530 (Escher-Vetter et al., 2014).

The DTM of Tyrol is available at https://www.data.gv.at/katalog/dataset/land-tirol_tirolgelnde (Land Tirol, 2016).

Land cover data are available at https://www.data.gv.at/katalog/dataset/clc2018 (Umweltbundesamt, 2018).

Glacier inventories are available at DOI 10.1594/PANGAEA.844985 (Fischer et al., 2015) and DOI 10.1594/PANGAEA.887415 (Buckel and Otto, 2018). Glacier mass

balances are available at DOI 10.5904/wgms-fog-2021-05, 2021 (World Glacier Monitoring Service, 2021). Snow cover data are available via DOI 10.3390/data5010001 (Matiu et al., 2020).

2.7 COMPETING INTERESTS

The authors declare that they have no conflict of interest.

2.8 ACKNOWLEDGMENTS

We thank the Hydrographic Service of Tyrol, Austria, the TiWAG Tirolean hydropower corporation and the Bavarian Academy of Sciences and Humanities for the provision of data as well as logistical support and fruitful discussions. We thank Peter Grosse and Marvin Teschner for their support in field, laboratory work and data analyses, Nina Lena Neumann and Joseph Pscherer for their laboratory work and Daniel Bazant for his support during the GIS analysis. We thank Stefan Achleitner, Carolina Kinzel and the Environmental Engineering laboratory at the University of Innsbruck for their kind support during field and laboratory work. We thank Anatoly Tsyplenkov and Ronald Pöppl for their detailed and constructive reviews of this paper.

2.9 FINANCIAL SUPPORT

This research has been supported by the Deutsche Forschungsgemeinschaft Research Training Group 'Natural Hazards and Risks in a Changing World' (NatRisk Change GRK 2043/1 and NatRisk Change GRK 2043/2 grants) as well as a fieldwork fellowship from the German Hydrological Society (DHG)

3 RECONSTRUCTING THE PAST

Published as: ***Schmidt, L. K.****, Francke, T., Grosse, P. M., Mayer, C., and Bronstert, A.: Reconstructing five decades of sediment export from two glacierized high-alpine catchments in Tyrol, Austria, using nonparametric regression, Hydrol. Earth Syst. Sci., 27, 1841–1863, https://doi.org/10.5194/hess-27-1841-2023, 2023.*

KEY POINTS

- Exploring a machine-learning approach (Quantile Regression Forest) to model sediment export
- Based on temperature, discharge and precipitation as predictors and suspended sediment concentrations as response
- Model performs well in an extensive validation and outperforms sediment rating curves
- Application to five decades of predictor data suggests that sediment export has increased
- Step-like increases after 1981 are linked to temperature-driven enhanced glacier melt

ABSTRACT

Knowledge on the response of sediment export to recent climate change in glacierized areas in the European Alps is limited, primarily because long-term records of suspended sediment concentrations (SSCs) are scarce. Here we tested the estimation of sediment export of the past five decades using quantile regression forest (QRF), a nonparametric, multivariate regression based on random forest. The regression builds on short-term records of SSCs and long records of the most important hydro-climatic drivers (discharge, precipitation and air temperature – QPT). We trained independent models for two nested and partially glacier-covered catchments, Vent (98 km^2) and Vernagt (11.4 km^2), in the upper Ötztal in Tyrol, Austria (1891 to 3772 m a.s.l.), where available QPT records start in 1967 and 1975. To assess temporal extrapolation ability, we used two 2-year SSC datasets at gauge Vernagt, which are almost 20 years apart for a validation. For Vent, we performed a five-fold cross-validation on the 15 years of SSC measurements. Further, we quantified the number of days where predictors exceeded the range represented in the training dataset, as the inability to extrapolate beyond this range is a known limitation of QRF. Finally, we compared QRF performance to sediment rating curves (SRC). We analysed the modelled sediment export time series, the predictors and

glacier mass balance data for trends (Mann–Kendall test and Sen's slope estimator) and step-like changes (using the widely applied Pettitt test and a complementary Bayesian approach).

Our validation at gauge Vernagt demonstrated that QRF performs well in estimating past daily sediment export (Nash–Sutcliffe efficiency (NSE) of 0.73) and satisfactorily for SSCs (NSE of 0.51), despite the small training dataset. The temporal extrapolation ability of QRF was superior to SRCs, especially in periods with high-SSC events, which demonstrated the ability of QRF to model threshold effects. Days with high SSCs tended to be underestimated, but the effect on annual yields was small. Days with predictor exceedances were rare, indicating a good representativity of the training dataset. Finally, the QRF reconstruction models outperformed SRCs by about 20 percent points of explained variance. Significant positive trends in the reconstructed annual suspended sediment yields were found at both gauges, with distinct step-like increases around 1981. This was linked to increased glacier melt, which became apparent through step-like increases in discharge at both gauges as well as change points in mass balances of the two largest glaciers in the Vent catchment. We identified exceptionally high July temperatures in 1982 and 1983 as a likely cause. In contrast, we did not find coinciding change points in precipitation. Opposing trends at the two gauges after 1981 suggest different timings of peak sediment. We conclude that, given large-enough training datasets, the presented QRF approach is a promising tool with the ability to deepen our understanding of the response of high-alpine areas to decadal climate change.

3.1 INTRODUCTION

Sediment production rates per unit area are highest in the world's mountains (Hallet et al., 1996), headed by modern glacierized basins (Hinderer et al., 2013). As a consequence, sediments transported from these rapidly deglaciating high-alpine areas have substantial effects on downstream hydropower production and reservoir sedimentation (Schöber and Hofer, 2018; Guillén-Ludeña et al., 2018; Li et al., 2022), flood hazard (Nones, 2019; Brooke et al., 2022) and water quality, nutrient and contaminant transport and aquatic habitats (Gabbud and Lane, 2016; Bilotta and Brazier, 2008; Vercruysse et al., 2017) and impact global sediment and biochemical balances (Herman et al., 2021). Thus, there is considerable interest in water resource research and management to gain better understanding of sediment dynamics in high-alpine areas and to mitigate and adapt to future changes.

However, there is still limited quantitative understanding of sediment transport in high-alpine rivers and their relation to changes in climatic forcing over temporal scales relevant to investigating changes associated with anthropogenic climate change, i.e. at decadal and centennial scales as opposed to longer ones (Huss et al., 2017; Antoniazza and Lane, 2021; Herman et al., 2021). This is partly due to the complexity of sediment dynamics in high-alpine areas, which are the result of an intricate system of climatic forcing and hydrogeomorphological processes (Costa et al., 2018b; Vercruysse et al., 2017; Zhang et al., 2022).

A significant body of knowledge exists on how some of the components of these complex systems have changed in recent decades due to rising temperatures. Cryospheric changes include widespread and accelerating glacier retreat (Abermann et al., 2009; Sommer et al., 2020) and reduced extent and duration of snow cover (Beniston et al., 2018; Chiarle et al., 2021). As a result, hydrological regimes are changing from glacial to nival regimes and from nival to pluvial regimes (Beniston et al., 2018), which results in changes in water quantities (Vormoor et al., 2015; Wijngaard et al., 2016), streamflow variability (van Tiel et al., 2019) and hydrograph timing (Kormann et al., 2016; Kuhn et al., 2016; Hanus et al., 2021; Rottler et al., 2020, 2021). These hydrological changes can translate to changes in erosivity, sediment transport capacities and fluvial erosion. At the same time, sediment supply changes, as glacier retreat uncovers large amounts of sediment previously inaccessible to pluvial and fluvial erosion (Carrivick and Heckmann, 2017; Leggat et al., 2015), subglacial sediment discharge transiently increases (Costa et al., 2018b; Delaney and Adhikari, 2020) and continuing permafrost thaw destabilizes slopes and facilitates mass movements (Huggel et al., 2010, 2012; Beniston et al., 2018; Savi et al., 2020). Adding to this, erosive precipitation has a higher chance of affecting unfrozen material during prolonged snow-free periods (Kormann et al., 2016; Rottler et al., 2021; Wijngaard et al., 2016).

However, the magnitude of these impacts is catchment-specific, as it depends, e.g., on the area occupied by glaciers and permafrost or basin hypsometry (Huss et al., 2017) and is thus not easily transferable from one site to another. Aggravatingly, high-alpine sediment dynamics are highly variable, so that long time series are required to assess systematic changes. However, most records are too short for such analyses and long-term data are extremely rare, especially in glacierized headwaters, which are often especially challenging to monitor.

To our knowledge, only very few examples of decadal sediment records from the European Alps exist in the current literature, as opposed to their availability for, e.g., High Mountain Asia (Singh et al., 2020; Li et al., 2020, 2021b; Zhang et al., 2021), the Andes (Vergara et al., 2022) or the Arctic (Bendixen et al., 2017a) (for an extensive review, see Zhang et al., 2022). Costa et al. (2018b) report on an exceptional record of suspended sediment concentrations from the upper Rhône basin, Switzerland, of almost five decades, though these recordings are severely affected by anthropogenic impacts (hydropower generation and gravel mining) and integrate over an area of 5340 km². Michelletti and Lane (2016) and Lane et al. (2017) reconstructed coarse sediment export from hydropower intake flushings at decadal scales in three small catchments in the Hérens Valley, Switzerland, not taking into account however the amount of suspended sediment transport, which is often at least as large as the amount transported as bedload (Schöber and Hofer, 2018; Mao et al., 2019; Turowski et al., 2010). Further long-term sediment records can be inferred from sediment stratigraphy (e.g., Bogen, 2008; Lane et al., 2019), yet such studies are of course confined to catchments where lakes or reservoirs are present. To compensate for this lack of measurement data, we aim to estimate longer-term past suspended sediment dynamics based on the available shorter records of suspended sediment concentrations.

Quantile regression forest (QRF) (Meinshausen, 2006) represents an approach that has been successfully applied to modeling suspended sediment concentrations in past geomorphological studies, in badland-dominated catchments in Spain (Francke et al., 2008a, b) and in a tropical forest in Panama (Zimmermann et al., 2012). QRF is a multivariate, nonparametric regression technique based on random forest, from the category of machine-learning (ML) approaches, which generally seek to identify patterns from complex data (Tahmasebi et al., 2020). Comparative studies have reported that QRF performs favorably compared to sediment rating curves and generalized linear models (Francke et al., 2008a) and that performance of random forest (which QRF is based on) was superior to support-vector machines and artificial neural networks (Al-Mukhtar, 2019) in modeling suspended sediment concentrations. Importantly, as an advantage to other ML approaches, QRF allows us to quantify the model uncertainty by estimating prediction accuracy (Francke et al., 2008a; Al-Mukhtar, 2019).

Thus, the first objective of this study was to extensively test QRF as an approach for estimating past suspended sediment dynamics at decadal scales in high-alpine areas. Previous studies have included proxies for drivers of sediment transport and erosive processes, e.g., precipitation, discharge, seasonality and antecedent conditions (Francke et al., 2008a, b; Zimmermann et al., 2012). We built on this setup and adapted it by including air temperature as a predictor, since many processes relevant to sediment dynamics in high-alpine areas are temperature-sensitive (e.g., snowmelt and glacier melt, thawing of topsoil). To assess model performance, we evaluated several validations and compared the results to sediment rating curves based on data from the two gauges 'Vent Rofenache' and 'Vernagt' that are located in a nested catchment setup in the Rofental, within the upper Ötztal in Tyrol Austria. This nested setup provides a favorable opportunity to test the QRF model and gives a good overview of sediment dynamics in this catchment.

The second objective of this study is to examine the resulting estimates of annual suspended sediment yields with respect to changes at decadal scales. Thus, we analyzed the time series for trends, some of which could be expected, e.g., due to ongoing temperature increase. However, the possibility of sudden, tipping-point-like shifts in response to climatic changes has been suggested for cryospheric geomorphic systems as well (Huggel et al., 2012), and sediment dynamics especially (Vercruysse et al., 2017) and indeed step-like increases in suspended sediment concentrations have been observed in other catchments (Costa et al., 2018b; Li et al., 2020, 2021b; Zhang et al., 2021). Hence, we used change point detection methods to assess whether the detected trends are gradual or follow a step-like pattern. We extended these analyses to the predictors (temperature, discharge and precipitation) and annual mass balances to assess possible reasons for changes in suspended sediment yields.

3.2 STUDY AREA

The study area is located in the 'Rofental', a valley in the upper Ötztal in the Tyrolean Alps, Austria. For more than 100 years, the area has been subject to intense glaciological and hydrometeorological research, yielding outstanding datasets (Strasser et al., 2018). The entire catchment is 98.1 km² upstream from gauge 'Vent Rofenache' (hereafter 'Vent'), and nested within is the 11.4 km² catchment upstream from gauge 'Vernagt' (see Figure 3.1). Gauge Vent is run by the Hydrographic Service of Tyrol and gauge Vernagt by the Bavarian Academy of Sciences and Humanities. The catchments' elevations range from 1891 m a.s.l. at gauge Vent and 2635 m at gauge Vernagt to the summit of Wildspitze, the highest peak in Tyrol, at 3772 m.

The study area's shielded location in the inner Alpine region leads to the relatively warm and dry climate (Kuhn et al., 1982). Mean annual temperature and precipitation at the gauge in Vent are 2.5°C and about 660 mm (Hanzer et al., 2018; Hydrographic yearbook of Austria, 2016; Strasser et al., 2018), but a considerable precipitation gradient with elevation of about 5 % per 100 m has been described (Schöber et al., 2014).

Both catchments are heavily glacierized, with approximately 28 % and 64 % glacier cover in 2015 (Buckel and Otto, 2018). The two largest glaciers within the Vent catchment, Vernagtferner and Hintereisferner, have been systematically observed since the 1950s and 1960s and have shown accelerating retreat since the beginning of the 1980s (Abermann et al., 2009), which is expected to continue in the future (Hanzer et al., 2018).

The catchment is drained by the river Rofenache, which flows into the Ötztaler Ache, one of the largest tributaries to the river Inn. The hydrological regime (glacial to nival) shows a pronounced seasonality as most of the discharge is fed by snowmelt and glacier melt and about 89 % of the discharge in Vent occurs from April to September (Schmidt et al., 2022b; Hanzer et al., 2018).

The Ötztal Alps are part of the Ötztal–Stubai massif within the crystalline central-eastern Alps, and the catchment geology is dominated by biotite–plagioclase, biotite and muscovite gneisses, variable mica schists and gneissic schists (Strasser et al., 2018). The land cover of higher elevations is dominated by glaciers, bare rock or sparsely vegetated terrain, whereas mountain pastures and coniferous forests are present at lower altitudes.

Suspended sediment concentrations at the gauge in Vent proved to be the highest in an Austria-wide comparison (Lalk et al., 2014), and annual suspended sediment yields are about 1500 t km^{-2} on average (Schmidt et al., 2022b). Suspended sediment dynamics showed an even more pronounced seasonality compared to discharge, as 99 % of the annual suspended sediment yields are transported from April to September (ibid.).

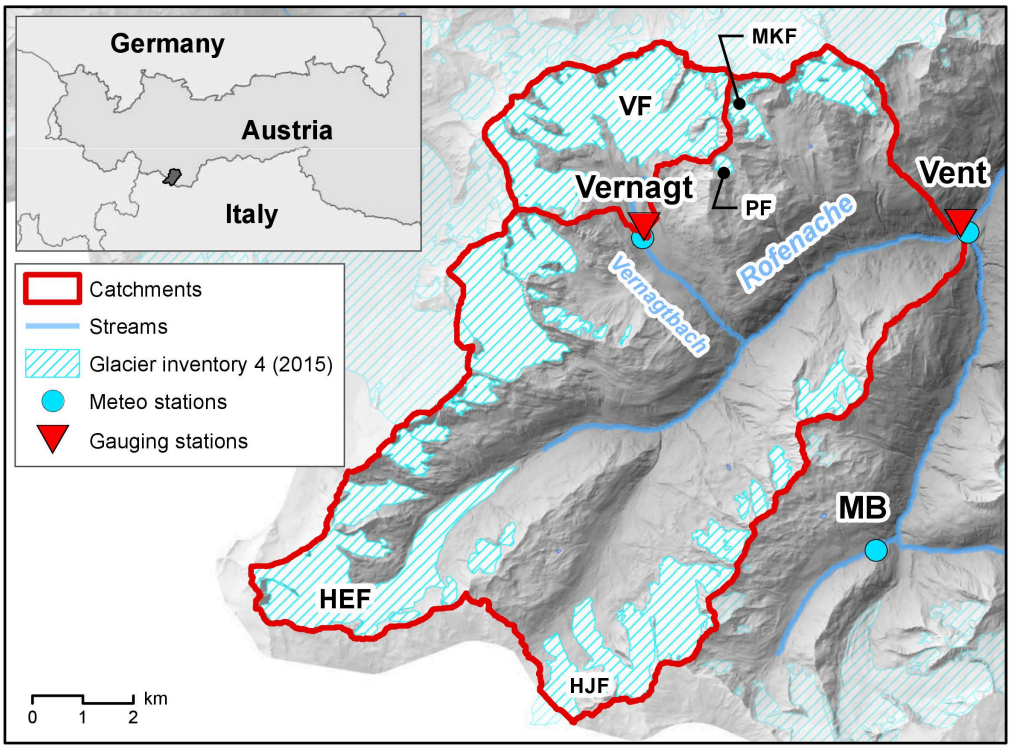

Figure 3.1. *Map of the catchment area upstream gauge Vent, and nested within the Vernagt catchment, with glaciers Vernagtferner (VF) and Hintereisferner (HEF) as well as the measurement station Martin-Busch-Hütte (MB). Smaller glaciers Hochjochferner, Platteiferner and Mitterkarferner are denoted by HJF, PF and MKF, respectively. Sources: 10 m DTM of Tyrol (Land Tirol, 2016), glacier inventory 4 (2015) (Buckel and Otto, 2018), and rivers from tiris open government data (Land Tirol, 2021).*

3.3 METHODS

In essence, we trained a nonparametric model on suspended sediment concentrations and predictors (discharge, temperature, precipitation) and then used this model and long-term records of the predictors to reconstruct past suspended sediment concentrations (SSCs) and derive annual suspended sediment yields. We then analyzed the resulting time series with respect to trends and change points.

In the following section, we briefly describe the general modeling approach and the validations, the QRF approach and its predictors, the input data and their preparation for the model as well as the statistical tools used for analyzing the results.

In our analyses, we focus on (annual) suspended sediment yields instead of concentrations, due to the strong seasonality in discharge (Schmidt et al., 2022b). This gives more weight to days with higher discharge, which are more influential for overall sediment export to downstream areas and the potential resulting problems, as opposed to, e.g., mean annual SSCs, which weigh days at the beginning and end of the season, with low discharge and low

concentrations, and days during the glacier melt period equally. We use the term 'reconstructing' to describe the estimates of SSCs (or the resulting yields) from our model predictions.

3.3.1 GENERAL MODELING APPROACH AND ADAPTATIONS TO CONDITIONS AT THE TWO GAUGES

We combined the analysis of the two gauges Vent and Vernagt to gain a more reliable and comprehensive understanding of past sediment dynamics in the Rofental from their distinct data context.

At gauge Vent, continuous turbidity-derived SSC time series have been recorded at high temporal resolution (15 min) since 2006, providing abundant training data for our model. Additionally, the long-term predictor data are available back until 1967, facilitating insights into long-term changes in catchment dynamics - yet only at daily resolution, which predetermines the temporal resolution of the reconstruction model. This is challenging as sediment concentrations vary considerably during 1 d, leaving us with the need to assess whether a daily model adequately represents sediment dynamics.

At gauge Vernagt, the availability of hourly discharge (Q), precipitation (P) and temperature (T) data back until 1974 is remarkable. However, turbidity-derived SSC data have only been recorded for the years 2000, 2001, 2019 and 2020 (see Figure 3.2, upper panel 'Vernagt', left-hand side, plots labeled 'SSC'). Additionally, the data in 2019 and 2020 are affected by episodic siltation and periods when the turbidity sensor reached saturation: 0.47 % of the two summers of data were affected by saturation, and about 8 % were affected by siltation. The latter was mainly due to one period of about 16 d in August 2019. Additionally, there were three shorter incidents (1.5 h to 1.5 d), two in 2019 and one in 2020. These issues first need to be dealt with in order to provide accurate training data for our model, as it is sensitive to the range of values represented in the training data (Francke et al., 2008a). However, the 16-year gap between the measurement periods provides the rare opportunity to verify the model's skill in estimating past SSCs against real measurement data.

To address these issues and benefit from these opportunities, we preformed three preparatory steps before the final reconstruction models (Figure 3.2).

Gap-filling model: at gauge Vernagt, we trained a model on SSCs determined from 131 water samples and the predictors (Q, P, T) at the highest possible (i.e., 10 min) resolution (Figure 3.2, upper panel). We used the resulting modeled SSC to replace periods in the 2019/2020 SSC data that were affected by siltation or sensor saturation. As the sampling scheme was customized to cover hydro-sedimentological conditions as widely as possible (see

Schmidt et al., 2022b), the water samples also partially cover the periods to be addressed by the gap filling.

Validation A - temporal resolution: we ran models at both hourly and daily resolution on all available training data at gauge Vernagt to assess the error magnitude due to the coarser temporal resolution in the final reconstruction models.

Validation B – extrapolation: we trained a model on the corrected Vernagt SSC data of 2019 and 2020 at daily resolution and estimated SSC back until 2000 for validation against the 2000-2001 measurement data (Figure 3.2, center).

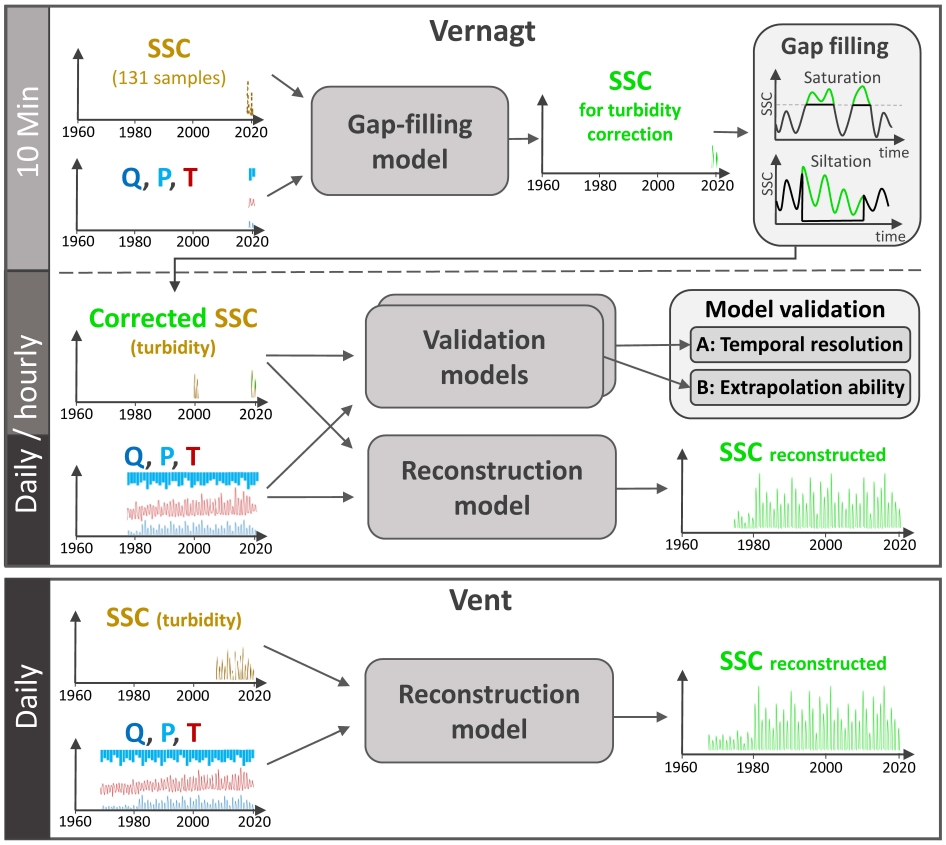

Figure 3.2. *Overview of the modeling approach. SSC: suspended sediment concentration; Q: discharge; P: precipitation; T: temperature.*

Finally, we ran the 'reconstruction models' at daily resolution (for consistency between the two gauges), taking into account all available training data to estimate SSC back until 1967 and 1975, respectively.

Beyond Validations A and B, we assessed whether and how often the ranges of the predictors in the training data were exceeded during the reconstruction period, since it is a known limitation of QRF that it is not possible to extrapolate beyond the range of values represented in the training data (Francke et al., 2008a). For example, if the discharge measured

on a day in the reconstruction period exceeds the maximum discharge within the training period ($Q_{train,\ max}$), the model potentially underestimates SSCs on that day.

Additionally, we compared QRF performance to the performance of sediment rating curves, one of the most commonly used approaches to estimate suspended sediment concentrations (Vercruysse et al., 2017), by fitting a power function between SSC and Q of the form $SSC = a \cdot Q^b$, where a and b are regression coefficients.

3.3.2 QRF FOR MODELING SUSPENDED SEDIMENT CONCENTRATIONS

To reproduce suspended sediment dynamics, the desired models have to account for a multitude of processes controlling SSCs (discharge dynamics, temperature-dependent activation of sediment sources and transport processes, precipitation, antecedent wetness conditions, etc.), need to deal with non-normal distributions of both predictor and response variables and have to handle correlations between the predictors (Zimmermann et al., 2012).

QRF (Meinshausen, 2006) represents a multivariate approach that can deal with nonlinearity, interactions and nonadditive behavior without making assumptions about underlying distributions. QRF performed favorably in reproducing sediment dynamics as compared to generalized linear models or sediment rating curves (Francke et al., 2008a). QRF is a generalization of random forest (RF) regression tree ensembles (Breiman, 2001). Regression trees (a.k.a. classification and regression trees – CARTs) (Breiman et al., 1984) apply recursive rule-based data partitioning in order to group data with similar values of the response variable (Francke et al., 2008a). To produce a 'forest', RF and QRF employ an ensemble of these trees, each one grown on a random subset (bootstrap sample) of the training data. Predictive performance is evaluated on those parts of the data that are not considered in the bootstrap sample, i.e., the out-of-bag data (OOB) (ibid.). Model predictions are then obtained from the mean of predictions of each single tree (RF) or are based on the distribution of these single-tree predictions (QRF). As QRF keeps the value of all observations within a node, it enables the quantification of the model uncertainty with the help of these inherent ensemble characteristics. This represents an advantage over other nonparametric approaches applied to SSC modeling, such as traditional fuzzy logic or artificial neural networks (ibid.).

Building on the developed model setup (Francke et al., 2008b; Francke, 2017; Zimmermann et al., 2012), we chose the predictors to represent proxies for processes important to sediment dynamics in high-alpine areas. For example, discharge is crucial for sediment transfer and, potentially, channel erosion, while precipitation drives hillslope erosion and mass wasting events. We extended the set of primary predictors by adding air temperature, as many processes determining sediment dynamics in high-alpine areas are temperature-sensitive (e.g., the activation of sediment sources, such as the occurrence of rain vs. snow, the availability of subglacial and proglacial sediments and their transport through glacier melt

waters, but also potential permafrost thaw). From these three primary predictors (discharge, precipitation and temperature, QPT), we derived information on antecedent conditions for each time step by computing ancillary predictors derived thereof. These ancillary predictors can capture that, e.g., longer-term discharge behavior is linked to potential exhaustion of sediment sources or storage, prolonged warm periods may lead to increased glacier ablation associated with intensified transport of glacial sediment, and high antecedent moisture conditions prior to a precipitation event may favor mass movements. To keep correlation between these derived predictors as low as possible, we used non-overlapping windows of increasing sizes (e.g., 24 h, 24 – 72 h, 72 h to 7 d and 7 d to 20 d ahead of each time step) to compute sums of the primary predictors (Zimmermann et al., 2012). To complete the set of predictors, we used the day of year to capture the pronounced seasonality in high-alpine sediment dynamics (Schmidt et al., 2022b) and the rate of change in discharge (see also Francke et al., 2008b; Zimmermann et al., 2012).

Further, we tuned the model with respect to the length of the antecedent periods considered: we optimized the length of the time windows for the highest model performance with respect to daily or hourly SSCs using the Nash–Sutcliffe efficiency index (see section 3.3.4.1). Besides the length of the antecedent periods, the two most important hyperparameters for QRF are the number of trees in a "forest" and the number of selected predictors at each node, implemented as parameter 'mtry' in R. To increase robustness, we set the number of trees to 1000, which is twice the default value. The parameter 'mtry' is optimized for maximum performance in the modeling process. Additionally, we optimized model performance in a cross-validation with five folds, as is commonly done (Murphy, 2012). However, unlike cross-validation approaches in the classical sense, which randomly pick a set of individual data points, we divided the training data into five equal temporally contiguous chunks to avoid unrealistically good performance simply due to autocorrelation of temporally close points in time. Finally, in the 'reconstruction model', we derived annual suspended sediment yields by performing 250 Monte Carlo realizations of the annual SSY for each year, which allows for assessing the prediction uncertainty, from which the mean and quartiles of annual suspended sediment yields were computed. We chose 250 Monte-Carlo realizations as this yields sufficiently robust estimates of the mean annual SSY (the confidence intervals of the mean are ca. ± 1.25 % of the mean) while keeping computation times reasonable.

3.3.3 CHARACTERISTICS, SOURCES AND ADJUSTMENTS OF INPUT DATA

Here we describe the input data and their preparation for modeling. An overview of details such as coordinates of stations and gauges, the temporal resolution of the different time series, their sources and data availability can be found in Table 3.A1 in the appendix.

3.3.3.1 DISCHARGE DATA, PRECIPITATION AND TEMPERATURE DATA

Gauge Vent has been operated continuously by the Hydrographic Service of Tyrol since 1967 (Strasser et al., 2018) and discharge has been measured at 15 minute resolution through water stage recordings, complemented by a radar probe since 2000. At gauge Vernagt, discharge has been recorded since 1974 (Bergmann and Reinwarth, 1977) and is determined through water stage recordings and tracer-calibrated stage–discharge relations. Additionally, this is complemented by ultrasonic stage measurements, providing nearly uninterrupted discharge series since 1974 (Braun et al., 2007). The temporal resolutions of the discharge time series at both gauges vary over time (from five and ten to 60 minutes; for details, see Table 3.A1 in the appendix).

Precipitation and temperature have been recorded close to the gauge in Vent (see Figure 3.1) since 1935 and are available at daily resolution. Both time series showed gaps, which creates a problem when using the chosen QRF approach. Thus, to fill the gaps in the precipitation time series, we used data recorded at gauge Vernagt: we derived a linear model between all days when daily precipitation sums were available from both stations and used the resulting linear model for conversion (i.e., $P_{Vent} = P_{Vernagt}/1.3$). Likewise, temperature data recorded at Martin-Busch-Hütte (see Figure 3.1) were aggregated to daily means and used to fill gaps in the temperature time series ($T_{Vent} = T_{MB} \cdot 2.8089$). As a result, 2 % of the precipitation and 0.25 % of the temperature time series were filled (see Figure 3.A1 in the appendix).

At gauge Vernagt, precipitation and temperature have been recorded at high temporal resolution (5 to 60 min; for details, see Table 3.A1 in the appendix) next to the gauge since 1974. To fill the present gaps, we used data recorded by the Hydrographic Service since 2010 in close proximity to the Vernagt station. As some gaps still remained, we subsequently used data recorded at Martin-Busch-Hütte (conversion factors: $Temp_{Vernagt} = -0.002536 \cdot Temp_{MB}^2 + 0.9196 \cdot Temp_{MB} - 0.474$; $Precip_{Vernagt} = 0.895 \cdot Precip_{MB}$). With this, 12 % of the precipitation time series and 9 % of the temperature time series were filled, although many of these filled gaps occur during the winter months, when the discontinued discharge data inhibit QRF modeling anyway (see Figure 3.A1 in the appendix). Some gaps still remain, but these, too, are mostly restricted to winters. We excluded the data from 1974 from the analyses at gauge Vernagt, as data were not available for the entire year.

3.3.3.2 TURBIDITY AND SUSPENDED SEDIMENT CONCENTRATION DATA

At gauge Vent, turbidity has been measured since 2006 using two optical infrared turbidity sensors (Solitax ts-line and Solitax hs-line by Hach). To calibrate the turbidity measurements to SSCs, water samples are taken manually from the stream close to the turbidity sensors

frequently (Lalk et al., 2014). Turbidity measurements are paused every winter (between October and April) to avoid damage to the equipment. However, the equipment is reinstalled early enough to capture the spring rise in concentrations, and winter sediment transport can be considered negligible (Schmidt et al., 2022b).

At gauge Vernagt, water is diverted into a measuring chamber (Bergmann and Reinwarth, 1977), where turbidity can be recorded while avoiding damage to the equipment by large rocks in the main channel. Turbidity was recorded in the summers of 2000 and 2001 (Staiger-Mohilo STAMOSENS 7745 UNIT) (Naeser, 2002) and 2019 and 2020 (Campbell OBS501). Water samples for calibration of turbidity to SSC were taken directly next to the turbidity sensor by hand in 2000 and 2001 (57 samples) and by means of an automatic sampler (ISCO 6712) in 2019 and 2020 (131 samples). The latter initiated sampling if one of two criteria was met: (i) regular sampling to avoid long gaps between two samples or (ii) threshold-based sampling to obtain samples across the whole range of possible turbidity values. Gravimetric sediment concentrations SSC_g were then determined in the laboratory and used to convert turbidity to SSC (2000–2001: SSC (in g L^{-1}) = 0.1583 · turbidity (in V) $^{-13.0877}$ (Naeser, 2002); 2019–20: SSC (in g L^{-1}) = 0.00212 · turbidity (in FNU)).

3.3.3.3 AGGREGATION/DISAGGREGATION TO DIFFERENT TEMPORAL RESOLUTIONS

As temporal resolutions varied between the different time series, we aggregated or disaggregated the data to achieve homogenous temporal resolutions for the respective QRF models at daily, hourly and 10 min resolution. Data at 10 min resolution were only needed for the gap-filling model at gauge Vernagt. For this, we had to disaggregate precipitation and temperature data from 60 min resolution in 2000 and 2001 by dividing hourly precipitation sums by 6 and replicating mean hourly temperature values for the six corresponding 10 min time steps.

For the analysis of annual Q, P and T, we summed up daily discharge volumes as derived from daily mean discharge (Q_{sum} (in m^3 d^{-1}) = 60 · 60 · 24 · Q_{mean} (in m^3 s^{-1})), added up daily precipitation sums and computed annual averages of daily mean temperature. At gauge Vernagt, we only considered data between 1 May and 30 September of each year due to inconsistent gaps in winter temperature and precipitation measurements.

3.3.4 ANALYSIS OF THE RESULTS

3.3.4.1 UNITS, CONVERSIONS AND PERFORMANCE MEASURES

From SSCs (modeled and from turbidity) and discharge (Q), we calculated sediment discharge Q_{sed} (in mass/time) (for analyses at high temporal resolution), daily Q-weighted SSC averages SSC_{daily} (in kg m^{-3}) (i.e., the total daily sediment discharge $\Delta t \cdot \Sigma Q_{sed}$ divided by the daily discharge volume $\Delta t \cdot \Sigma Q$; this assigns more weight to time steps with higher discharge, which are more influential for sediment export), annual SSYs (in t a^{-1}) and specific annual sSSY (in t km^{-2} a^{-1}) (for comparability among the gauges) as follows:

$$Q_{sed}(t) = SSC(t) \cdot Q(t), \quad (1)$$

where Q is discharge (in m^3 s^{-1}),

$$SSC_{daily} = \frac{\Delta t \cdot \sum Q_{sed}(t)}{\Delta t \cdot \sum Q(t)}, \quad (2)$$

where Δt is the corresponding temporal resolution (in s) and Σ sums over all time steps of the day,

$$annual\ SSY = \Delta t \cdot \sum Q_{sed}(t)\ , \text{and} \quad (3)$$

$$annual\ sSSY = \frac{annual\ SSY}{A}, \quad (4)$$

and where A (in km²) is the catchment area and Σ sums over all timesteps of the year.

To quantify model performance, and for our validation, we used the Nash–Sutcliffe efficiency (NSE) index:

$$NSE = 1 - \frac{\sum_{i=1}^{n}[SSC_{obs}(i) - SSC_{mod}(i)]^2}{\sum_{i=1}^{n}[SSC_{obs}(i) - \overline{SSC_{obs}}]^2}, \quad (5)$$

where "obs" and "mod" refer to observed and modeled SSC values and $\overline{SSC_{obs}}$ is the mean of observed SSC values (Zimmermann et al., 2012, based on Nash and Sutcliffe, 1970). The NSE is dimensionless and ranges from -∞ to 1, and a model with a NSE over 0.5 can be considered accurate (Moriasi et al., 2007; Mather and Johnson, 2014). However, sediment export in the study area is highly seasonal (see also Schmidt et al., 2022b), so that the NSE might be misleading, as models reproducing seasonality but failing to reproduce smaller

fluctuations can still report a good NSE value (Schaefli and Gupta, 2007). Thus, we additionally computed the normalized benchmark efficiency (BE) as follows:

$$BE = 1 - \frac{\sum_{i=1}^{n}[SSC_{obs}(i) - SSC_{mod}(i)]^2}{\sum_{i=1}^{n}[SSC_{obs}(i) - SSC_{bench}(i)]^2}, \quad (6)$$

where SSCbench refers to the benchmark model suspended sediment concentration at time step i. Commonly, this benchmark model is the mean of the observations for every Julian day over all years within *n* (i.e., the mean annual cycle) (see, e.g., Pilz et al., 2019). However, this is heavily influenced by individual events in our case, so we used the 60 d moving average of the mean SSC for every Julian day instead. As for the NSE, a BE value of 1 corresponds to perfect agreement of simulation to measurements, and a model with BE > 0 is able to reproduce dynamics better than simply using statistics (Pilz et al., 2019).

3.3.4.2 METHODS FOR TREND ANALYSIS AND CHANGE POINT DETECTION

In order to quantify time series behavior, we generally followed the approach of first analyzing for the existence of a trend. If a trend was detected, we assessed whether the trend was homogenous by analyzing for change points. If a change point was identified, we then examined the resulting segments of the time series for trends.

Most of the investigated time series are not normally distributed, and some show autocorrelation. Thus, to calculate trend significance, we used the nonparametric Mann–Kendall test for linear trend detection in a version that was modified to detect trends in serially correlated time series (Yue and Wang, 2004) as recommended by Madsen et al. (2014). To estimate trend magnitude, we used Sen's slope estimator (Sen, 1968). Both methods are implemented in the mkTrend function of the R package "FUME" (Santander Meteorology Group, 2012). In our results, we only plot and refer to trends that were significant at least at a significance level $\alpha = 0.05$ after correction for autocorrelation.

For change point (CP) detection, we used the nonparametric Pettitt test (Pettitt, 1979), which is commonly used as it is a powerful rank-based test for a change in the median of a time series and is robust to changes in distributional form (Yue et al., 2012), as implemented in the R package 'trend' (Pohlert, 2020). However, it only gives one change point location without uncertainty quantification around its location and was shown to be sensitive to the position of the change point within the time series; i.e., detection at the beginning and end of the series is unlikely (Mallakpour and Villarini, 2016).

Thus, as a complementary advanced approach that counterbalances the weaknesses of Pettitt's test, we used Bayesian regression with change points as implemented in the R package "mcp" (which stands for "multiple change points"; hereafter we refer to this method as "MCP") (Lindeløv, 2020). This represents a much more flexible approach which allows

us to assess uncertainty through the resulting posterior distributions of the change point location and is applied in an increasing number of studies in different fields of research (e.g., Veh et al., 2022; Yadav et al., 2021; Pilla and Williamson, 2022). Although MCP allows us to detect multiple change points, we only considered one change point as we aimed to detect the largest shift in the time series and to ensure comparability with Pettitt's test. Unless specified otherwise, we used the uninformative default prior, allowed free slope estimation before and after the change point, assumed a disjoined slope (i.e., step-like change) at the change point and allowed for changes in variance at the change point.

As mentioned earlier, we computed 250 Monte Carlo realizations of the annual SSY as a result of the QRF model. We propagated this uncertainty by applying the trend and change point detection methods not only to the mean estimates but also to the 250 resulting time series realizations.

All calculations were done in R version 4.2.1 (R Core Team, 2018).

3.4 RESULTS PART I – MODEL EVALUATION

3.4.1 VALIDATION A: INFLUENCE OF THE REDUCTION OF TEMPORAL RESOLUTION

The temporal resolution for long-term reconstruction is limited to daily, as the respective long-term predictor data are available only at daily resolution at gauge Vent. As a result, we can expect some loss of information, e.g. on short-term precipitation intensity, which can be crucial for sediment dynamics. To assess the error magnitude, we ran two variants of the models at gauge Vernagt, at daily and hourly resolution based on all available training data (i.e. 2000, 2001, 2019 and 2020). We then compared daily sediment discharge (Q_{sed}) calculated from the OOB model estimates to Q_{sed} calculated from measured turbidity (Figure 3.3a). It is important to stress that OOB estimates of any given day represent model predictions of only those regression trees where the particular day was not part of the training data. Both models reproduced daily Q_{sed} very well, where the daily model showed a larger scatter, which is also reflected in the slightly lower NSE and BE. The comparison of annual sSSY (Figure 3.3b) showed very similar estimates in most years. To rule out that model performances were strongly influenced by discharge (which is both a predictor in the model and is used to calculate Q_{sed}), we also compared hourly and daily out-of-bag SSC instead of Q_{sed}. However, the resulting NSEs of 0.97 and 0.82 and BEs of 0.95 and 0.73 for the hourly and daily models, respectively, still represent very good model performance in general and show that the loss of model skill between the two models because of different temporal resolutions is acceptable. Thus, we used the daily-resolution models at both gauges in the following analyses for better comparability and applicability to the full length of the available time series.

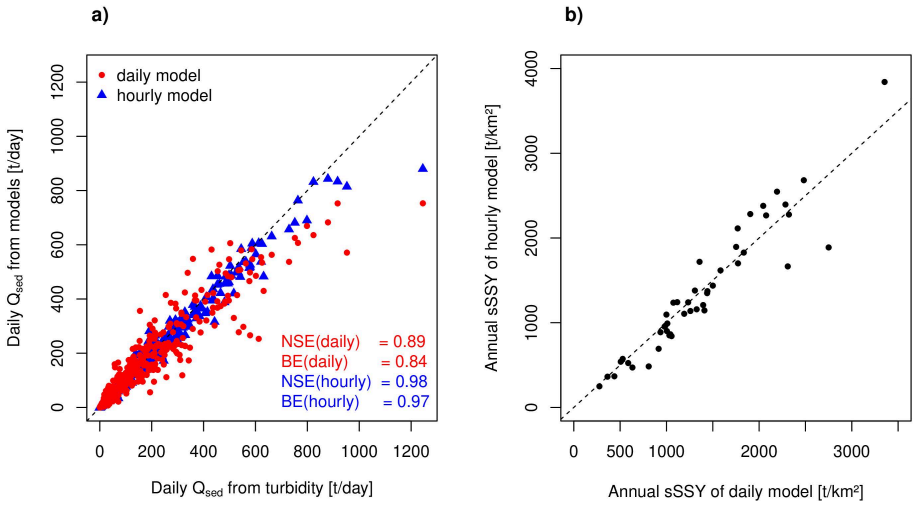

Figure 3.3. *(a) Daily Qsed calculated from out-of-bag prediction of daily and hourly models vs. Qsed calculated from turbidity at gauge Vernagt. (b) Comparison of mean annual sSSY estimates of the daily and hourly models at gauge Vernagt. NSE: Nash–Sutcliffe efficiency; BE: benchmark efficiency. Dashed lines indicate a ratio of 1:1.*

3.4.2 VALIDATION B: CAPABILITY OF TEMPORAL EXTRAPOLATION

To evaluate the capability of the QRF models to reconstruct past sediment dynamics, we trained a daily model on the 2019-2020 (n = 212) data at gauge Vernagt and used the data of 2000-2001 (n = 367) for validation. The comparison of Q_{sed} determined from turbidity to modeled Q_{sed} showed that the model underestimates high daily Q_{sed} (Figure 3.4a). Nevertheless, the NSE of 0.73 and BE of 0.66 are indicative of a good representation of sediment dynamics at daily resolution. Comparing mean daily measured and modeled SSC instead of Q_{sed}, the NSE of 0.51 and BE of 0.33 still represent a satisfactory model performance (Moriasi et al., 2007; Pilz et al., 2019). Conversely, when training the model on the data from 2000 and 2001 and estimating Q_{sed} (and SSC) for 2019 and 2020, performance was slightly lower, with an NSE of 0.6 (0.45) and BE of 0.38 (0.15) (Figure 3.4a).

In the 'validation model' results, annual yields were affected by overestimation in late August 2000 and underestimation in July 2001 (Figure 3.4b). As a result, the mean annual sSSY estimates were 31 % higher and 16 % lower than observed annual sSSY in 2000 and 2001, respectively. Considering the spread of the model results (i.e., the 2.5 and 97.5 percentiles of the 250 model predictions as depicted by the whiskers in Figure 3.4b, which were chosen as they are more robust than the extremes while covering 95 % of the estimates), 19 % overestimation compared to the maximum model estimate in 2000 and 4 % underestimation compared to the minimum model estimate in 2001 remained. Unfortunately, annual yields of the validation model trained on the 2000-2001 data cannot be compared in the same way, since observations show gaps in both 2019 and 2020 (see also the caption of Figure 3.4a).

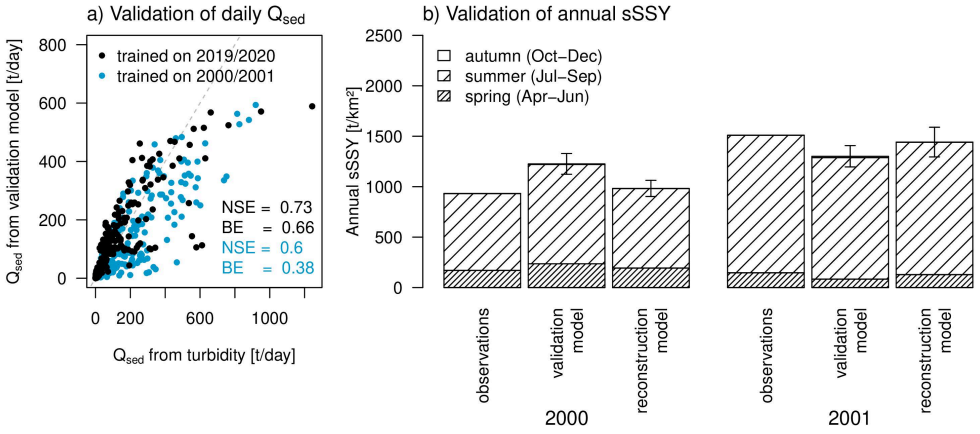

Figure 3.4. *(**a**) Daily Q_{sed} estimates from QRF validation models vs. Q_{sed} from turbidity at gauge Vernagt. (**b**) Annual sSSY based on turbidity observations, estimates of the validation model (without 2000-2001 data) and estimates of the reconstruction model (all training data) in 2000 (left) and 2001 (right). This comparison was not possible for 2019 and 2020, since observation data are missing in May - July 2019 and May - June 2020. Boxes depict mean model estimates and whiskers depict the 2.5 and 97.5 percentiles of model predictions. NSE: Nash–Sutcliffe efficiency; BE: benchmark efficiency.*

At gauge Vent, more years of data were available, so that the results of the five-fold cross-validation provided a more detailed picture of the temporal extrapolation ability (Table 3.1). Some cross-validation periods showed rather low NSE values, which indicates that they are harder to predict with only the remaining training data, and therefore contain more valuable data for training the full QRF model. For example, the period 2012 to 2014 with the lowest NSE contains the most extreme event in August 2014, which was likely linked to mass movements (Schmidt et al., 2022b). Similarly, the period 2018 to 2020 also shows a low NSE and a mass-movement event was observed in 2020 (ibid.). Including such periods in the training data apparently is of importance to the fidelity of the model. Conversely, the same cross-validation with a sediment rating curve shows that QRF performance is much better, especially in those periods that are harder to predict. Consequently, QRF clearly excels over the traditional approach (see also section 3.4.4).

Table 3.1. *Results of the five-fold cross-validation at gauge Vent for QRF and SRCs, with respect to mean daily SSC compared to turbidity measurements, expressed as Nash–Sutcliff efficiency (NSE) of the model estimates for each one-fifth of the time series in the cross-validation (with corresponding years in parentheses) and the full models (OOB: out-of-bag in the case of QRF).*

	NSE (OOB) full	**NSE (2006–2008)**	**NSE (2009–2011)**	**NSE (2012–2014)**	**NSE (2015–2017)**	**NSE (2018–2020)**
QRF	0.6	0.48	0.55	0.21	0.69	0.39
SRC	0.41	0.41	0.33	0.09	0.61	-0.055

3.4.3 EXCEEDANCES OF PREDICTOR RANGES IN THE PAST

At gauge Vent, the maximum temperature of the training period ($T_{train,\ max}$) was not exceeded during the reconstruction period. The maximum discharge of the training period ($Q_{train,\ max}$) was overstepped on 4 d in 1987, and precipitation within the reconstruction period was larger than the maximum precipitation during the training period ($P_{train,\ max}$) on 3 d within the reconstruction period.

At gauge Vernagt, $Q_{train,\ max}$ was exceeded six times in the reconstruction period, and four of these days occurred in 2003. There was one day at gauge Vernagt, where $T_{train,\ max}$ was exceeded in 2017. $P_{train,\ max}$ was exceeded on 5 d within the reconstruction period; however on two of these days, the temperature was below zero and discharge was very low, so we considered these days negligible for annual sediment export.

There were also days at both gauges when discharge was lower than the minimum discharge measured during the training period ($Q_{train,\ min}$). Yet all of these days were in April, May or October, when SSCs are very low, and as very low discharge also translates to very low transport capacities, we considered the error negligible for annual sediment yields.

3.4.4 PERFORMANCE OF THE RECONSTRUCTION MODELS

To test the performance of the reconstruction models, we compared out-of-bag SSC estimates of the reconstruction models and SSC estimates of sediment rating curves (trained on all available data) to turbidity measurements at both gauges (Figure 3.5).

QRF performance is superior to sediment rating curves (SRCs) at both gauges with respect to mean daily SSCs: as can be seen in Figure 3.5 and the NSE and BE values, SRCs are generally less capable of capturing the variability in the training data. The NSE and BE values of the QRF model represent a satisfactory performance at gauge Vent and very good performance at gauge Vernagt (Moriasi et al., 2007). Considering mean annual SSCs at gauge Vent, QRF performs much better than SRCs. At gauge Vernagt, QRF performs very well and slightly better than SRCs, but there are only four years available for comparison, which confines the representativity of this analysis.

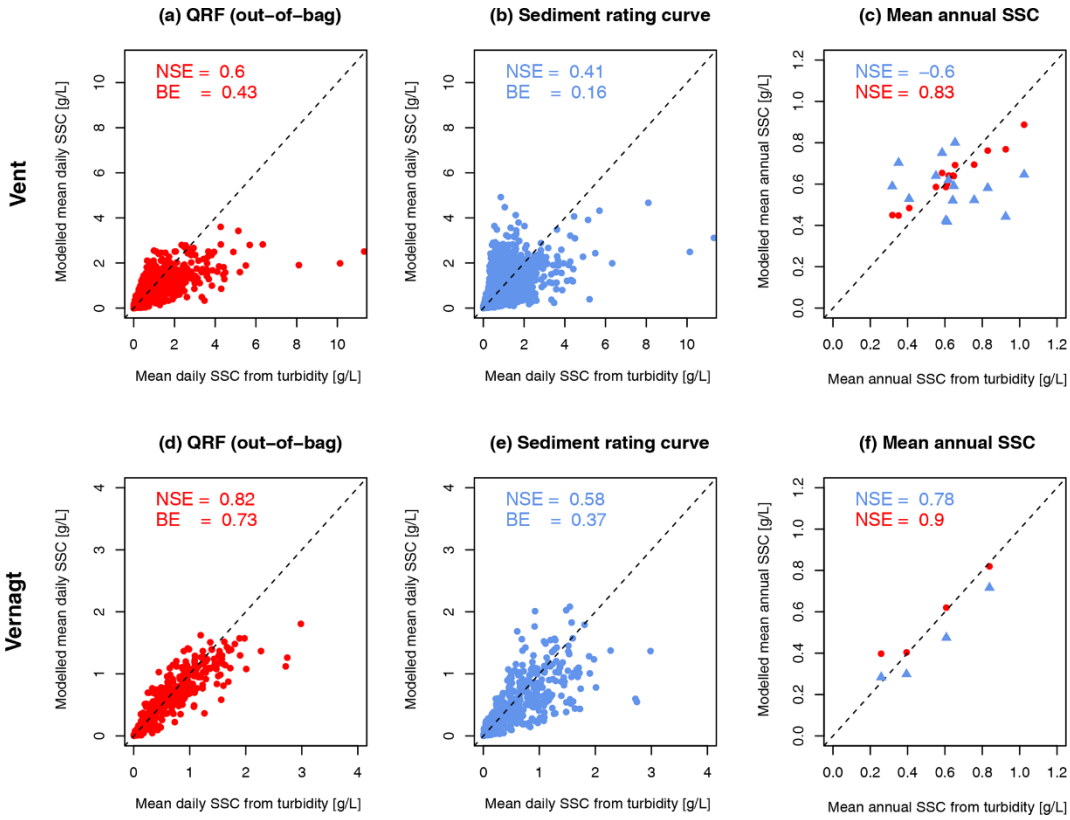

Figure 3.5. *Measured versus modeled sediment concentration and yield using QRF (OOB estimates, red) and SRC (blue). (**a, b, c**) Gauge Vent; (**d, e, f**) gauge Vernagt; (**a, d**) QRF, daily values; (**b, e**) SRC, daily values, (**c, f**) QRF and SRC, annual values. NSE: Nash– Sutcliffe efficiency; BE: benchmark efficiency.*

Performance with respect to Q_{sed} is slightly better for both models as compared to SSC. SRC estimates yield values for NSE of 0.73 and BE of 0.61 at gauge Vernagt and NSE of 0.49, and BE of 0.35 at gauge Vent. Still, QRF performance is superior (NSE of 0.89 and BE of 0.84 at gauge Vernagt and NSE of 0.64 and BE of 0.54 at gauge Vent). For both models, performance is better at gauge Vernagt than at gauge Vent.

Rare days with extremely high SSC (and Q_{sed} above ca. 7000 t d^{-1}) are systematically underestimated by both models. However, it is important to emphasize that Figure 3.5 shows OOB predictions, i.e., the QRF model predictions for these 'extreme' days if the particular day in question is not part of the training data. To quantify the effect of this underestimation of daily Q_{sed} on annual SSY for the QRF model, we calculated the difference between measured and estimated daily Q_{sed} (OOB) for the 10 d with the highest Q_{sed} in the turbidity time series at both gauges. The differences correspond to 0.6 to 2.8 % of the annual SSY at gauge Vernagt and 1.7 to 19.1 % of the annual SSY at gauge Vent. However, the 19.1 % underestimation is attributable to the most extreme event in the time series, where 26 % of the annual SSYs were exported within 25 h in August 2014, likely in association with a mass-movement event (see Schmidt et al., 2022b). The full model estimate of the 'reconstruction model' (i.e. not OOB estimates) for this day shows an underestimation of only 6 %.

3.5 RESULTS PART II: ANALYSIS OF ESTIMATED ANNUAL SSSYS, PREDICTORS AND MASS BALANCES

3.5.1 ANNUAL SSSYS AND THEIR DEVELOPMENT OVER TIME

In the resulting time series, the average sSSY of all years (± 1 standard deviation) is 1401 (± 453) t km^{-2} a^{-1} at gauge Vent and 1383 (± 668) t km^{-2} a^{-1} at gauge Vernagt. This indicates overall similar magnitudes of sediment export per catchment area but with much higher variability at gauge Vernagt. To assess how suspended sediment dynamics changed over time, we analyzed the time series of annual sSSYs at the two gauges for trends and change points.

At both gauges, mean modeled annual sSSYs show significant positive trends (Figure 3.6). In Vent, 97.6 % of the 250 time series realizations show significant positive trends (Sen's slope (SS): 9 – 15 t km^{-2} a^{-1}), and at gauge Vernagt, all realizations show significant positive trends (SS: 28 – 35 t km^{-2} a^{-1}). At gauge Vent, Pettitt's test yields a significant change point in 1981 in annual sSSY, which is also true for 99.6 % of the realizations (for one realization, the change point was detected in 1980). Accordingly, the MCP analysis shows a rather narrow probability density distribution around 1980/81 for all realizations, with a maximum probability density in 1981.

At gauge Vernagt, MCP shows very similar probability density distributions to those of Vent with maximum probabilities in 1981 for all realizations. However, Pettitt's test detects a change point in 1989 ($p < 0.01$; 66 % of realizations in 1989 and 27 % in 2002). As we elaborate in the discussion, this is likely due to a limitation of Pettitt's test. Thus, we divided both time series in 1981 to examine the resulting segments for trends.

In the first segment, no significant trends were detected at gauge Vernagt, and at gauge Vent, only 2 of the 250 realizations show significant positive trends (SS of 11.1 and 3.9 t km^{-2} a^{-1}; see Figure 3.5). In the second segment (i.e. after 1981), we detected a negative trend in mean annual sSSY at gauge Vent (SS = - 7.6 t km^{-2} a^{-1}) and in 42 realizations (SS of - 13.1 to - 5.9 t km^{-2} a^{-1}). In contrast, at gauge Vernagt, mean sSSYs (SS = 23.5 t km^{-2} a^{-1}) as well as 248 of the realizations (SS of 20.2 to 27.9 t km^{-2} a^{-1}) show strong positive trends. The average sSSYs (± 1SD) of all years after 1981 are 1579 (± 391) t km^{-2} a^{-1} at gauge Vent and 1537 (± 603) t km^{-2} a^{-1} at gauge Vernagt.

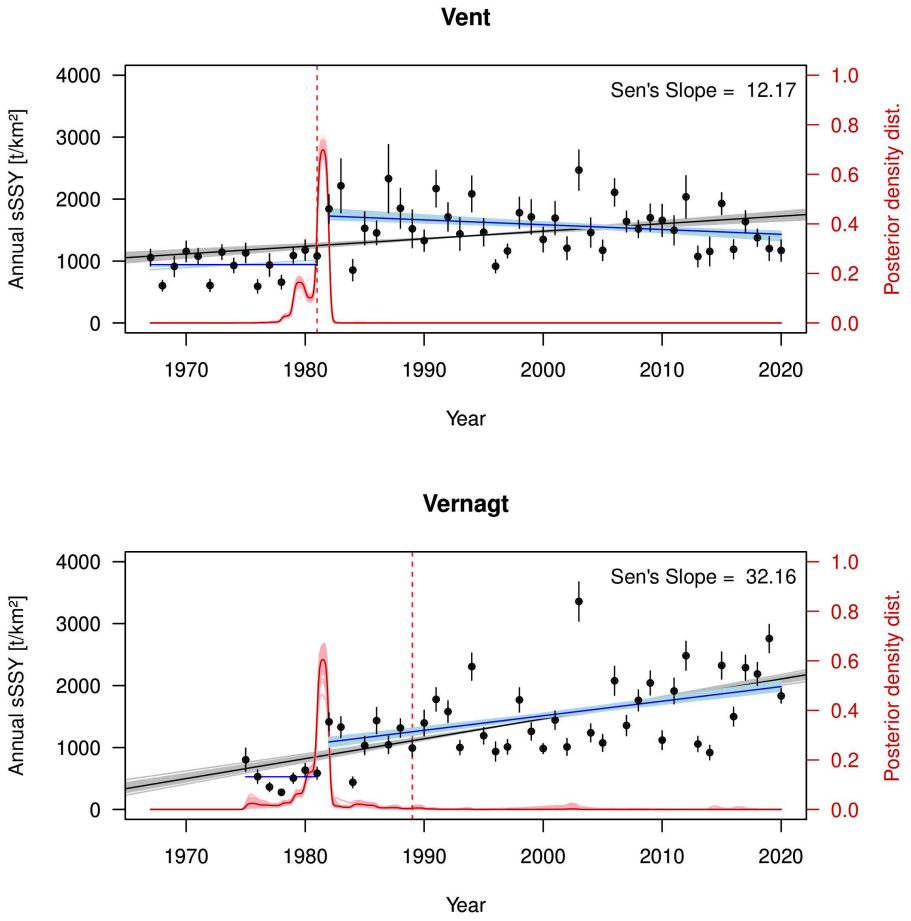

Figure 3.6. *Mean specific annual suspended sediment yields (sSSYs) as reconstructed by the QRF model (black points). Whiskers depict 2.5 % and 97.5 % quantiles of the 250 QRF realizations. The overall trend of mean annual sSSY is given by Sen's slope (black line) and trends of all 250 QRF realizations in grey. Change points determined by Pettitt's test (red dashed line) and MCP (posterior distributions of 250 realizations as solid light red and mean as dark red lines). Trends in the time series segments before and after 1981 are given as dark blue (mean) and light-blue (realizations) lines (only plotted if significant).*

3.5.2 RESULTS PART III: ANALYSIS OF PREDICTORS AND GLACIER MASS BALANCES

We found positive trends in annual sSSYs at both gauges with high probabilities of a step-like increase around 1981. To assess whether this coincides with changes in temperature (i.e., changes in snowmelt and/or glacier melt and discharge) or changes in precipitation, we analyzed time series of the predictors, temperature, discharge and precipitation, as well as glacier mass balance data with respect to trends and change points.

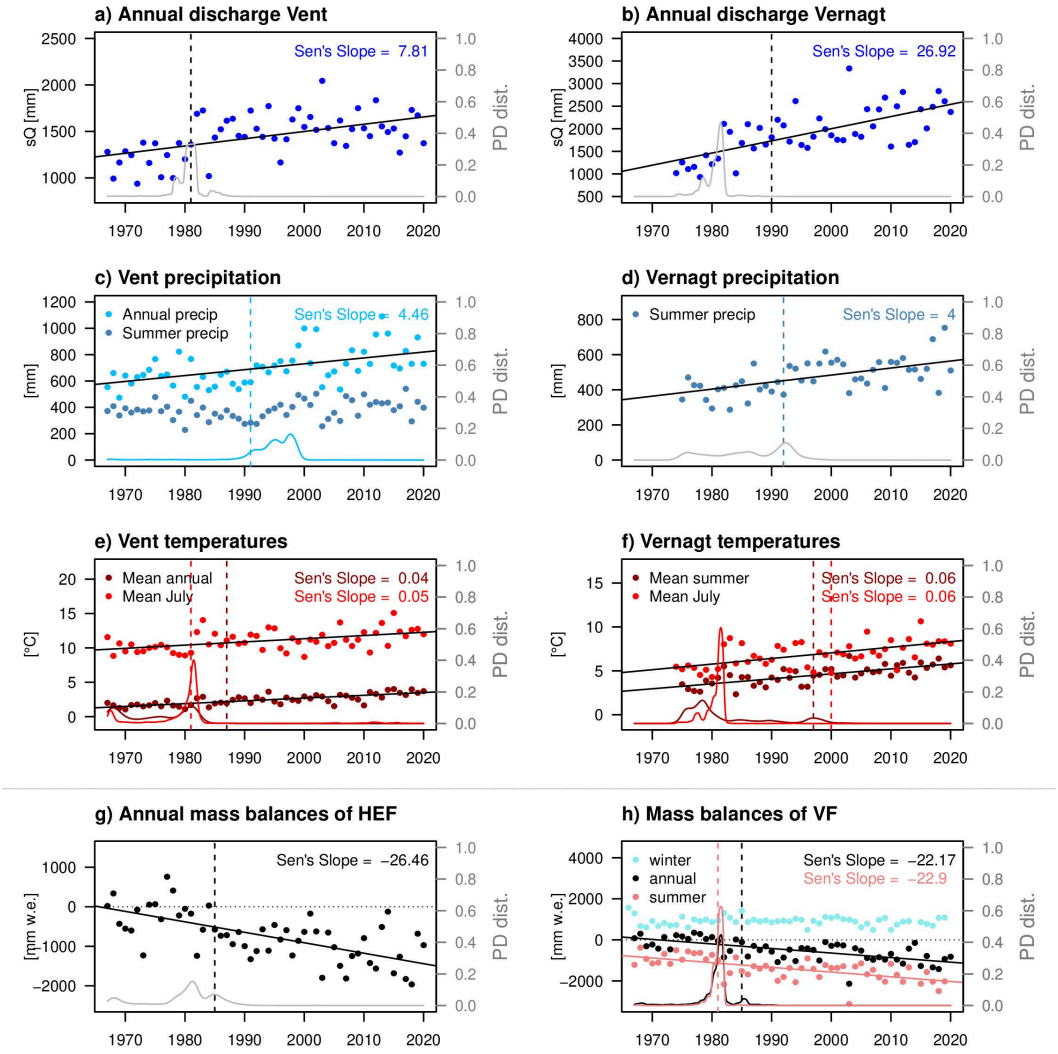

Figure 3.7. *(**a, b**) Annual discharge yields at gauges Vent and Vernagt. (**c**) Annual and summer (May – Sept) precipitation in Vent. (**d**) Summer (May – September) precipitation at gauge Vernagt. (**e**) Mean annual and July temperatures in Vent. (**f**) Mean summer (May – Sept) and July temperatures at gauge Vernagt. (**g**) Annual mass balances of the Hintereisferner (HEF). (**h**) Annual, winter and summer mass balances of VF. Dashed vertical lines show change point locations according to Pettitt's test, and solid lines show Sen's slope. Both are only drawn if they are significant at a = 0.01. Lines at the bottom show posterior density distributions of MCP change point locations, with colors corresponding to the respective variables if several variables are depicted within one plot.*

Annual specific discharge sums at both gauges show significant positive overall trends (Figure 3.7a) and b). In Vent, both change point detection methods indicate high probabilities of a change point in 1981. At gauge Vernagt, annual discharge volumes roughly doubled within the examined period, from ca. 1250 mm to ca. 2500 mm. The two change point (CP) detection methods disagree as in the case of annual sSSYs, as Pettitt's test detects a change point in 1990 while MCP suggests a change point with high probability in 1981. Dividing both time series in the year 1981, both segments of the Vent time series show insignificant trends, while both segments at gauge Vernagt show significant positive trends (first segment: Sen's slope = 32.7 mm a^{-1}, $p < 0.01$; second segment: Sen's slope = 17.2 mm a^{-1} $p < 0.001$).

We analyzed mean monthly discharge volumes and found significant positive trends in May and June in Vent (a detailed figure can be found in Appendix Figure 3.A2). As with temperature, change points are indicated by both methods in 1981 for July discharge and around 1995 for June discharge. At gauge Vernagt, discharge shows significant positive trends from May through August (see Figure 3.A3 in the Appendix). In June, a CP is indicated around 1995 by both methods, and in July, MCP indicates a CP around 1981, but Pettitt's test does not yield a significant change point. For May and August discharge, Pettitt's test yields change points in the late 1990s and mid-1980s, respectively, but MCP shows very widespread probability distributions.

Summer precipitation sums (May – September) at gauge Vent (Figure 3.7c) show no significant trend, while annual precipitation sums show a significant positive trend. A change point is identified by Pettitt's test in 1991 ($p < 0.001$) while MCP yields a widespread probability distribution with the highest probability in the late 1990s. At gauge Vernagt, we confined the analysis to summer precipitation (May – September) as the time series is affected by gaps in some winters (see Figure 3.A1 in the appendix). Summer precipitation at gauge Vernagt shows a significant positive trend (Figure 3.7d). Pettitt's test yields a significant change point in 1992 while MCP gives a very widespread distribution.

We derived mean annual temperatures at gauge Vent, however, at gauge Vernagt, we computed mean summer temperatures (between May and September) instead, as temperatures are missing in winter in many years (see also Figure 3.A1 in the appendix). Both time series show significant positive trends but no clear change points, as Pettitt and MCP disagree and MCP yields a very widespread probability distribution (Figure 3.7e and f). Additionally, we analyzed mean monthly temperatures over time and found that while most months show positive trends, at both gauges July is the only month with a high change point probability around 1981 (Figure 3.7e and f). At both stations, July temperatures in 1982 and 1983 were exceptionally warm.

In addition to the hydroclimatic predictors considered in the QRF model, we analyzed independent data of annual mass balances of the Vernagtferner (VF) and Hintereisferner (HEF), the two largest glaciers in the Vent catchment with long glaciological mass balance records. Since 1965 (VF) and 1952 (HEF), the two glaciers have been regularly and extensively surveyed for volume changes (World Glacier Monitoring Service, 2021; Strasser et al., 2018). Annual mass balances of both glaciers show significant negative trends (Figure 3.7g and h). Significant change points are indicated in 1985 for both glaciers by the Pettitt test, while MCP attributed (much) higher probabilities for change points to the year 1981. Notably, annual mass balances of both glaciers are almost exclusively negative after 1980 (with the exception of 1984, where mass balances are barely positive). Dividing the time series in 1981, no significant trends are detected in the first segments of both time series and significant negative trends in the second segments (HEF: -20 mm a^{-1}; VF: -17 mm a^{-1}).

Summer mass balances were only (continuously) available for the Vernagtferner and show a strong negative trend and both Pettitt and MCP detect change points in 1981 (Figure 3.7h).

No significant trends are detected in the resulting time series segments. Winter mass balances do not show a significant trend or change points.

3.6 DISCUSSION

3.6.1 MODEL EVALUATION

The presented study aimed to examine extensively whether quantile regression forest is a suitable method for estimating past sediment export. Overall, the final QRF reconstruction models outperformed SRCs by about 20 percent points in explained variance at both gauges – even though we assessed OOB estimates of QRF versus rating curves based on all available data. OOB performance was better at gauge Vernagt (NSE of 0.82 with respect to daily SSCs) than at gauge Vent (NSE of 0.6), although even the latter corresponds to a satisfactory performance (Moriasi et al., 2007). We suggest that there are three reasons for this difference in performance. First, the Vent catchment is much larger (almost 100 km²) than the 11.4 km² Vernagt catchment. Thus, suspended sediment dynamics at gauge Vent integrate over more different processes, which adds to the complexity compared to the mostly melt-driven Vernagt catchment. Second, precipitation measurements at gauge Vent are unlikely to be representative of the entire catchment, due to the catchment size and especially due to topographical effects. Thus, more localized rainstorms are likely to be captured more poorly. Third, SSCs at gauge Vent reach much higher values than at gauge Vernagt, so that uncertainties in the turbidity measurement are more relevant: at low concentrations, the light emitted by the turbidity sensor is predominantly scattered by solid particles, while at high concentrations, absorption becomes the dominant process. This causes the relation between the light detected by the photo sensor in the turbidity probe and SSCs to become nonlinear (Merten et al., 2014) and leads to a much higher variance in the SSC–turbidity relationship. However, despite these effects and the lower NSE with respect to daily Q_{sed} at gauge Vent, annual sSSYs show very good agreement. Thus, we conclude that – given the availability of a large-enough and varied training dataset and sufficiently long records of the predictors – QRF represents a reliable tool with the ability to broaden our understanding of the response of high-alpine areas to climate change in the past decades.

Nevertheless, a few limitations need to be considered. As a major limitation, QRF cannot extrapolate if predictors in the reconstruction period exceed the range of values represented in the training dataset (Francke et al., 2008a). In these cases, the modeled values will potentially suffer from overestimation or underestimation. At the same time, assessing the number of such exceedances in the period of model application provides an indication of the representativity of the training dataset, which must be sufficiently large and varied for such data-driven approaches (Vercruysse et al., 2017). In our case, exceedances were rare (7 d at gauge Vent and 10 d at gauge Vernagt), so we consider the error negligible for annual sediment export. We strongly encourage future studies to assess the number and severity of such

exceedances for this purpose, especially in view of changing conditions, e.g., due to (prospective) climate change.

More generally, the QRF model can only reproduce the quantitative and qualitative conditions as represented within the training data. This has several implications. First, the spread of the QRF model results needs to be interpreted as a minimum estimate of uncertainty, as it can only reproduce the 'known unknown', i.e., the variability represented in the training data and their respective relationships or the lack thereof. Second, major qualitative changes in the functioning of the modeled system, such as changes in connectivity, e.g., through the formation of proglacial lakes or large-scale storage of sediments along the flow paths, cannot be captured. However, for the catchments considered in this study, such major changes are at least not indicated in historic aerial images (Laser- und Luftbildatlas Tirol, 2022) and the longitudinal profiles of the major water courses are very steep, which precludes significant sediment storage.

We found that our models at both gauges underestimated rare, high daily SSCs and Q_{sed} (Figure 3.3 – Figure 3.5). This is not surprising given that these events are rare and that Figure 3.3 to Figure 3.5 show out-of-bag predictions, which means that the respective estimates are based only on those trees that have seen few or none of these conditions. Including them in the training of the final reconstruction model alleviated this effect.

Further, we suspected that the aggregation of precipitation and discharge to daily values might involve some loss of information e.g. on subdaily precipitation intensity and maximum discharge, which would very likely affect sediment export estimates. Indeed, the underestimation is a little more pronounced in the daily model as compared to hourly resolution, yet the difference was relatively small (Validation A, Figure 3.3a). Adding to this, the underestimation at the daily scale does not seem to propagate to annual estimates, as high annual sSSYs are not systematically underestimated to the same extent (Figure 3.5b) and the underestimation of rare events at the daily scale has a limited effect on the annual estimates (section 3.4.4). This is in accordance with the finding that only about one-fourth of the annual yield in Vent is transported during (precipitation) events (Schmidt et al., 2022b), as opposed to other fluvial systems where the majority of the annual sediment yield is transported by several extreme events (Delaney et al., 2018b). Consequently, the proposed QRF model is also applicable at daily resolution, enabling its application to the longer time series available.

We assessed temporal extrapolation ability at gauge Vernagt by training a model on the data of 2019/20 and comparing the estimates to measurements in 2000 and 2001 (Validation B; Figure 3.4), which showed overestimation and underestimation of annual sSSYs by 31 % and 16 %, respectively. In interpreting these results, it has to be considered that the amount of data used for training is very small and less than half of the final reconstruction model (212 of 579 d), while the amount of training data is known to be crucial in data-driven models (e.g., Vercruysse et al., 2017). Specifically, turbidity recordings only started in mid-July 2019, so that only one spring season was available for training. Thus, given the rigorousness of this test and the temporal distance of 20 years, we find that the validation yields satisfactory results with

good agreement of dynamics on short timescales and annual estimates. The validation model trained on the data of 2000/2001 yielded lower but still satisfactory NSE values. We attribute this to higher discharge and temperature values in 2019 and 2020, which, again, points to the importance of exceedances. With better data availability at gauge Vent, we assessed temporal extrapolation ability through a five-fold cross-validation. This showed that some periods were harder to model based solely on the remaining data. This means that these periods contain rather distinct data and are thus especially valuable as training data for the full QRF model, as they contained the highest SSC and Q_{sed} in the time series. We repeated this cross-validation with the SRCs. It proved to be inferior to QRF in most periods, which showed that in our case QRF is better able to extrapolate from limited data, especially with respect to periods containing extreme events, which are difficult to describe per se, due to threshold effects such as the activation of mass movements (Zhang et al., 2022). This seems to contradict the fact that, numerically, a SRC is indeed capable of extrapolating beyond the range of the training data, whereas QRF is not. As QRF still performed better in modeling periods with extreme events in the cross-validation, we attribute this to the circumstance that QRF is able to model interactions and is not bound to a linear or monotonous relationship between the predictors and SSC estimates. Apparently, these features are more important and influential than extrapolation in the sense of sheer "extension of a curve".

3.6.2 ANALYSIS OF ANNUAL SSSYS, PREDICTORS AND MASS BALANCES

The overall magnitudes of annual yields at the two analyzed gauges fall at the high end compared to an extensive collection from the European Alps (Hinderer et al., 2013) and are in good accordance with yields from other catchments in the Stubai and Ötztal Alps (Schöber and Hofer, 2018; Tschada and Hofer, 1990) (see also Schmidt et al., 2022b). Their reconstruction for the past five decades constitutes an important contribution to the understanding of long-term sediment budgets, as other existing records commonly only cover some decades.

The reconstructed annual sSSYs at both gauges show overall positive trends and change points around 1981. The two change point detection methods did not agree at gauge Vernagt, where MCP yielded high change point probabilities around 1981, whereas Pettitt's test detected a significant change point in 1989 (or 2002 in some realizations). Similarly, the results did not agree for July temperatures and discharge at gauge Vernagt. We attribute this to a limitation of Pettitt's test, which is known to be much less sensitive to break points located near the beginning or end of the time series (Mallakpour and Villarini, 2016). Notwithstanding, we conclude that there is a high probability of change points around 1981 in the reconstructed sSSY as well as discharge and July temperature time series at gauge Vernagt, as the MCP probability distributions are very narrow and similar to the corresponding probability distributions in Vent.

Our results suggest that the step-like increase in modeled sSSY is linked to the onset of increased ice melt. Mean annual temperature in Vent and mean summer temperature at gauge Vernagt at both locations show gradual positive trends without a clear change point. However, mean July temperatures show high change point probabilities around 1981 at both locations, which is probably heavily influenced by extraordinarily high temperatures in July 1982 and 1983. July temperatures are especially relevant for firn and glacier melt, since July is the month with the highest firn and ice melt contribution to discharge after snowmelt contributions have peaked in June and snow cover has decreased substantially (Kormann et al., 2016; Weber and Prasch, 2016a; Schmieder et al., 2018a; Schmidt et al., 2022b). This shift is reflected in discharge, which shows a step-like increase around 1981 at both gauges and continues to be elevated after this change point. The analyses of monthly discharge showed that July was the only month with a change point around 1981 at both gauges, which again emphasizes the dominance of increased firn and ice melt. In contrast, we did not find evidence of a change in precipitation sums around 1981, which would indicate that enhanced hillslope erosion on snow- or ice-free surfaces played a crucial role in the sSSY increase. With regard to suspended sediment dynamics, the increase in ice melt may translate to an increase in sediment-rich glacial meltwater (Delaney and Adhikari, 2020) and intensified fluvial erosion of sediment-rich proglacial areas.

These changes in the predictors of our QRF model are also reflected in the mass balance time series of the Hintereisferner and Vernagtferner, which were almost exclusively negative after 1980, with very negative summer mass balances in 1982 and 1983. Escher-Vetter (2007) and Abermann et al. (2009) also showed that mass loss started in 1981 at both glaciers, resulting from negative summer balances. With respect to the Vernagtferner, the drastically higher ablation area ratio of almost 80 % in 1982 as compared to around 25 % in the preceding years (Escher-Vetter and Siebers, 2007) indicates that large areas of the glacier became snow-free in 1982. This entails crucial changes in albedo and therefore intensified ice melt and thinning of firn areas due to rising energy absorption at the glacier surface (Escher-Vetter, 2007; Braun et al., 2007). We interpret this as a regime shift as summer mass balances continue to be lower than before 1981 although (July) temperatures decrease again, with the exception of 1984, which was characterized by a relatively high number of snowfall days during the ablation period (Escher-Vetter and Siebers, 2007).

Similar step-like increases in sediment export have been reported from the upper Rhône basin in Switzerland (Costa et al., 2018b) (only slightly later, around 1985, which is likely due to lower average temperatures) and for the headwaters of the Yangtze River on the Tibetan Plateau (Li et al., 2020; Zhang et al., 2021) and 28 headwater basins in High Mountain Asia (Li et al., 2021b). Thus, we deem it unlikely that the change points identified in the present study are related, e.g., to a change in measurements, also because they were detected at both gauges in the same year and in both (July) temperature and discharge. More generally, substantial increases in sediment export in response to climate change have been reported from cold environments around the globe (e.g., Bogen, 2008; Koppes et al., 2009; Bendixen et al., 2017b; Singh et al., 2020; Vergara et al., 2022) and are in accordance with state-of-the-art conceptual models, which expect that phases of glacier retreat (and re-advance) will lead to the highest

increase in sediment yield across glacial cycles (Antoniazza and Lane, 2021), as has been confirmed by several studies (Lane et al., 2017, 2019; Micheletti and Lane, 2016).

Interestingly, we found opposing trends in the time after 1981, with strongly increasing annual sSSY at gauge Vernagt and decreasing sSSY at gauge Vent. To some extent, this is reflected in changes in discharge, where we found no significant trend (and Sen's slope close to zero) after 1981 at gauge Vent, but a strong positive trend at gauge Vernagt. Altogether, this could indicate different timings of *peak sediment* (Ballantyne, 2002; Antoniazza and Lane, 2021) and thus a stabilization or compensation of the larger Vent catchment as opposed to the nested Vernagt catchment. Some independent observations support this notion: for example, the glacier tongue of the Hochjochferner (denoted as "HJF" in Figure 3.1), located in the southernmost tributary valley to the Rofental, has retreated by about 2 km since the 1970s (determined based on historic aerial image collection of the State of Tyrol, Laser- und Luftbildatlas Tirol, 2022) and has now retreated behind a rock sill. Additionally, several small lakes have formed in its glacier foreland that likely act as sediment sinks. Another two smaller glaciers in the northeastern part of the Vent catchment, Mitterkarferner and Platteiferner ("MKF" and "PF" in Figure 3.1), have disappeared almost completely since the 1970s. Conversely, the Vernagtferner glacier has also experienced considerable loss in area and volume but lacks such pronounced qualitative changes thus far.

3.7 CONCLUSIONS

In the presented study, we tested a quantile regression forest (QRF) model, which enabled the estimation of sediment export of the past five decades for the two gauges Vent and Vernagt. This allowed us to analyze annual specific suspended sediment yields (sSSYs) for trends and change points. Annual sSSYs show positive trends as well as step-like increases after 1981 at both gauges. As this coincides with exceptionally high July temperatures in 1982 and 1983, distinct changes in the glacier mass balances of the two largest glaciers in the catchment area and a sudden increase in the ablation area of one of the glaciers, we conclude that temperature-driven enhanced glacier melt is responsible for the step-like increase in sSSYs. This is also mirrored in discharge measurements at both gauges, which show change points around 1981 as well. Opposing trends after 1981 at the two gauges could indicate different timings of peak sediment. These analyses also demonstrated the value of assessing change points in addition to trend analyses, in order to detect sudden changes in the analyzed geomorphic systems and thus facilitate a better understanding of critical time periods.

Further, we explored advantages and limitations of the QRF approach. As a major limitation, QRF may yield underestimates if predictors exceed the range of values represented in the training dataset. To estimate the effect on the model results, we suggest assessing the number of such exceedances, which can also be leveraged to evaluate the representativity of the training dataset. Further, we found that events with very high SSC and Q_{sed} tend to be underestimated. While this is not surprising given the rareness of such events, the

effect of such underestimations on the annual yields was small. The assessment of the temporal extrapolation ability revealed a satisfactory performance of QRF and illustrated again the importance of a sufficiently varied dataset, i.e., including larger events. A comparison of QRF to sediment rating curves in a five-fold cross-validation showed that QRF was better able to model periods that contain very high SSCs caused by mass movements. This points to the favorable ability of QRF to model threshold effects, which is a major advantage compared to approaches bound to continuous relationships. The final QRF reconstruction models showed good performance at both gauges and outperformed SRCs by about 20 percent points of the explained variance. We conclude that the presented approach is a helpful tool for estimating past sediment dynamics in catchments where long-enough SSC measurement series are lacking. Future studies could help gain more knowledge on decadal-scale sediment export from high-alpine areas by applying the presented approach to other catchments. In turn, advancing knowledge on past changes will support and prepare the development of management and adaptation strategies.

3.8 CODE AVAILABILITY

The code of the quantile regression forest model, including the preprocessed data and raw model results, is available on B2Share (https://b2share.109960a9fb42427b9d0a85b998b9d18c, Schmidt et al., 2022a).

3.9 DATA AVAILABILITY

See column 'data availability' in Table 3.A1 in Appendix A.

3.10 ACKNOWLEDGEMENTS

We were supported by the Hydrographic Service of Tyrol, Austria, by providing data as well as logistical support and fruitful discussions.

We thank Oliver Korup for his encouraging advice on statistical analyses, Matthias Siebers, Andreas Bauer, Irene Hahn, Theresa Hofmann, Marvin Teschner, Nina Lena Neumann and Joseph Pscherer for their help and support during fieldwork and laboratory work, and Stefan Achleitner, Carolina Kinzel and the Environmental Engineering laboratory at the University of Innsbruck for their kind support during fieldwork and laboratory work. We thank Anna Costa, Dongfeng Li and an anonymous referee for their thorough and valuable comments that helped enhance and refine the manuscript.

3.11 FINANCIAL SUPPORT

This research has been supported by the Deutsche Forschungsgemeinschaft research training group 'Natural Hazards and Risks in a Changing World' (grant nos. NatRisk Change GRK 2043/1 and NatRisk Change GRK 2043/2) and a fieldwork fellowship of the German Hydrological Society (DHG).

3.12 APPENDIX

Table 3.A1. *Characteristics of input data. Q: discharge, T: temperature, P: precipitation, SSC: suspended sediment concentration. HD: Hydrographic Service of the State of Tyrol, Austria. BAdW: Bavarian Academy of Sciences and Humanities, Munich, Germany.*

Variable	Location	Coordinates (lon, lat; WGS84)	Length	Temporal resolution	Source	Data availability
Q	Vent	10 54 39, 46 51 25	01.01.1967 – 31.12.2017	Daily means	HD	eHYD (2021)
			01.01.1967 – 31.12.2020	15 min mean		Can be requested via wasserwirtschaft@tirol.gv.at
T, P	Vent	10 54 46, 46 51 26	01.01.1935 – 31.12.2011	Daily mean (*T*) and sum (*P*)	Institute of Meteorology and Geophysics, Innsbruck, Austria	Institute of Meteorology and Geophysics (2013)
			01.01.2012 – 31.12.2016	Daily mean (*T*) and sum (*P*)	Institute of Atmospheric and Cryospheric Sciences, Innsbruck, Austria	Juen and Kaser (2017)
			01.01.2017 – 31.12.2020	Daily mean (*T*) and sum (*P*)	HD	Can be requested via wasserwirtschaft@tirol.gv.at
SSC (turbidity)	Vent	10 54 39, 46 51 25	01.05.2006 – 31.10.2020	15 min mean	HD	Schmidt and Hydrographic Service of Tyrol, Austria (2021)
Q, P, T	Vernagt	10 49 43, 46 51 24	01.05.1974 – 31.10.2001	60 min mean	BAdW	Escher-Vetter et al. (2012)

Q	Vernagt		01.05.2000 – 20.10.2001	10 min mean		
Q, P, T	Vernagt		01.05.2002 – 31.12.2012	5 min mean		Escher-Vetter et al. (2014)
Q, P, T	Vernagt		01.05.2013 – 15.10.2020	5 min mean		Data will successively be made available on PANGEA.
SSC (turbidity)	Vernagt		01.05.2000 – 20.10.2001	10 min mean		
SSC (turbidity)	Vernagt		30.04.2019 – 03.11.2020	5 min mean		
SSC samples	Vernagt		23.05.2019 – 30.08.2020	131 samples	This study	
P, T	Vernagt (HD)	10 49 42, 46 51 24	07.10.2010 – 31.12.2020	15 min mean (*T*) and sum (*P*)	HD	Can be requested via wasserwirtschaft@tirol.gv.at
P	Martin-Busch-Hütte	10 53 18 46 48 03	23.09.2010 – 31.12.2020	15 min mean (*T*) and sum (*P*)	HD	Can be requested via wasserwirtschaft@tirol.gv.at

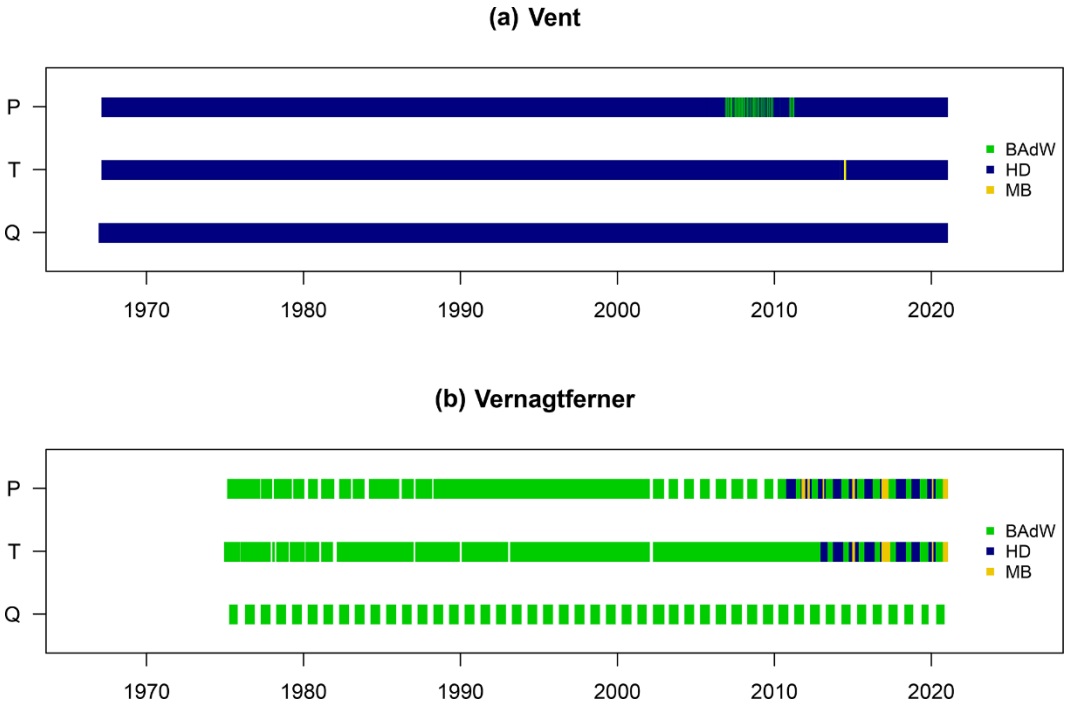

Figure 3.A1. *Discharge (Q), temperature (T) and precipitation (P) data at the two gauges after the gap-filling procedure. The color indicates the data source (BAdW: Bavarian Academy of Sciences and Humanities, HD: Hydrographic Service of Tyrol stations at gauges Vent* ***a*** *and Vernagt* ***b****, MB: Martin-Busch Hütte).*

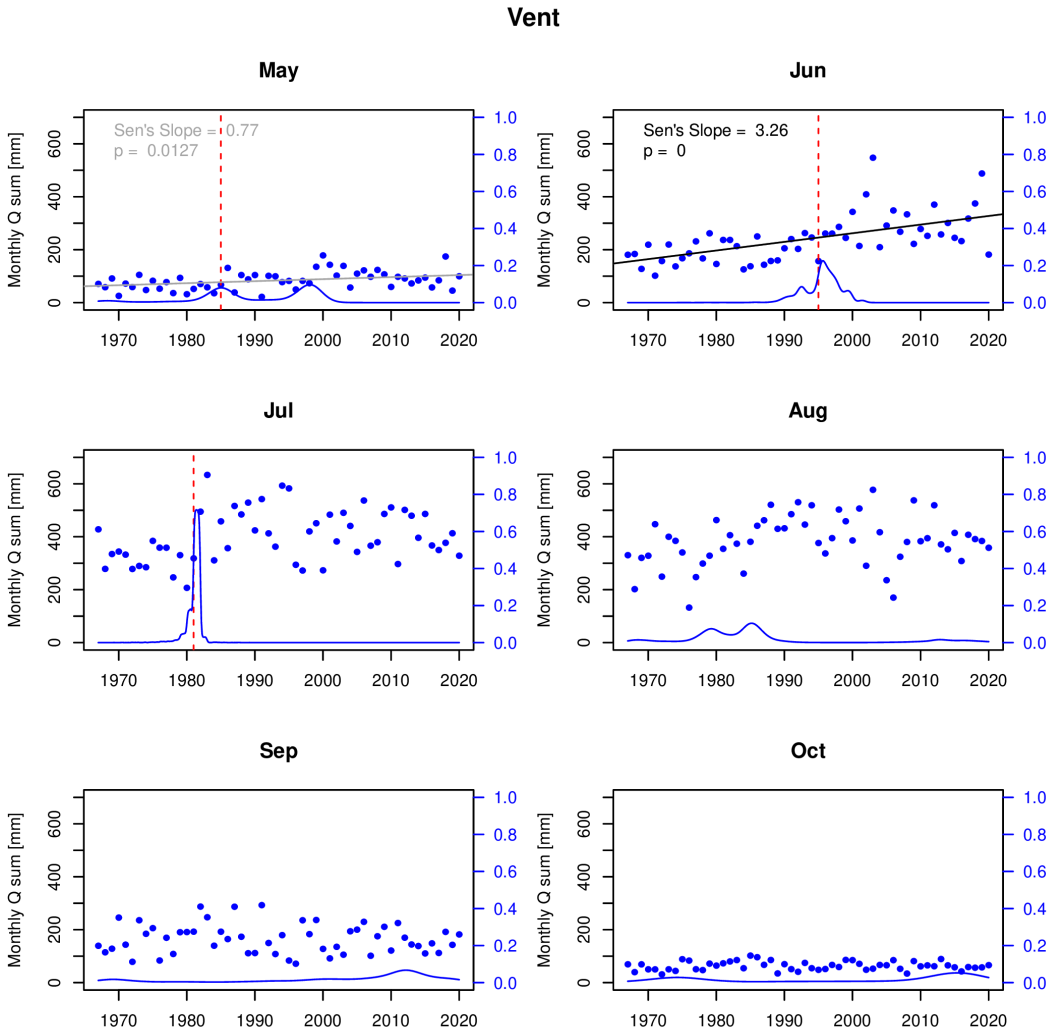

Figure 3.A2. *Trends and change points in monthly discharge sums at gauge Vent. Dashed red lines indicate change points according to Pettitt's test (significant at a = 0.01), blue lines represent change point probability distributions of MCP, and solid black (and grey) lines indicate trends according to Mann–Kendall test significance at a = 0.01 (and 0.05).*

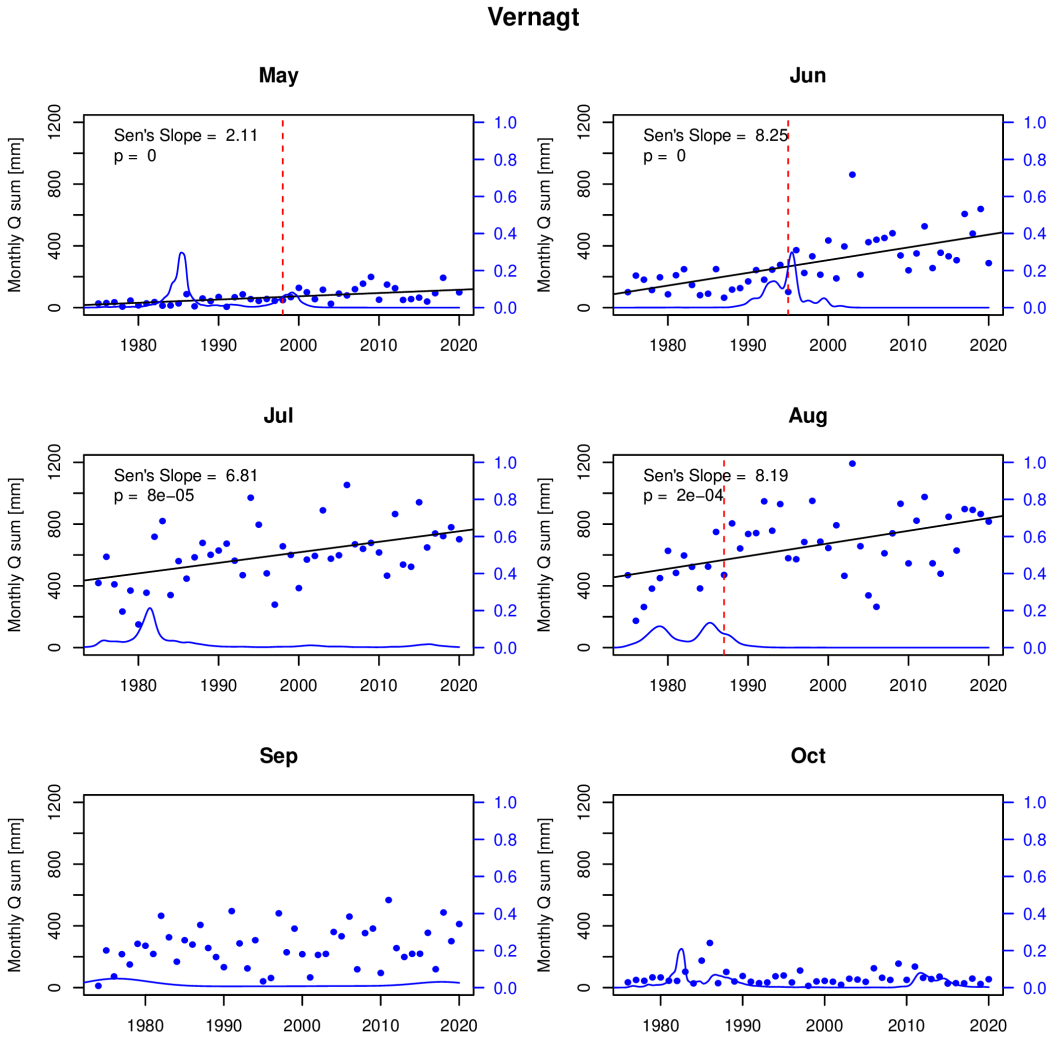

Figure 3.A3. *Trends and change points in monthly discharge sums at gauge Vernagt. Dashed red lines indicate change points according to Pettitt's test (significant at a = 0.01), blue lines represent change point probability distributions of MCP, and solid black lines indicate trends according to Mann–Kendall test significance at a = 0.01.*

4 ESTIMATING THE FUTURE

Under review as: ***Schmidt, L. K.****, Francke, T., Grosse, P. M., and Bronstert, A.: Projecting sediment export from two highly glacierized alpine catchments under climate change: Exploring non-parametric regression as an analysis tool. Under review in Hydrology and Earth System Sciences, EGUsphere [preprint]: https://doi.org/10.5194/egusphere-2023-1063.*

KEY POINTS

- Applying QRF models developed in chapter 3 to temperature, precipitation and discharge projections
- Estimating sediment export for three emission scenarios (RCP2.6, RCP4.5 and RCP8.5) until 2100
- Analysis indicates that uncertainties associated with technical limitation of QRF model (out-of-observation-range values) are small before 2070
- Results suggest overall decrease in sediment export regardless of emission scenario
- However, high yields are projected in response to heavy summer precipitation

ABSTRACT

Future changes in suspended sediment export from deglaciating high-alpine catchments affect downstream hydropower and reservoirs, flood hazard, ecosystems and water quality. Yet so far, quantitative projections of future sediment export have been hindered by the lack of physical models that can take into account all relevant processes within the complex systems determining sediment dynamics at the catchment scale. As a promising alternative, machine-learning (ML) approaches have recently been successfully applied to modeling suspended sediment yields (SSY).

This study is the first to our knowledge exploring machine-learning approach to derive sediment export projections until the year 2100. We employ Quantile Regression Forest (QRF), which proved to be a powerful method to model past SSY in previous studies, at two nested high-alpine gauges in the Ötztal, Austria, i.e. gauge Vent (98.1 km² catchment area, 28 % glacier cover in 2015) and gauge Vernagt (11.4 km² catchment area, 64 % glacier cover). As predictors, we use temperature and precipitation projections (EURO-CORDEX) and discharge projections (AMUNDSEN physically-based hydroclimatological and snow model)

for the two gauges. We address uncertainties associated with a known limitation of QRF, i.e., that underestimates can be expected if out-of-observation-range (OOOR) data points (i.e., values exceeding the range represented in the training data) occur in the application period. For this, we assess the frequency and extent of these exceedances and the sensitivity of the resulting mean annual suspended sediment concentration (SSC) estimates. We examine the resulting SSY projections for trends, the estimated timing of peak sediment and changes in the seasonal distribution.

Our results show that the uncertainties associated with the OOOR data points are small before 2070 (max. 3 % change in estimated mean annual SSC). Results after 2070 have to be treated more cautiously, as OOOR data points occur more frequently and as glaciers are projected to have (nearly) vanished by then in some projections, which likely substantially alters sediment dynamics in the area. The resulting projections suggest decreasing sediment export at both gauges in the coming decades, regardless of the emission scenario, which implies that peak sediment has already passed or is underway. Nevertheless, high(er) annual yields can occur in response to heavy summer precipitation, and both developments would need to be considered in managing sediments as well as e.g. flood hazard. While we chose the predictors to act as proxies for sediment-relevant processes, future studies are encouraged to try and include geomorphological changes more explicitly, e.g. changes in connectivity, landsliding / rockfalls, or vegetation colonization, as these could improve the reliability of the projections.

4.1 INTRODUCTION

Fluvial suspended sediment export from glacierized, high-alpine areas can be up to a magnitude higher (per unit area) than in non-glacierized downstream areas (Hinderer et al., 2013; Beniston et al., 2018). Thus, sediment dynamics in these high-alpine areas and changes therein have important implications for downstream hydropower generation and reservoir sedimentation (Schöber and Hofer, 2018; Guillén-Ludeña et al., 2018; Li et al., 2022), water quality (as well as nutrient and contaminant transport) (Bilotta and Brazier, 2008), aquatic species and riverine ecosystems (Milner et al., 2009, 2017; Gabbud and Lane, 2016; Huss et al., 2017), but also flood hazard (Nones, 2019) and carbon cycling (Tan et al., 2017; Syvitski et al., 2022).

High-alpine areas are particularly sensitive to climate change, experience above-average warming (Gobiet et al., 2014) and hence crucial cryospheric changes, such as ongoing and accelerating deglaciation, permafrost melt and snow cover changes (Huss et al., 2017; Beniston et al., 2018; Abermann et al., 2009). These changes go hand in hand with changes in discharge volumes, timing and magnitude (Vormoor et al., 2015; Kuhn et al., 2016; van Tiel et al., 2019; Rottler et al., 2020; Hanus et al., 2021). This in turn affects sediment export, and past changes have been observed frequently, e.g. due to enhanced subglacial sediment evacuation and increased sediment accessibility in expanding erodible landscapes (Micheletti and Lane, 2016;

Carrivick and Heckmann, 2017; Lane et al., 2017, 2019; Costa et al., 2018a; Delaney and Adhikari, 2020; Li et al., 2020; Vergara et al., 2022).

Nevertheless, future changes in sediment export are understudied (Zhang et al., 2022) and questions such as 'Are sediment yields from deglaciating catchments increasing, decreasing or is there no pattern?' or 'to what extent is it possible to quantify spatio-temporal patterns of future sediment yields?' (Carrivick and Tweed, 2021) have yet to be answered – although projections of climatological (e.g. Gobiet and Kotlarski, 2020; Gobiet et al., 2014) , glaciological (e.g. Stoll et al., 2020; Bolibar et al., 2022; Huss, 2011) and hydrological changes (e.g. Madsen et al., 2014; Hanzer et al., 2018; Hanus et al., 2021; Huss and Hock, 2018; Tecklenburg et al., 2012; Wijngaard et al., 2016), that could serve as a basis for estimating future changes in sediment export, are numerous.

The main reason why answering such questions is challenging is that modeling sediment export at the catchment scale with process-based models remains difficult – if not impossible – because it is determined by a complex system of interconnected processes that is not straightforward to capture. For example, the relationship between suspended sediment concentrations and discharge is most often nonlinear in time and space, and univariate models relying solely on discharge are often insufficient (Vercruysse et al., 2017; Zhang et al., 2021). Hence, in addition to variations in discharge, changes in sediment availability, entrainment, transport and deposition would have to be considered, there may be threshold effects and nonlinear responses of geomorphic processes (e.g. triggering of mass movements or debris flows), correlated influencing factors, hysteresis and seasonality (Huggel et al., 2012; Landers and Sturm, 2013; Vercruysse et al., 2017; Costa et al., 2018a; Schmidt et al., 2022b; Zhang et al., 2022). Additionally, long-term field observations (i.e. several decades and covering a wide range of conditions) that provide enough training and validation data to develop sediment-yield models or to analyze trends are very rare (Zhang et al., 2022; Schmidt et al., 2023).

There are conceptual models on (suspended) sediment export from deglaciating areas (Antoniazza and Lane, 2021; Carrivick and Tweed, 2021; Zhang et al., 2022), which expect an initial increase in sediment export as glaciers begin to retreat, and an eventual decrease – after *peak sediment* – once the glaciers have disappeared and the landscape stabilizes. The timing of peak sediment is presumed to depend i.a. on changes in erosive precipitation, i.e. a negative trend in erosive precipitation implies that peak meltwater and peak sediment may co-occur, while a positive trend or no change in erosive precipitation result in a lag between peak meltwater and peak sediment. However, deducing estimates of future sediment export and implications for individual catchments based on these conceptual considerations is not straightforward or even possible.

Common approaches to model sediment yields at the catchment scale, such as SWAT (e.g. Vigiak et al., 2017), BQART (Syvitski and Milliman, 2007), WBMsed (Cohen et al., 2013), WASA-SED (Mueller et al., 2010) or SAT (Zhang et al., 2021), are mostly empirical or conceptual in their sediment modules, do not consider all relevant erosion processes (i.e. neglecting glacial, gully erosion and landslides in the case of SWAT) and often concentrate on

large spatial scales (i.e. sediment fluxes to the oceans for large basins, entire continents or at global scale) and / or large temporal scales (i.e. multiyear averages and long-term fluxes). On the other end of the spectrum, models for individual parts or processes within glacierized catchments exist, as for example a numerical approach to model subglacial fluvial sediment transport (Delaney et al., 2019) that has also been coupled with models for ice dynamics and bedrock erosion (Delaney et al., 2021), or e.g. probabilistic or physical models of mass wasting processes, such as landslide or debris flows (Iverson and George, 2014; Hirschberg et al., 2021; Campforts et al., 2022). However, as of yet, there is no all-in-one physical model (fully-distributed, incorporating thermal and pluvial drivers of sediment mobilization and transport) to simulate sediment export from cryospheric basins (Zhang et al., 2022) at the catchment scale.

Accordingly, studies that have attempted to project future suspended sediment yields (SSY) chose rather qualitative approaches, such as comparing sediment yield observations of warmer and colder ablation seasons (Stott and Mount, 2007; Bogen, 2008), using responses of SSY to past predictor changes and applying this to projected changes in the future (Li et al., 2021b) or fitting a multiple regression model to past data (of only one year) and increasing the temperature input in the model (Stott and Convey, 2021). However, these approaches may preclude modeling decreases or accounting for interactions between variables.

As a promising alternative, geoscientific machine-learning approaches have emerged, and have recently been acknowledged for their potential in applications to Earth System Science (Reichstein et al., 2019). Indeed, first studies showed that machine-learning approaches can easily outperform well-known existing models for sediment yield (Gupta et al., 2021; Rahman et al., 2022; Jimeno-Sáez et al., 2022; Schmidt et al., 2023). In a previous study, we have developed and validated a Quantile Regression Forest (QRF) approach to model SSY in two nested high-alpine catchments and estimate yields for the past five decades (Schmidt et al., 2023). This showed that the QRF model outperformed commonly applied sediment rating curves by about 20 % of explained variance, and other studies found that regression trees and Random Forest models (which QRF is based on) even outperformed other machine-learning approaches in modeling sediment dynamics (Talebi et al., 2017; Al-Mukhtar, 2019).

Thus, the present study is motivated to explore QRF to model future SSY based on measurement data, emission scenarios and subsequent hydrological model results. We test the approach in two glacierized high-alpine catchments in the Ötztal in Austria, where projections of future climatological and glacio-hydrological conditions from the AMUNDSEN model are available (Hanzer et al., 2018), and where we have successfully trained and applied QRF models to reconstruct past sediment export, using records of discharge, precipitation and air temperature (Schmidt et al., 2023).

The goals of the present study are (i) to derive estimates of future changes in sediment export with respect to trends in annual yields, shifts in the seasonal distribution and the timing of peak sediment and (ii) to assess uncertainties of the model due to known limitations of the QRF method in order to identify the limitations of the approach.

4.2 METHODS

In a previous study, we trained and validated quantile regression forest models to retrospectively estimate SSY at two gauges for the past 5 decades, using the available records of turbidity-derived suspended sediment concentrations (four and 15 years) and long-term records of the predictors, i.e. discharge, precipitation and temperature (Schmidt et al., 2023) (Figure 4.2, dashed-line box). In the present study, we use these models and apply them to downscaled and bias-corrected EURO-CORDEX temperature and precipitation projections that were used as input data for the glacio-hydrological model AMUNDSEN as well as the discharge projections of AMUNDSEN (Hanzer et al., 2018)(Figure 4.1). In the following, we outline the Quantile Regression Forest approach including its advantages and limitations with respect to modeling suspended sediment dynamics and the choice of predictors to model sediment dynamics in high-alpine areas. Then, we describe the study area, input data and necessary adjustments, as well as how we analyzed the limitations, sensitivities and the resulting SSY estimates.

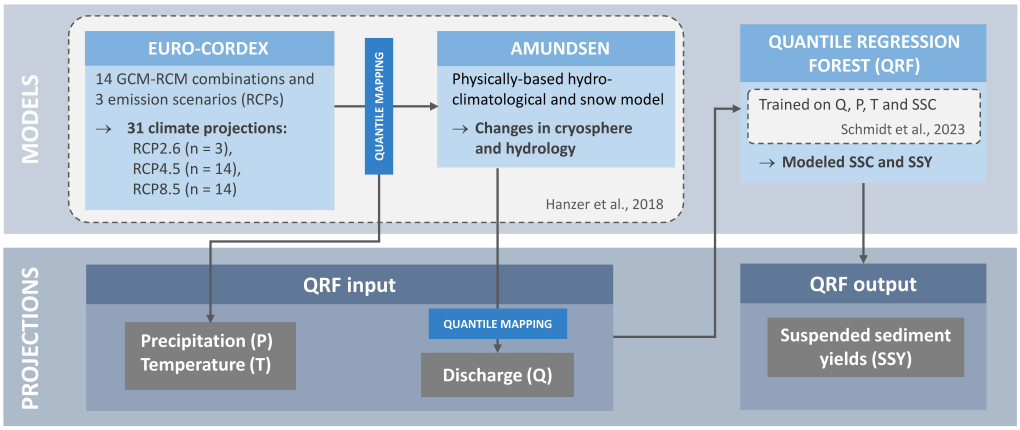

Figure 4.1. *Overview of models and resulting projections used in this study. Bias-corrected EURO-CORDEX climate projections and AMUNDSEN model results serve as input data for the QRF models. Q: discharge, P: precipitation, T: temperature, SSC: suspended sediment concentrations, SSY: suspended sediment yields.*

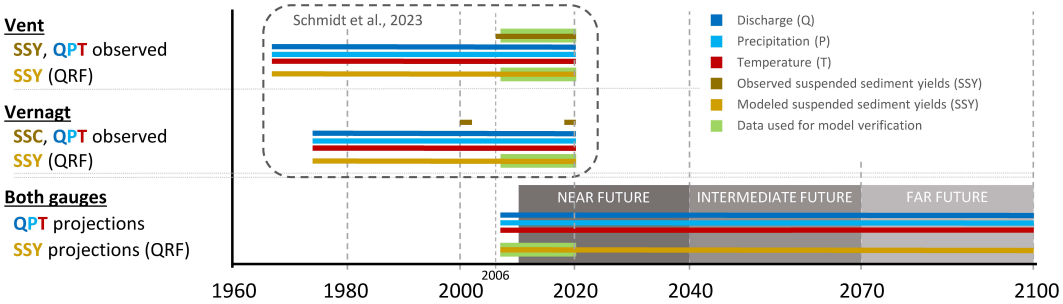

Figure 4.2. *Temporal extent of input data as well as modeled suspended sediment yields (SSY) in the previous study (dashed-line box, topleft), as well as projections (discharge (Q), precipitation (P), temperature (T)) as input data and SSY estimates from this study. 2006 – 2020 is the training data period at gauge Vent. At gauge Vernagt, the QRF model was trained on the years 2000, 2001, 2019 and 2020, when SSC data were available. Thus, to verify model results in the present study, we use the QRF estimated yields at gauge Vernagt of the years overlapping with the climate and hydrology projections, i.e. the 'overlap period' 2007 – 2020 (section 4.2.4.1).*

4.2.1 QUANTILE REGRESSION FOREST FOR SUSPENDED SEDIMENT CONCENTRATION MODELING

Quantile Regression Forest (QRF) (Meinshausen, 2006) is a non-parametric regression technique, that is based on Random Forest (RF) and can be classified as a machine-learning approach. It learns from the training data by growing ensembles of regression trees on random subsets (bootstrap samples) of the training data (Francke et al., 2008a; Schmidt et al., 2023). In each regression tree, the data are recursively partitioned based on splitting rules, where both RF and QRF randomly select the predictors used for splitting. In contrast to Random Forest, QRF keeps all observations within a node (whereas RF only keeps the mean), which allows to construct prediction intervals and to assess uncertainty (ibid.).

The advantages of QRF include that it can handle multiple input variables, makes no assumptions on distributions and can deal with interactions, non-linearity and non-additive behavior. As limitations, it does not allow for easy interpretation of effects of single predictors and model predictions will always be within the range of observations, i.e. if the predictors in the period of application exceed the range represented in the training dataset (hereafter called 'out-of-observation-range (OOOR) data points'), we can expect over- (or under-) estimations (ibid.) of the target variable, if the respective predictor has a continuing monotonic effect in this range.

With respect to modeling suspended sediment concentrations, studies have shown that QRF is very well-suited to model sedigraphs and estimate annual SSY (Francke et al., 2008b, a; Zimmermann et al., 2012) and that it performs favourably compared to sediment rating curves and generalized linear models (Francke et al., 2008a; Schmidt et al., 2023). On a related note, RF (which QRF is based on) outperformed support-vector machines and artificial neural networks (Al-Mukhtar, 2019) in modeling suspended sediment concentrations.

In a previous study (Schmidt et al., 2023), we trained QRF models on data of the two gauges Vent and Vernagt, using the limited available time series of turbidity (4 and 15 years) and long records of the primary predictors, discharge (Q), precipitation (P) and air temperature (T) (Figure 4.2). These can be seen as drivers or proxies for processes and catchment conditions crucial to sediment dynamics in high-alpine areas: e.g. discharge determines sediment transfer and erosion within the channel, precipitation is key for runoff formation and hillslope erosion, hillslope-channel coupling and the triggering of mass movement events, and air temperature controls the activation of sediment sources (e.g. sub- and proglacial sediments and their transport by glacier meltwaters or hillslope destabilization by permafrost thaw) and whether precipitation occurs as rain or snow. In addition to these primary predictors, we derived ancillary predictors to describe antecedent conditions and cumulative effects thereof: e.g. longer-term discharge behavior may exhaust sediment sources or lead to sediment storage, long warm periods may deplete snow cover and accelerate glacier melt associated with increased subglacial sediment transport, and high antecedent moisture conditions may amplify surface runoff or promote mass movements in response to precipitation events. The final

models performed well and favorably to sediment rating curves, even with respect to threshold effects. For the past 5 decades, OOOR data points (see section 4.2.4.2) were rare, which strengthened the notion that the available training data covered the majority of typical situations.

4.2.2 STUDY AREA

The two studied gauges Vent Rofenache (hereafter 'Vent', operated by the Hydrographic Service of Tyrol) and Vernagt (operated by the Bavarian Academy of Sciences and Humanities) are located in the Rofental in the Ötztal Alps, Austria (Figure 4.3). The two corresponding nested catchments of 98.1 km² and 11.4 km² span elevations ranging from 1891 m a.s.l. at gauge Vent and 2635 m a.s.l. at gauge Vernagt to 3772 m a.s.l. The area is characterized by a relatively warm and dry climate (for this alpine setting), with average annual precipitation as low as 660 mm at gauge Vent but a strong precipitation gradient with elevation (Schmidt et al., 2023). Both catchments are heavily glacierized (28 % and 64 % glacier cover in 2015; Buckel and Otto, 2018), but accelerating glacier retreat has been observed since the beginning of the 1980s (Escher-Vetter and Siebers, 2007; Braun et al., 2007; Abermann et al., 2009). Apart from the glaciers, land cover at high elevations is dominated by bare rock or sparsely vegetated terrain, whereas mountain pastures and coniferous forests occupy lower elevations. Geology is dominated by biotite-plagioclase, biotite and muscovite gneisses, variable mica schists and gneissic schists (Strasser et al., 2018).

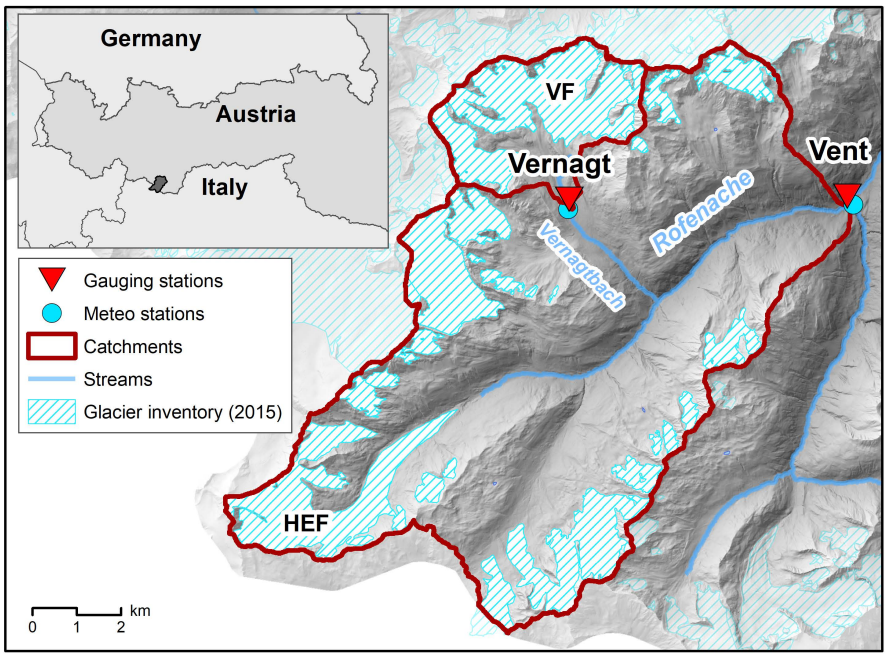

Figure 4.3. *Map of the catchment area above gauge Vent , with nested catchment above gauge Vernagt and major glaciers Vernagtferner (VF) and Hintereisferner (HEF). Meteo stations recording precipitation and temperature are located close to the gauges. (Map based on 10 m DEM of Tirol (Land Tirol, 2016), glacier inventory of 2015 (Buckel and Otto, 2018) and river network from tiris open government data (Land Tirol, 2021).)*

The river Rofenache is a tributary stream of the Ötztaler Ache, one of the largest tributaries to the river Inn. The glacial to nival hydrological regime shows a pronounced seasonality, with almost 90 % of discharge occurring during snow and glacier melt from April to September (Schmidt et al., 2022b). Mean annual suspended sediment concentrations at gauge Vent were the highest in an Austria-wide comparison (Lalk et al., 2014). Annual suspended sediment yields in Vent averaged 1500 t km^{-2} a^{-1} with an even more pronounced seasonality compared to discharge (99 % of the annual SSY transported from April to September) (Schmidt et al., 2022b).

4.2.3 INPUT DATA

4.2.3.1 CLIMATE PROJECTIONS

We used projections of air temperature and precipitation of the European part of the COordinated Regional Downscaling Experiment (EURO-CORDEX) (Jacob et al., 2014), that have been downscaled and bias-corrected for use in their hydrological model by Hanzer et al., 2018. The EURO-CORDEX initiative provides regional climate model results to enable exploring impacts of future climate change at comparatively high horizontal resolution. This is beneficial for modeling future sediment export, for examples since regional climate model simulations provide higher precipitation intensities, which are entirely missing in the global climate model simulations (Jacob et al., 2014), and are thus more likely to capture erosion-relevant changes in precipitation. The data used in this study and by Hanzer et al., 2018, were the result of six different regional climate models (RCMs) driven by five different global climate models (GCMs), resulting in a total of 14 different GCM-RCM modeling chains (Table 4.1). These are forced by three different emission scenarios expressed as representative concentration pathways (RCP), which correspond to an added radiative forcing of 2.6, 4.5 and 8.5 W/m^2 at the end of the 21st century relative to pre-industrial conditions, i.e. RCP2.6 (intervention scenario assuming peak CO_2 concentrations in the middle of the century, followed by slow decline and negative emissions), RCP4.5 (intermediate scenario with peak emissions mid-century followed by strong decline) and RCP8.5 (assuming no implementation of climate mitigation policies, considerably and steadily increasing emissions and greenhouse gas concentrations over time) (Jacob et al., 2014; Hanzer et al., 2018). This results in a total of 31 RCP-GCM-RCM combinations. The horizontal resolution of the original EURO-CORDEX projections is 0.11° (≈ 12.5 km).

Hanzer et al. used statistical downscaling to represent the local scale, i.e. quantile mapping, to match the distributions of the climate model simulations of the current climate to the distributions of observations from stations. This is necessary, especially in Alpine regions, because the 12.5 km spatial resolution of RCMs (despite being comparatively high) can not sufficiently resolve topographical and climatological heterogeneities (Hirschberg et al., 2021). Hanzer et al. interpolated the meteorology to a 100 m grid and we used the projections for the two grid cells that are located closest to the gauges Vent and Vernagt. EURO-CORDEX

simulations are provided at daily resolution, and Hanzer et al., have disaggregated them to 3 h resolution to capture diurnal variability in the energy fluxes. We re-aggregated these data to daily resolution to match the temporal resolution of our QRF models (see section 4.2.3.3).

Table 4.1. Overview of EURO-CORDEX scenario simulations used in this study (unaltered from Hanzer et al. (2018), distributed under CC BY 3.0 https://creativecommons.org/licenses/by/3.0/).

ID	RCM	GCM	RCPs
1	CCLM4-8-17	CNRM-CM5	4.5, 8.5
2	CCLM4-8-17	EC-EARTH	4.5, 8.5
3	CCLM4-8-17	HadGEM2-ES	4.5, 8.5
4	CCLM4-8-17	MPI-ESM-LR	4.5, 8.5
5	HIRHAM5	EC-EARTH	2.6, 4.5, 8.5
6	RACMO22E	EC-EARTH	4.5, 8.5
7	RACMO22E	HadGEM2-ES	4.5, 8.5
8	RCA4	CNRM-CM5	4.5, 8.5
9	RCA4	EC-EARTH	2.6, 4.5, 8.5
10	RCA4	CM5A-MR	4.5, 8.5
11	RCA4	HadGEM2-ES	4.5, 8.5
12	RCA4	MPI-ESM-LR	4.5, 8.5
13	REMO2009	MPI-ESM-LR	2.6, 4.5, 8.5
14	WRF331F	CM5A-MR	4.5, 8.5

4.2.3.2 HYDROLOGICAL PROJECTIONS

We used discharge projections of the physically-based hydroclimatological and snow model AMUNDSEN (Hanzer et al., 2018), which is a fully distributed energy and mass balance model including glacier evolution (Δh method) and particularly adapted to high mountain catchments of small to regional scale. It comprises a glacier retreat module and has been extensively validated for historic conditions, especially with respect to snow distribution (Hanzer et al., 2016). This is especially beneficial for modeling sediment dynamics, since AMUNDSEN can model processes such as changes in glacier melt that govern discharge dynamics and are crucial to sediment fluxes in these high-alpine areas. AMUNDSEN was forced by the downscaled, bias-corrected and temporally disaggregated EURO-CORDEX simulations of precipitation and air temperature described above (as well as relative humidity, global radiation and wind speed), and modeled snow, glaciers and hydrology in the Ötztal Alps until 2100 (ibid.). Hanzer et al. have bias-corrected all RCM outputs using at least 20 years of observations in the period 1971 to 2005, and concluded that the corrected RCM outputs adequately represent the mean and variability of the observed climate. The AMUNDSEN model was calibrated and extensively validated for the period 1997 – 2013, using water-balance-derived mean areal precipitation, snow depth recordings, Landsat and MODIS-derived snow extent maps, glacier mass balances and runoff recordings (Hanzer et al., 2016).

The temporal extent of both the meteorological and the hydrological projections is 2006 to 2100, but since data are not available for the entire year of 2006, we use the period of 2007 to 2100. Additionally, three HadGEM-driven models ended in November 2099. The years 2007 to 2020 overlap with observation data at gauge Vent and results of the previous study at

gauge Vernagt (Figure 4.2), which we utilize to verify our model results (see sections 4.2.4.1 and 4.3.2).

4.2.3.3 ADJUSTMENT OF INPUT DATA FOR THE QRF MODEL

As the QRF models were trained at daily resolution, we aggregated the Q and T projections from 3 h resolution to daily means and P projections to daily sums. However, comparing the AMUNDSEN Q projections to observations in the overlap period (2007 – 2020; see Figure 4.2), showed that underestimation of Q during the glacier melt period at gauge Vernagt and substantial overestimation of Q during the snowmelt period at gauge Vent. Hanzer et al. (2018) have acknowledged that, but have left the overestimations (percent bias (PBIAS) of up to 23 %) unaltered, since 'mainly changes than absolute values are analyzed; these partial biases likely do not affect the main conclusions'. However, in our case, it is necessary to correct the discharge data, since SSY are sensitive to discharge amounts and additionally, unrealistic discharge amounts exceeding the maximum discharge value in the training data represent a challenge (see section 4.2.4.2). Also, it is necessary to represent discharge seasonality, and thus discharge origins, as accurately as possible, as usually more sediment is exported during glacier melt than at similar discharge levels during snowmelt (Schmidt et al., 2022b).

For consistency, we applied the same bias-correction as Hanzer et al., i.e. quantile mapping, using the methodology by (Gudmundsson et al., 2012) as implemented in the R package *qmap* (Gudmundsson, 2016). Due to strong season-dependent biases, Hanzer et al. have performed quantile mapping for each season individually. We followed this approach, yet in order to best represent discharge seasonality, we shifted the limits of the seasons by one month (NDJ, FMA, MJJ, ASO instead of DJF, MAM, JJA, SON), as this corresponded better to seasons with similar characteristics of over- or underestimation.

4.2.4 ANALYSES OF MODEL LIMITATIONS AND UNCERTAINTIES

To analyze model performance and identify the limits of the applicability of the presented QRF modeling approach, we verified the modeled SSY against measurement data in the overlap period (2007 – 2020) (section 4.2.4.1), assessed the frequency of OOOR data points as well as by how much the observation range of the predictors is exceeded in the projections and analyzed whether the modeled SSY are sensitive to changes in these predictors (section 4.2.4.2).

4.2.4.1 VERIFICATION OF MODEL RESULTS BASED ON OBSERVED DATA

To determine how well the SSY projections of our QRF models correspond to SSY derived from turbidity measurements, we compared model results in the overlap period (2007 to 2020) to measurements at gauge Vent. Lacking continuous direct measurements at gauge Vernagt, we used estimated SSY for the years 2007 - 2020 from the QRF model trained on measurements for the years 2000, 2001, 2019 and 2020 (Schmidt et al., 2023) for the comparison (see also Figure 4.2). To simplify the descriptions in the results, we hereafter refer to these estimates as 'observations' as well. As the hydroclimatic projections (and, thus, the SSY projections resulting from thereof) do not mimic the characteristics of single years (let alone month or days), but merely reproduce their distribution, we compared the distributions of observed and simulated annual SSY. To test for significant differences between these distributions, we used the two-sample Kolmogorov-Smirnov test, which is able to handle the non-normal distribution of some groups, as implemented in the R package *stats* version 3.5.1 (R Core Team, 2018). Additionally, we assessed whether the seasonality of sediment export is accurately represented in the model results, by comparing mean monthly SSY.

4.2.4.2 ASSESSMENT OF LIMITS OF APPLICABILITY

As mentioned in section 4.2.1, a known limitation of QRF is that model bias can potentially result if the predictors in the application period exceed the range of observed values used as training data. This limitation is a direct consequence of the numerical characteristics of RF and QRF, which are incapable of extrapolation. In order to assess, how often and to what extent the model results are affected, we performed a series of analyses (overview in Figure 4.4), described in the following.

ANALYSIS OF OUT-OF-OBSERVATION-RANGE DAYS

First, we quantified how often OOOR days occurred for each projection *proj* and predictor *p* (i.e. Q, P or T), as the mean annual number of OOOR days per year:

$$\overline{n_{p,proj}} = \frac{1}{n_{years}} \cdot \sum_{i=1}^{n_{years}} n_{p,proj,i} \,, \qquad (1)$$

where n_{years} is the number of years, and $n_{p,proj,i}$ is the number of OOOR days in a given predictor and projection in a given year *i*. Additionally, we determined the **exceedance extent** (in % of the maximum value in the training data $max(x_{p,train})$), i.e. by how much the maxima in the observations (i.e. the training period) $max(x_{p,train})$ were exceeded on the OOOR days *j* (i.e. in the projection period),

$$e_{p,j} = \frac{x_{p,j} - \max(x_{p,train})}{\max(x_{p,train})} \cdot 100 \quad \forall \quad x_{p,j} > \max(x_{p,train}), \tag{2}$$

where $x_{p,j}$ is the value of the predictor *p* on OOOR day *j*.

Although the same limitations of QRF theoretically also apply to predictors falling *below* the training minima, we did not consider them, since Q and P already contained very low or zero values and cannot fall below zero. Likewise, for T, minimum temperatures are already well below zero and further decrease (if it occurs) is not further physically relevant to sediment transport. Similarly, we only considered summer precipitation at both gauges (i.e. May – September), to exclude snowfall events that are not directly relevant to sediment dynamics.

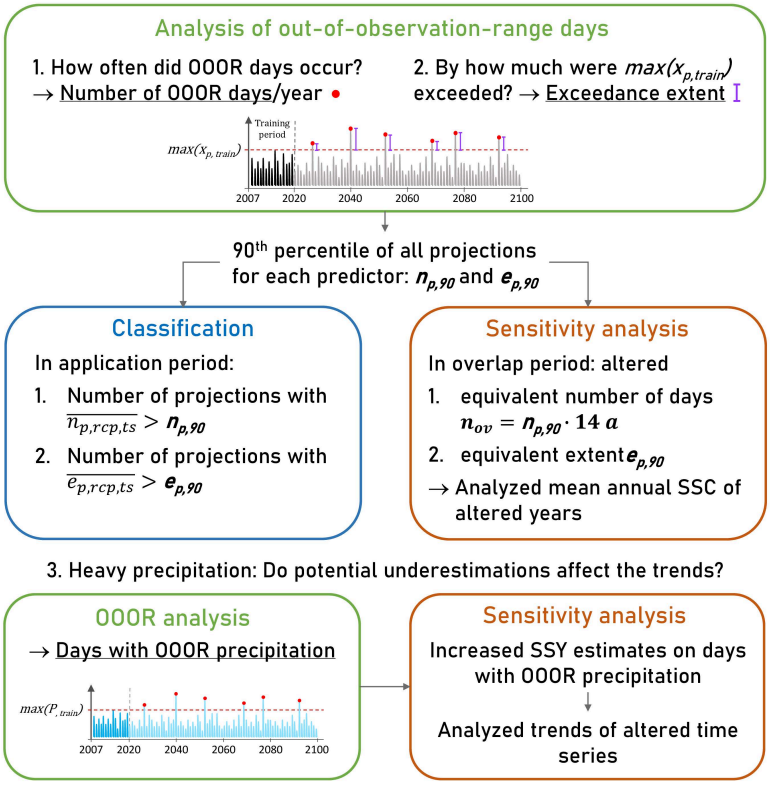

Figure 4.4. *Overview of analyses performed with respect to OOOR days. Max(xp,train) denotes the maximum value in the training data, n refers to the number of OOOR days and e to the exceedance extent. Subscripts: p for predictor, rcp for emission scenario, ts for time slice. The analysis of OOOR precipitation days (3.) is described in section 4.2.5.*

SENSITIVITY ANALYSIS

Second, we performed sensitivity analyses for the three primary predictors Q, P, and T (Figure 4.4), to assess the effects of the abovementioned exceedances on the model results. For this, we determined the 90th percentiles of the number of exceedances $\overline{n_{p,proj}}$, and the exceedance extents $e_{p,j}$ of all projections, i.e. $n_{p,90}$ (in d a^{-1}) and $e_{p,90}$ (in % of $max(x_{p,train})$), for each predictor *p*. These values were considered to represent a severe case for possible model

deficits due to lacking extrapolation capability. We created a respective test datasets for the sensitivity analysis from the 14-year overlap period (2007 – 2020): We selected the corresponding number of days n_{ov} with the highest values of the respective predictor in the, as

$$n_{ov} = \overline{n_{p,90}} \cdot 14\ a \quad \text{(rounded to whole days)}, \tag{3}$$

and altered them by adding or subtracting the respective $e_{p,90}$. For example, $n_{p,90}$ of Q in Vent is 0.55 d a^{-1}, therefore we changed $n_{ov} = 0.55 \cdot 14 \approx 8$ days by the $e_{p,90}$ of 9.6 m³ s-1 (Table 4.2).

We used the resulting altered time series of the primary predictors to compute the corresponding ancillary predictors (that describe antecedent conditions, see section 4.2.1), ran the QRF model with them and compared mean annual SSC after the alterations to the original dataset. Thus, we performed six individual runs for the sensitivity assessment at each gauge, two (one where the predictor was increased and one where it was reduced) for each of the three primary predictors Q, P and T. We chose to compare mean annual SSC instead of annual SSY, as discharge is needed to compute SSY so that the alterations in Q would have affected the estimated SSY twice.

Table 4.2. *Amount of reduction/increase in in the sensitivity models (average exceedance extent $\overline{e_p}$ in units of the corresponding predictor) and number of days with reduction/increase on average per year ($\overline{n_p}$) and in total in the 14-year period (n_{ov}).*

	Q			**P (summer)**			**T**		
	$e_{Q,90}$ [m³ s^{-1}]	$n_{Q,90}$ [d a^{-1}]	n_{ov} [d]	$e_{P,90}$ [mm]	$n_{P,90}$ [d a^{-1}]	n_{ov} [d]	$e_{T,90}$ [°C]	$n_{T,90}$ [d a^{-1}]	n_{ov} [d]
Vernagt	1.5	0.32	4	28.86	0.45	6	3.3	2.75	38
Vent	9.6	0.55	8	25.95	0.54	8	2.02	0.22	3

CLASSIFICATION

Third, we assessed whether the sensitivity analysis was informative for the different RCPs, time slices and predictors, i.e. if the sensitivity analyses contained sufficiently extreme conditions to represent the projections. For this, we determined the mean exceedance extent per predictor p, emission scenario rcp and time slice ts $\overline{e_{p,rcp,ts}}$ and the mean number of OOOR days per year $\overline{n_{p,rcp,ts}}$. We compared these to the ep,90 and np,90, and marked the respective predictor-time slice-RCP combination yellow, if ≥ 1/3 of projections had $\overline{n_{p,rcp,ts}} > n_{p,90}$ or $\overline{e_{p,rcp,ts}} > e_{p,90}$, and red if this applied to ≥ 2/3 of the projections (see Figure 4.5 and Table 4.5).

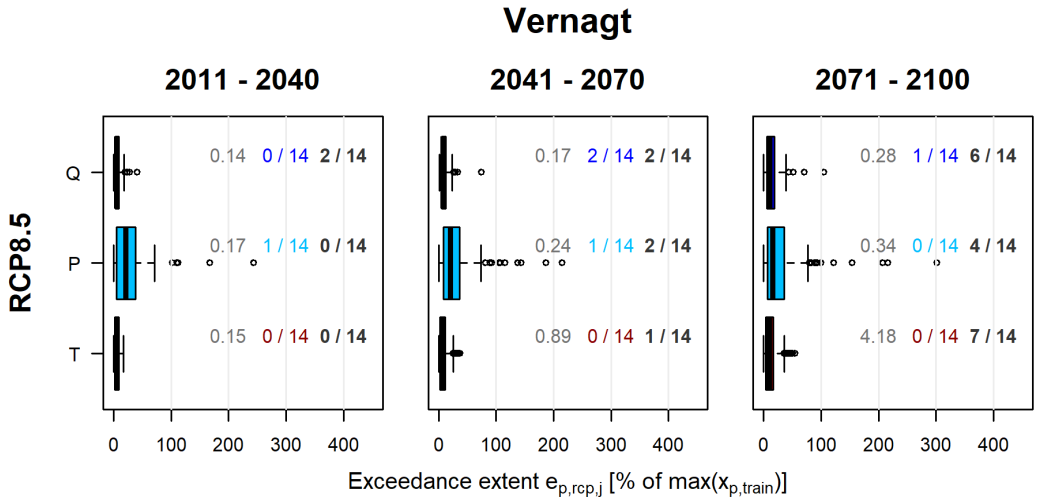

Figure 4.5. *Example of the classification based on the OOOR analysis. The boxplots show the distribution of exceedance extents ep,rcp,j per RCP and predictor on all days j within the respective time slice ts. Grey numbers denote the average* $\overline{n_{p,rcp,ts}}$ *of all projections within the respective RCP, time slice and predictor. Colored numbers indicate the number of projections with mean exceedance extent* $\overline{e_{p,rcp,ts}} > e_{p,90}$*, i.e. projection more extreme than the sensitivity analysis. Black numbers indicate the number or projections with the mean number of OOOR days per year* $\overline{n_{p,rcp,ts}} > n_{p,90}$*, , i.e. projection more extreme than the sensitivity analysis.*

4.2.5 ANALYSIS OF MODEL RESULTS

We analyzed the model results, i.e. estimated annual yields in the application period for trends as well as shifts in seasonality. To assess trends, we used two methods implemented in the R package *FUME* (Santander Meteorology Group, 2012): the Mann-Kendall test, which is a non-parametric tool to detect linear trends (specifically, we used a version that was modified to detect trends in serially correlated time series; Madsen et al., 2014; Yue et al., 2012) and Sen's slope estimator (Sen, 1968) to assess trend magnitude. Further, we compared the estimated yields in three time slices (near future: 2011 – 2040, intermediate future: 2041 – 2070, and far future: 2071 – 2100; see also Figure 4.2), comparable e.g. to Jacob et al. (2014) and Hanzer et al. (2018). To assess changes or shifts in the seasonality of sediment export, we compared the mean monthly yields of the observations and the projections.

To assess whether the detected trends are sensitive to the potential underestimation of yields on OOOR precipitation days, we multiplied the daily yields estimated by our QRF model on these days by a factor of 5, i.e., assuming a very severe underestimation in the original estimates (Figure 4.4). We chose this factor, as it is close to the most severe exceedance extents in precipitation at both gauges, which are 456 % at gauge Vernagt and 442 % at gauge Vent (see also section 4.3.3). We then compared the trends in annual SSY of the altered time series to the trends in the original QRF estimates. All analyses were conducted with the statistical software R (R Core Team, 2018).

4.3 RESULTS

4.3.1 VERIFICATION OF BIAS-CORRECTED DISCHARGE FOR THE PRESENT CLIMATE (2007 – 2020)

The bias-corrected discharge data yield more adequate representations of measured monthly discharge amounts and their seasonal distribution (Figure 4.6), as well as mean annual discharge volumes (Table 4.3). At gauge Vernagt for example, maximum mean monthly Q in the observations and the bias-corrected data is in August, whereas the original AMUNDSEN simulations suggested a maximum in July. Nevertheless, some underestimation of August discharge remains at gaute Vernagt. At gauge Vent, the original AMUNDSEN simulations substantially overestimated discharge amounts in April to July, i.e. the snowmelt period, which was successfully corrected by the bias-correction.

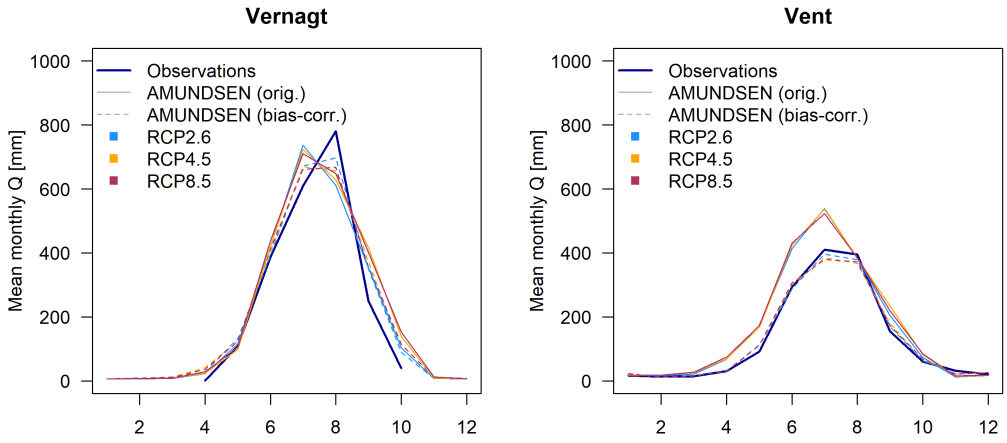

Figure 4.6. *Comparison of mean monthly discharge [mm] at gauge Vernagt (left) and Vent (right) derived from measurements, unaltered multi-model means of the original AMUNDSEN output and multi-model means of the bias-corrected AMUNDSEN output in the overlap period (2007-2020).*

Table 4.3. *Comparison of mean annual discharge volumes based on the original AMUNDSEN output, observations and bias-corrected AMUNDSEN estimates in the overlap period (2007 - 2020).*

Mean annual Q (2007 – 2020) [mm]	Vernagt	Vent
AMUNDSEN (orig.)	2530	1990
Observations	2310	1537
AMUNDSEN (corr.)	2400	1555

4.3.2 VERIFICATION OF MODELED SSY FOR THE PRESENT CLIMATE (2007 – 2020)

We find good agreement between observed and modeled annual SSY at both gauges (Figure 4.7), and the Kolmogorov-Smirnov test does not yield significant differences between the observations and model results in mean annual sediment yields. Nevertheless, years with extremer annual yields (both lower and higher) occur in the model results, especially under RCP4.5 and RCP8.5 (e.g. for Vent, max. 3250 t a^{-1} in RCP4.5 vs. 2120 t a^{-1} in the observations), likely due to the higher sample size in the projections (42 or 196 years in the projections compared to 14 years in the observations, see also description of Figure 4.7).

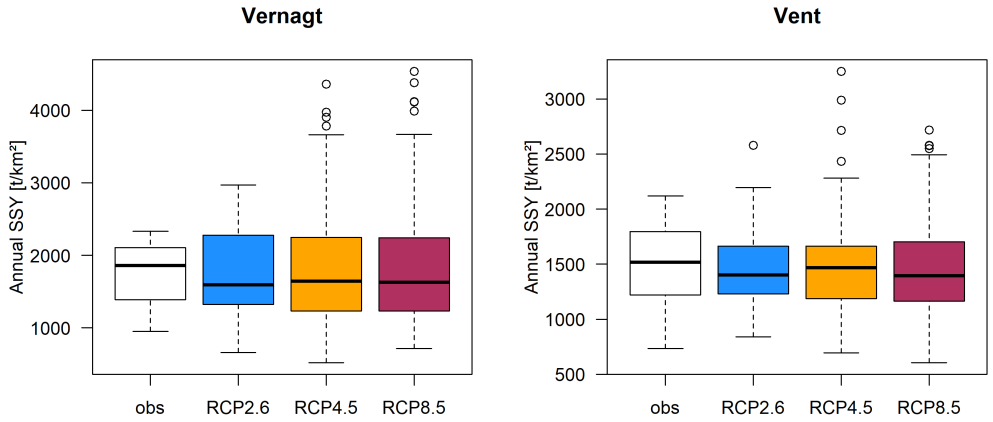

Figure 4.7. *Comparison of annual specific SSY in the overlap period (2007 – 2020) derived from measurements ('obs', n = 14 years) and QRF modeling results per RCP (n = 42 for RCP2.6 and n = 196 for RCP4.5 and RCP8.5, resp.) at gauges Vernagt (left) and Vent (right).*

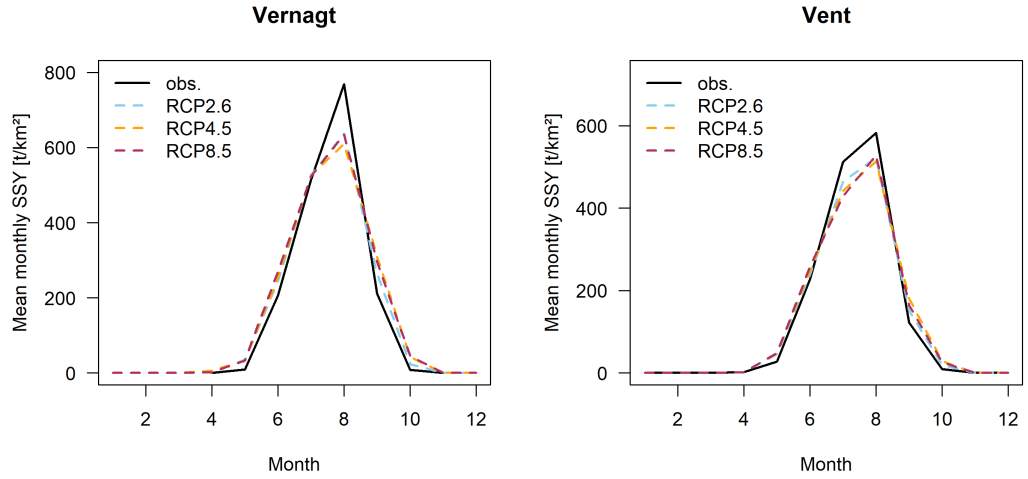

Figure 4.8. *Comparison of observations (see also Figure 4.2) to QRF model forced by climate projections (multi-model means per emission scenario) during the overlap period (2007-2020).*

Similarly, the seasonality of sediment export is well represented in overlap period of the projections (Figure 4.8), and the Kolmogorov-Smirnov test does not yield significant differences to the seasonal distribution of the measurements. Monthly SSY tend to be slightly lower in the projections in August at gauge Vernagt and in July and August at gauge Vent. Similar patterns had already become apparent in the comparison of mean monthly discharges at gauge Vernagt (Figure 4.6).

4.3.3 ASSESSMENT OF LIMITS OF APPLICABILITY

OUT-OF-OBSERVATION-RANGE DAYS

Generally, we find more frequent OOOR days and higher exceedance extents in later time slices and in the higher emission scenarios (Figure 4.A1). At both gauges, OOOR days in Q are relatively rare, but in the higher emission scenarios and later time slices, OOOR days become more frequent and individual exceedance extents of more than 100 % occur (Figure 4.A1 and Table 4.4). Exceedances in temperature are more frequent at gauge Vernagt, especially under RCP8.5 and after 2040. At gauge Vent, there are only few OOOR days in T, except under RCP8.5 after 2070.

Table 4.4. *Mean and maximum exceedance extents ep of the three primary predictors discharge (Q), precipitation (P) and air temperature (T) across all emission scenarios and time slices, in percent of the maximum during the training period max($x_{p,train}$) and original units.*

e_p		Q [%]	Q [m³ s-1]	P [%]	P [mm]	T [%]	T [°C]
Vernagt	Mean	10.1	0.7	29.3	12.8	10	1.4
	Max	105	6.9	456	199.8	54.4	7.9
Vent	Mean	11.8	4.4	24.8	13.1	4.2	0.9
	Max	123	45.4	442	233	16.3	3.6

OOOR data points in summer precipitation are rather rare at both gauges. However, precipitation shows very high exceedances extents of up to ca. 450 % (RCP4.5 after 2070 and RCP8.5 before 2040 at gauge Vent; RCP4.5 after 2070 at gauge Vernagt, Figure 4.A1 and Table 4.4). This corresponds to daily precipitation sums of approx. 280 and 240 mm/day at gauge Vent and Vernagt, respectively, and is equivalent to over a third of the current mean annual precipitation at gauge Vent (687 mm; Hydrographic yearbook of Austria, 2016). Yet even without the most extreme cases, exceedance extents in precipitation can be quite severe, which corresponds to very heavy precipitation events.

SENSITIVITY ANALYSIS

Given the alterations corresponding to the respective $n_{p,90}$ and $e_{p,90}$, the most sensitive predictor is P at gauge Vernagt and Q at gauge Vent (Figure 4.9). Yet although the reductions on the days with the highest P in the overlap period were quite substantial (Table 4.2), the

maximum effect on the mean annual SSC is ≤ 3% at both gauges. Temperature is the second most sensitive parameter at gauge Vernagt, while the alterations at gauge Vent had little effect on mean annual SSC. At gauge Vent, P is the second most sensitive parameter, but with a maximum effect of < 2% on mean annual SSC.

The results of the sensitivity analysis also give indication of the behavior of the QRF model in response to OOOR data points: as expected, we generally observe a decrease in mean annual SSC if we decrease the predictors (Q, P and T), and vice versa. However, for most predictors, the decrease is more pronounced than the increase (although the same days were altered by the same extent). We presume that this is due to the described incapability of QRF to extrapolate. Thus, we can expect to underestimate the additional effect, e.g. of precipitation exceeding $max(P_{train})$.

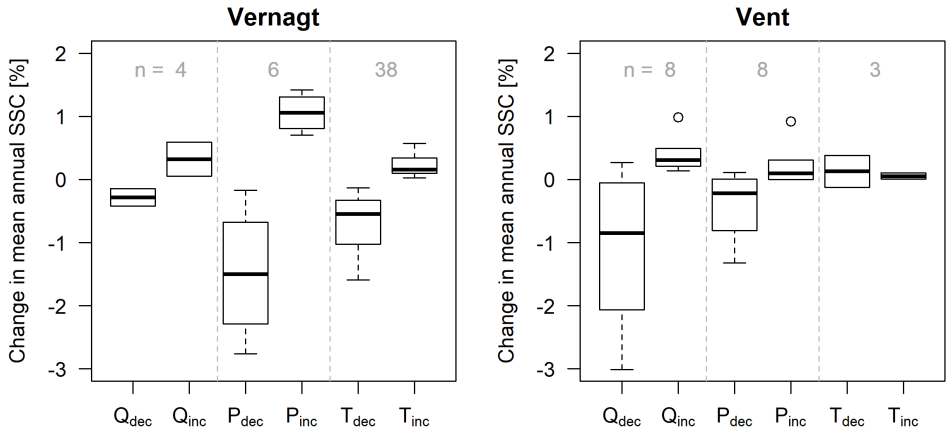

Figure 4.9. *Results of the sensitivity analysis for gauges Vernagt (left) and Vent (right) with respect to mean annual SSC of the years with altered days. Subscripts signify increase (inc) and decrease (dec) in the predictors by the respective average exceedance extent ep,90 and frequency np,90 as identified based on the exceedance analysis. Grey numbers represent the number of altered days.*

CLASSIFICATION

Table 4.5 shows, that until 2070, all predictors and RCPs fall within the conditions covered by the sensitivity analysis (with the exception of Q after 2040 at gauge Vent under RCP8.5). This implies that the results of the sensitivity analysis are informative in these cases, and that we expect similar or smaller effects of OOOR days on mean annual SSC or SSY in the application period. After 2070, exceptions occur at both gauges in two out of three RCPs and several predictors, which implies that the uncertainty is higher than in the results of the sensitivity analysis.

The OOOR analysis showed that very high exceedance extents occur in precipitation and that precipitation is a sensitive parameter at both gauges (although the effect on mean annual SSC was small). Additionally, we find that heavy summer precipitation becomes more intense

(and only slightly more frequent) (Figure 4.A2 in appendix): the 99.95th percentile of the summer precipitation projections increases over time, which suggests that precipitation events become more intense. At the same time, the number of precipitation events that exceed the 99.95th percentile determined from the precipitation observations in the overlap period (2007 – 2020) hardly increases on average, which suggest that precipitation events of a certain strength do not become (much) more frequent. We also find an increase in daily SSY associated with heavy precipitation events (Figure 4.A2 in appendix).

Thus, we additionally assessed whether the trends in annual yields were sensitive to changes in yields on days with OOOR precipitation (sections 4.2.5 and 4.3.4.1), as extreme precipitation can be very important for sediment dynamics (e.g. by triggering mass movements).

Table 4.5. *Results of the classification per emission scenario, predictor and time slice. The color of the field denotes more than 1/3 (yellow) and 2/3 (red, does not occur) of the projections with* $\overline{e_{p,rcp,ts}} > e_{p,90}$ *(assumed in sensitivity); N denotes more than 1/3 (yellow) and 2/3 (red, does not occur) of the projections with* $\overline{n_{p,rcp,ts}} > n_{p,90}$.

		Vernagt			Vent		
		2011 – 2040	2041 – 2070	2071 – 2100	2011 – 2040	2041 – 2070	2071 – 2100
RCP2.6	Q						N
	P			N			
	T						
RCP4.5	Q						
	P						
	T						
RCP8.5	Q			N		N	N
	P			N			
	T			N			N

4.3.4 PROJECTIONS OF FUTURE SEDIMENT EXPORT: CHANGES IN ANNUAL YIELDS, TIMING OF PEAK SEDIMENT AND CHANGES IN SEASONALITY

4.3.4.1 CHANGES IN ANNUAL YIELDS AND TIMING OF PEAK SEDIMENT

The resulting projections suggests an overall decrease in mean annual SSY for both gauges and each of the three emission scenarios, which is more pronounced at gauge Vernagt (Figure 4.10 and Table 4.6). Accordingly, we consistently find significant negative trends in the projections (2007 – 2100) in mean annual SSY (Table 4.6). The differences between the RCPs

are small, and smaller than the spread within individual RCPs (Figure 4.10). Accordingly, trends of mean annual SSY are only slightly more negative in the high-emission scenarios. With respect to the 99th percentile of annual SSY estimates, trends are less strong than for mean SSY estimates at gauge Vent, while at gauge Vernagt, the trends in the 99th percentile are even stronger than for mean annual SSY estimates.

Negative trends were detected for all individual projections as well: at gauge Vent, 26 (out of 31) are significant ($\alpha = 0.05$, Sen's slope ranging from -10.8 to -3.8 t km^{-2} a^{-2}), and at gauge Vernagt, 30 of 31 are significant a ($\alpha = 0.05$, Sen's slope ranging from -15.2 to -6.1 t km^{-2} a^{-2}).

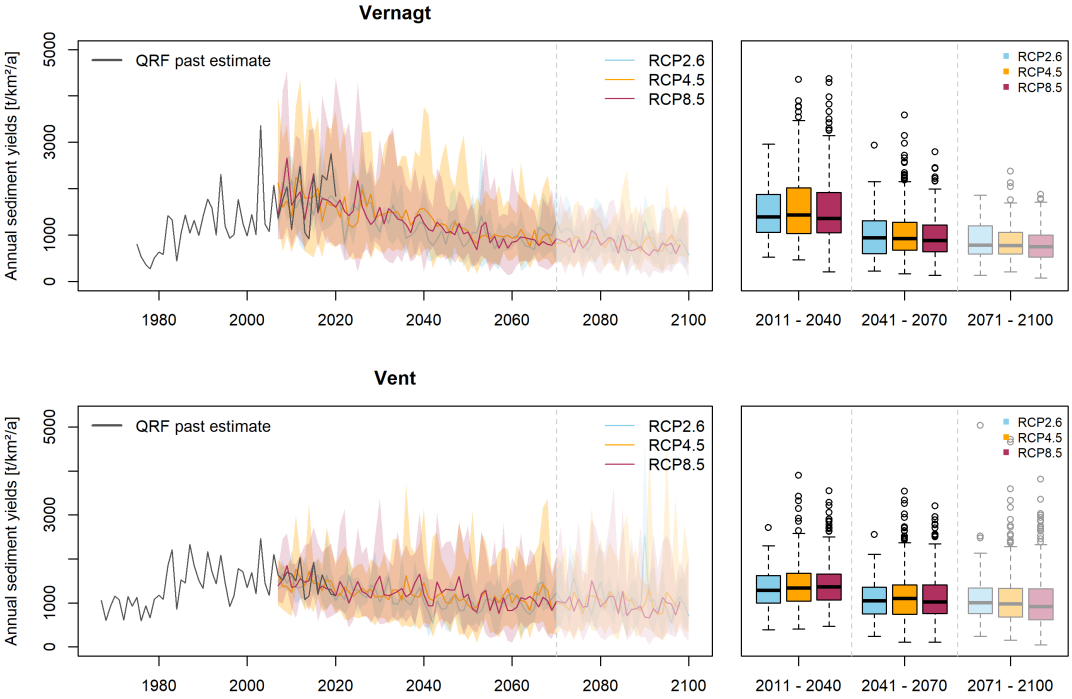

Figure 4.10*. Mean annual suspended sediment yields per RCP (left) with minima and maxima of the individual projections indicated by the colored envelopes. Right: Annual SSY of all respective years and projections within the three time slices.*

The trend in the altered time series (with 5-fold increased daily yields on days with OOOR precipitation; see section 4.2.5) hardly differs from the trend in the original time series (Table 4.6). Specifically, at gauge Vernagt, trend characteristics are basically unchanged. The only trend reversal occurs in the 99th percentile at gauge Vent under RCP8.5, where the trend is slightly positive (and significant) instead of negative. We conclude that the overall trend characteristics remain very robust, even if we assume as severe underestimation of the model on days with OOOR values in the predictors. Thus, the overall future sediment budget seems to be governed by their mean behavior rather than solitary extreme events.

The synopsis with estimates of annual SSY for the past decades shows that we find increases in annual yields at both gauges up until sometime between 2000 and 2020, and

decreases afterwards, which is much more distinct at gauge Vernagt (Figure 4.10). This suggests, that peak sediment has already been reached or is underway at both gauges and occurs simultaneously with peak water.

*Table 4.6. Trends in mean and 99th percentile of annual specific SSY projections (2007 – 2100) given as Sen's Slope [t km^{-2} a^{-2}] for the original estimates and the altered estimates (5-fold increased SSY on days with OOOR precipitation). Significance levels: * = 0.05, ** = 0.01, *** = 0.001.*

Sen's Slope of mean annual SSY [t km^{-2} a^{-2}]		RCP2.6 Original	RCP2.6 Altered	RCP4.5 Original	RCP4.5 Altered	RCP8.5 Original	RCP8.5 Altered
Vernagt	Mean	-10.6***	-10.7***	-11.6***	-11.5***	-12.4***	-12.1***
	99 percentile	-12.3***	-12.3***	-22.6***	-22.3***	-22.3***	-21.3***
Vent	Mean	-4.85 **	-4.97**	-5.0***	-4.67***	-6.41***	-5.6***
	99 percentile	-4.5**	-5.1***	0.5	2.3	-3.1*	0.1**

4.3.4.2 CHANGES IN SEASONALITY

Mean monthly SSY is projected to decrease substantially during the glacier melt period in August in all RCPs and at both gauges (Figure 4.11). This decrease amounts to approx. ⅓ to ½ at gauge Vernagt and approx. ⅓ at gauge Vent. As a result, the highest mean monthly SSY shifts from August to July, or even to June under RCP8.5 after 2070 at both gauges. Additionally, the spring onset of sediment export is projected to occur earlier in the year in the high emission scenarios. This represents a decrease in importance of glacier melt for sediment export. After 2070, only relatively minor further changes are projected under RCP2.6 and RCP4.5, whereas RCP8.5 experiences further decreases in mean monthly SSY throughout the year.

At gauge Vent, a slight increase in mean July SSY is projected after 2070 under RCP2.6. This is likely related to an increase in discharge, since this increase is not visible in mean monthly concentrations (not shown). It also has to be considered that only three projections are averaged for RCP2.6 (as compared to 14 in the other RCPs), which makes it less robust with respect to outliers.

A comparison to the seasonal distributions determined from the altered time series (5-fold increased SSY on days with OOOR precipitation), showed only very slight differences, which indicates that the seasonal distribution is also insensitive to underestimations of SSY on days with heavy precipitation.

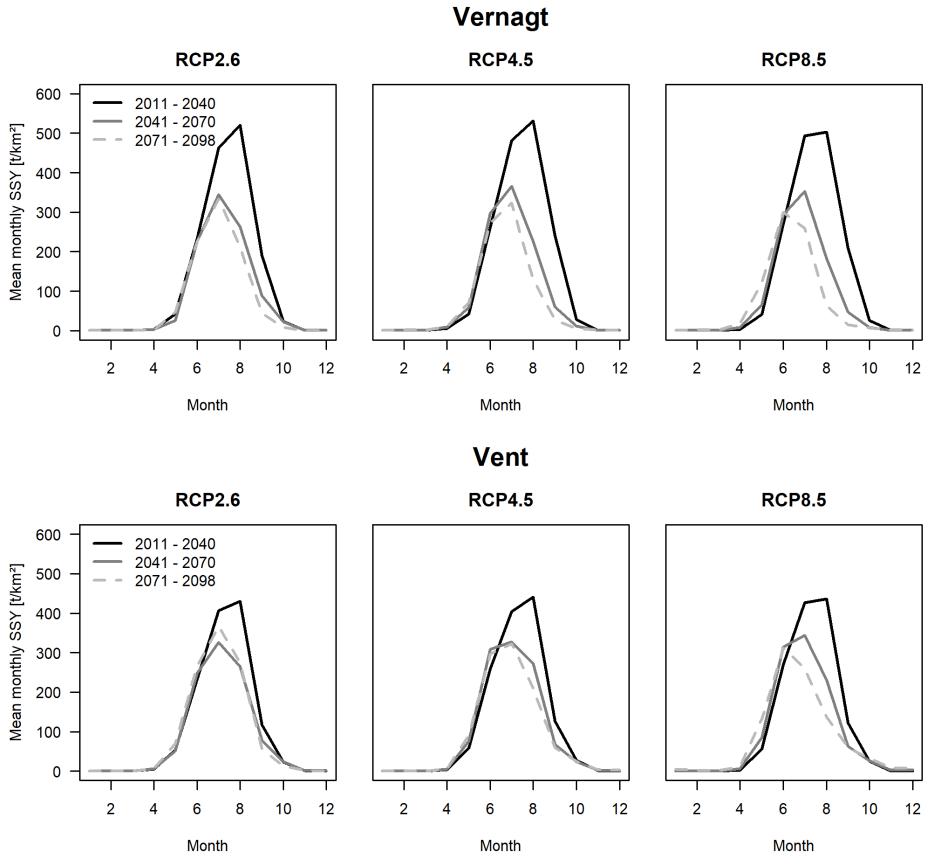

Figure 4.11. *Seasonality of mean monthly SSY in three time slices and emission scenarios.*

4.4 DISCUSSION

Testing new methods to estimate future suspended sediment export from glacierized high-alpine areas can provide important information, e.g. to flood hazard, sediment or water quality management, since estimating such changes had so far been limited to relatively rough approximations. This study represents the first attempt to our knowledge to derive SSY projections using a machine-learning approach and investigate them in synopsis with reconstructed past SSY.

PROJECTED CHANGES IN SEDIMENT EXPORT AND LOCATION OF PEAK SEDIMENT

The presented SSY projections in the Ötzal, Austria, suggest an overall decrease in annual SSY. This is consistent across emission scenarios as well as all individual projections (i.e. based on the 31 different RCP-GCM-RCM-chains). The decrease is much more distinct at gauge Vernagt, where a trend analysis in the previous study (Schmidt et al., 2023) showed significant

positive trends in the period until 2020. At gauge Vent, significant positive trends were detected if all data points since the 1970s are considered (ibid.). However, if only the years after the distinct increase around 1980 were considered, the trend was slightly negative (ibid.). This suggests that peak sediment has already been reached or is underway at both gauges and occurs simultaneously with peak water.

These findings match expectations of conceptual models, that sediment yield from deglaciating basins will initially increase (due to increases in glacial erosion, sediment supply accessibility, transport capacity and occurrences of extreme floods) and subsequently decrease, as glacier masses decline, meltwater volumes and freeze-thaw weathering decrease, and vegetation colonizes (Antoniazza and Lane, 2021; Zhang et al., 2022). It is expected that peak sediment may lag behind peak meltwater, with a lag that can be up to decades or centuries (Delaney and Adhikari, 2020). This lag is hypothesized to be scale-dependent, i.e. will be shorter for areas closer to the glacierized regions, and to depend on the changes in erosive precipitation: if erosive precipitation decreases, peak sediment occurs simultaneously with peak water, while increasing or stable erosive rainfall scenarios are associated with a lag (Zhang et al., 2022). Indeed, for the study area of this study, a decrease in summer precipitation sums (i.e. June to August, which is the time of minimum snow-cover and thus maximum erodibility) is projected (Hanzer et al., 2018), and our estimates suggest that peak sediment coincides with 'peak meltwater'.

Sediment export projections differed only slightly (if at all) between emission scenarios, i.e. the spread between projections within one emission scenario is much larger than differences between ensemble means of the three RCPs. It should be noted, that comparisons to RCP2.6 need to be treated with care, as it comprises less GCM-RCM combinations (only 3 as compared to 14 in the higher emission RCPs). Nevertheless, the absence of major differences between RCPs is in accordance with findings by Gobiet & Kotlarski (2020), that 'until the middle of the 21st century [...] it is projected that climate change in the Alpine area will only slightly depend on the specific emission scenario.' Accordantly, Hanzer et al. (2018) projected glacier volumes to decline by 60-65 % until 2050 'largely independent of the emission scenario'.

CHANGES IN SEASONALITY AND RESPONSE TO HEAVY PRECIPITATION EVENTS

Despite the overall decrease in SSY, our results suggest that high annual SSY are possible, especially at gauge Vent and towards the end of the century, and that yields on days with heavy precipitation may increase at both gauges – in absolute terms and in relation to the annual export. This is reasonable, given that increases in heavy precipitation intensity and/or frequency in the European Alps have been detected in measurement data from the past (e.g. Hiebl and Frei, 2018; Scherrer et al., 2016; Gobiet and Kotlarski, 2020), as well as future projections (Gobiet and Kotlarski, 2020; Jacob et al., 2014; Kotlarski et al., 2023) – despite the overall decrease in summer precipitation mentioned above. As a result, we can expect an increase in sediment-related harmful events triggered by heavy precipitation, such as flash

floods and gravitational mass movements (i.e. debris flows, landslides) (Huggel et al., 2012; Savi et al., 2020; Gobiet and Kotlarski, 2020). Similar expectations, i.e. increasing high-magnitude transport events in the context of an overall decrease, have e.g. been expressed with respect to bedload in South Tyrol (Coviello et al., 2022). Such a development would have important implications e.g. for flood hazard management, as the flood risk can increase if cross-sections are reduced after sedimentation and potential backwater effects need to be considered (Nones, 2019), and where much of the damage is associated with transported solids rather than the water itself (Badoux et al., 2014).

Our findings suggest a shift in sediment export seasonality, since the highest mean monthly SSY shifts from August to July (or even June), due to substantial reductions in sediment export in July, August and September at both gauges. This is linked to the projected distinct reductions in glacier melt (Hanzer et al., 2018) and appears reasonable given that glacier melt has so far been the dominant transport medium of suspended sediments at these gauges (Schmidt et al., 2022b). These results are not sensitive to potential underestimations of SSY on days with very heavy precipitation. Such shifts in seasonality and the concomitant overall reduction in fluvial sediment transport will likely have severe effects on biodiversity, i.e. flora and fauna of glacier-fed streams (Milner et al., 2009, 2017; Gabbud and Lane, 2016; Huss et al., 2017).

LIMITATIONS

As a potential limitation to the presented Quantile Regression Forest approach, out-of-observation-range data points in the predictors can lead to underestimates in SSY on the affected days. Yet, the analysis of such incidents in synopsis with the results of the sensitivity analysis showed that before 2070, the effect on annual yield estimates is ≤ 3%. This is very small given the overall high variability in SSC (Vercruysse et al., 2017; Delaney et al., 2018b; Schmidt et al., 2022b). On a similar note, even assuming rather generous increases of yields on days with OOOR precipitation altered the trends only marginally, which shows that underestimations on individual days with OOOR precipitation has little effect on long-term annual averages. However, we have less confidence in the model results after 2070 for two reasons. First, more frequent and severe OOOR incidents occur during this time, especially in the high-emission scenarios, and fewer projections are covered by the assumptions of the sensitivity analysis. We can therefore expect a higher uncertainty in the model results. Specifically, the effect of underestimation for single large events will aggravate. Second, more than a few glacier simulations suggest that glaciers could have disappeared almost entirely by 2070 (Hanzer et al., 2018), which implies a major shift in the hydro-sedimentological functioning of these catchments. While our QRF models were able to model threshold effects better than sediment rating curves (Schmidt et al., 2023) (likely because they are not bound to linear or monotonous relationships), this is only true for effects that are represented in the training data. Thus, the results for the period after 2070 need to be treated with caution. We have indicated this in the presentation of our results by using transparency or dashed instead of solid lines.

As a more general limitation, there are several other factors with the potential to substantially alter and influence sediment dynamics in the study area, which we cannot consider in our models. This concerns geomorphological changes, such as increased paraglacial erosion: debuttressed slopes may trigger landslides and rockfalls, and indeed, increased debris flow and rockfall activity have been shown in response to warming in other areas, likely associated with intensified alpine permafrost thaw (Savi et al., 2020; Hartmeyer et al., 2020; Huggel et al., 2012). Additionally, sediment availability and accessibility increase as erodible landscapes expand (Li et al., 2021a), and subglacial sediment availability might also increase (more subglacial sediment can be accessed by meltwaters as the equilibrium line altitude retreats upslope) until the glacier size becomes smaller than a critical size (Delaney and Adhikari, 2020; Zhang et al., 2022). Although these processes are likely already partially reflected in the observations used for the model training, their intensity may still be too low to be sufficiently learned by the model. Thus, future intensification of these processes could lead to higher sediment export rates than our estimates suggest, and might thereby affect the estimated location of peak sediment. Notwithstanding, there are also several factors that could lead to decreases in sediment export, such as decreases in connectivity (such as the formation of supra-, sub- or proglacial lakes or outwash fans which act as sediment traps) or decreasing glacial erosion as glaciers recede (Zhang et al., 2022). Additionally, freeze-thaw weathering may decrease (Hirschberg et al., 2021) and it is not clear how quickly the deglaciating landscapes will stabilize, e.g. through eluviation of fine materials and fluvial sorting of sediment, which progressively increases the resistance to entrainment and transport (Ballantyne, 2002; Lane et al., 2017), or vegetation colonization (Haselberger et al., 2021; Altmann et al., 2023; Musso et al., 2020; Eichel et al., 2018). Many of these processes are ultimately governed by temperature and/or precipitation, and we have chosen the predictors to act as proxies (e.g. antecedent moisture and temperature conditions could be crucial for mass movements). While this is out of scope of the presented study, we encourage future studies to work towards including more advanced proxies for geomorphological changes.

UNCERTAINTIES

The presented results are associated with uncertainties, which are a combination of uncertainties inherited from the underlying climatological and hydrological projections and uncertainties inherent in the QRF approach. Climate model uncertainty represents a combination of uncertainties in assumptions of future anthropogenic greenhouse gas emission, GCM uncertainty (different GCMs produce different responses to the same radiative forcing) and RCM uncertainty (different RCMs forced by same GCM produce different regional responses) (Evin et al., 2021; Gobiet et al., 2014). It has been found that EURO-CORDEX simulations may be biased towards 'too cold, too wet, too windy', but that these uncertainties are mostly within the observational uncertainties, and that simulations 'reproduce fairly well the recent past climate despite some biases' (Vautard et al., 2021). To address this, it was recommended to carry out bias-correction, which has been performed by means of quantile mapping for the precipitation and temperature projections (Hanzer et al., 2018). The hydrological model results are also associated with uncertainties, such as the tendency to overestimate spring runoff, winter snow accumulation and glacier mass balances. We have

addressed this through bias-correcting the discharge projections, which resulted in a more adequate representation of discharge seasonality and volumes. Certainly, bias-correction methods such as quantile mapping in turn introduce uncertainties, e.g. by assuming that the biases are stationary, i.e. do not change over time (Gudmundsson et al., 2012). Hydrological simulations that do not show the necessity for this correction could eliminate this issue. Uncertainties in the QRF approach have been addressed in a previous study, and include the tendency to underestimate rare, high-magnitude daily SSY (albeit with small effects on the respective annual yields), the underestimates on days with OOOR values (which had small effects until 2070, as discussed in detail above) and the choice of temporal resolution (i.e. daily compared to hourly resolution involves some loss of information, e.g. on precipitation intensities, but the effect was also found to be small) (Schmidt et al., 2023). Since QRF is a data-driven approach, the quality of the estimates hinges on the underlying training data set as well as the choice of predictors, i.e. a large and varied enough dataset in combination with predictors that meaningfully represent the most important processes improve the quality of the estimates (ibid.). Thus, future studies are recommended to explicitly sample extreme events, and/or verify the representativity of the training dataset.

4.5 CONCLUSION

We found decreasing trends in annual SSY at both gauges regardless of the emission scenario, which suggests that peak sediment was already reached between 2000 and 2020. These findings persist even if yields on days with projected heavy precipitation are inflated by a factor of five. Despite the projected overall decrease, high(er) annual yields are possible, likely in response to heavy summer precipitation. This discrepancy has important implications for sediment management, but also e.g. of flood management.

To our knowledge, this study represents the first attempt to combine machine learning for suspended sediment modeling with climate and hydrological projections, in order to derive projections of sediment export in high-alpine areas. It demonstrated that Quantile Regression Forest can be a valuable tool for this application. We addressed known issues of QRF, i.e. underestimations on days where predictors in the application period exceed the range represented in the training data. The influence on the results showed to be negligible until 2070. We conclude that the presented results are much more uncertain after 2070, partly because of more frequent and severe out-of-observation-range data points, but mainly since a major shift in the functioning of the hydro-sedimentological system can be expected as deglaciation is quasi completed.

However, while the chosen predictors represent proxies for crucial processes controlling sediment transport in these high-alpine environments, several potentially crucial geomorphological factors, that could increase or decrease sediment export (and thereby change the projected trends and location of peak sediment) could not be taken into account.

These include increases in rockfalls and landsliding, changes in connectivity or vegetation colonization. Future studies are encouraged include these factors more explicitly.

4.6 CODE AND DATA AVAILABILITY

The model code, input data and results are published under DOI 10.23728/b2share.5f706863fc5041c49cb8d1a8cd55f613.

4.7 ACKNOWLEDGEMENTS

This research was funded within the DFG Research Training Group 'Natural Hazards and Risks in a Changing World' (grant nos. NatRiskChange GRK 2043/1 and GRK 2043/2) and by a fieldwork fellowship of the German Hydrological Society (DHG).

The authors would like to thank Florian Hanzer and Ulrich Strasser for providing the projections required as input data for this study. We thank the Hydrographic Service of Tyrol, Austria, and the Bavarian Academy of Sciences and Humanities for the provision of data as well as logistical support. We thank Marvin Teschner for his support in data analyses.

4.8 APPENDIX

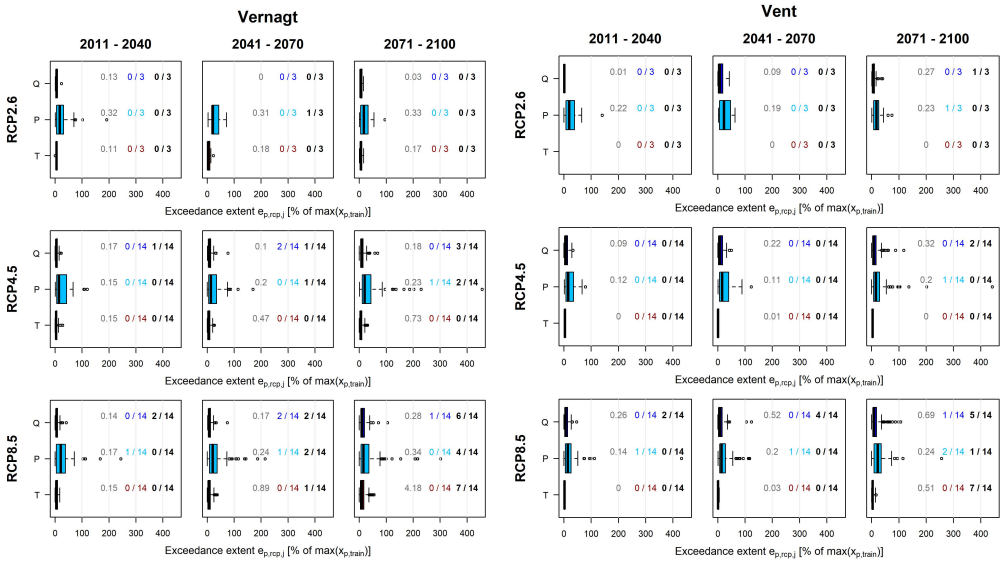

Figure 4.A1. *Results of the classification, based on the sensitivity and OOOR analyses. The boxplots show the distribution of exceedance extents for each RCP and predictor on all days j within the respective time slice ts. Grey numbers denote the average* $\overline{n_{p,rcp,ts}}$ *of all projections within the respective RCP, time slice and predictor. Colored numbers indicate the number of projections with mean exceedance extent* $\overline{e_{p,ts}} > e_{p,90}$ *(as used for the sensitivity analysis). Black numbers indicate the number or projections with the mean number of OOOR days per year* $\overline{n_{p,ts}} > n_{p,90}$ *(as used for the sensitivity analysis).*

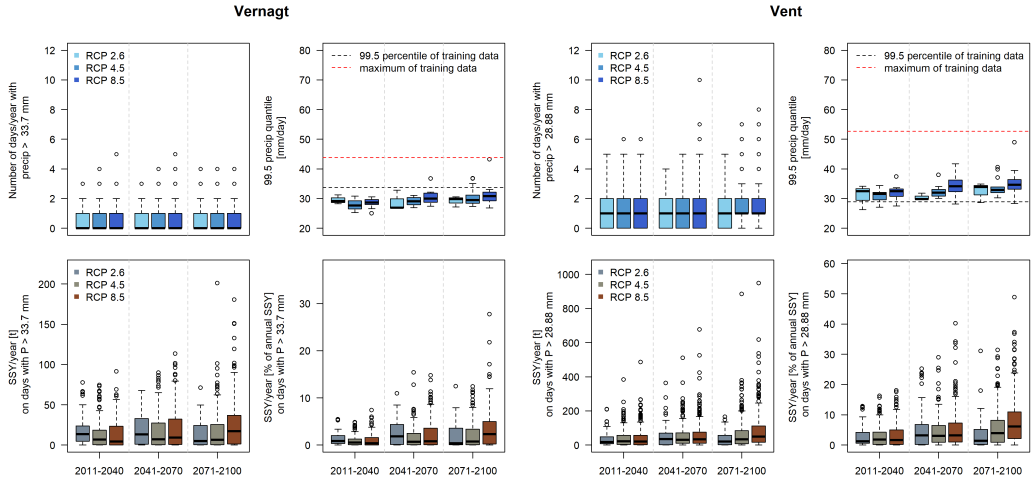

Figure 4.A2. *Analysis of summer precipitation projections (top) and SSY projections (bottom) at gauges Vernagt and Vent. Top left of each panel: frequency of days with heavy summer precipitation (> 99.5 percentile of the training data, i.e. and 33.7 mm/d (Vernagt) and 28.88 mm/d (Vent)). Top right: intensity of heavy summer precipitation events over time, expressed as the 99.5 percentile. Bottom left: Sediment export on days with precipitation > 99.5 percentile of the training data. Bottom right: Sediment export on days with precipitation > 99.5 percentile of the training data relative to the respective annual yields*

5 OVERARCHING DISCUSSION

The main purpose of this thesis was to estimate past and future sediment export from a high-alpine area, and investigate whether quantile regression forest can be a suitable approach for this purpose. In the following, I will proceed with an integrated discussion of how the results of the three manuscripts included in this thesis contribute to answering the research questions, and link the individual chapters to the overall aim. Finally, I will deduce future research directions in the outlook section and summarize what we have learned in the conclusion.

5.1 RQ 1: LEARNING FROM OBSERVATIONS OF PRESENT DYNAMICS

The first research question aimed to identify the predictors, areas within the catchments and time periods that are most important for sediment export in the study area, based on the years with available measurements (i.e. 'the present'), in order to be able to prioritize and inform the model setup for chapters 3 and 4. In the following, I will describe the findings and the decisions made in the model setup of chapters 3 and 4.

5.1.1 PREDICTORS

Chapter 2 showed that discharge alone was insufficient to explain sediment export in the study area. This became apparent through the virtually non-existent relationship between annual discharge and annual SSY at all three investigated gauges (Figure 2.5) and the lag between the spring increase in discharge and the spring onset of sediment transport (Figure 2.7 and Figure 2.8.). It is also reflected in the low performance of univariate sediment rating curves in chapter 3 (Figure 3.5). This illustrates that multivariate approaches are preferable.

Chapter 2 also concluded that in 'the present', sediment dynamics were dominated by melt-driven processes, i.e. that precipitation events played a subordinate role compared to thermally induced sediment transport. This was supported by the notion that annual glacier ablation of the two largest glaciers in the Vent catchment explained annual SSY much better than annual discharge yield (Figure 2.5 and Figure 2.6), that mean annual SSY increased with increasing glacier cover (Figure 2.4) and that differences between mean annual sQ and sSSY of the three sub-catchments were mainly due to differences during the glacier melt period (Figure 2.3.). While this might appear trivial, it constitutes an important difference to the non-cryospheric

environments that QRF models had been applied to in the past (Spain and Panama), and illustrates that it is crucial to include temperature as a predictor.

5.1.2 AREAS AND ALTITUDES

Chapter 2 showed that areas above 2500 m a.s.l. are crucial for sediment dynamics in the Ötztal, as the onset of sediment transport in spring, which lagged behind the spring increase in discharge, coincided with snow cover reductions above 2500 m (Figure 2.8). Thus, although discharge is available as a transport medium earlier in the year (Figure 2.7), sediment export only starts once the areas characterized by glacier tongues, the most recently deglaciated proglacial areas, a high permafrost probability, a low vegetation cover and bare rock surfaces (Figure 2.9) become snow-free. Assuming that the reduction of snow cover is a proxy for whether or not an area is frozen and thus active in terms of sediment dynamics, this can be interpreted as the susceptibility of unfrozen and not glacier-covered, loose material to detachment, by means of fluvial transport as well as pluvial erosion. Additionally, once the snow covering the glaciers starts to melt (which may not be visible in the MODIS data), this likely initiates the onset of glacier melt and thus also subglacial sediment transport. While the MODIS-derived snow cover data were only available for the years 2002 to 2018 and thus could not be considered as a predictor directly, these findings informed the decision about which sub-catchments the modeling should focus on.

5.1.3 TIME PERIODS

Chapter 2 showed that precipitation events – so far – played a subordinate role as compared to thermally induced sediment transport, but still constituted around ¼ of the annual export in the Vent and Tumpen catchments. This was surprising, given that experts familiar with the catchments and sediment dynamics in the area had expected that individual high-magnitude events might contribute a higher share (around 50 %) of the annual yield (pers. comm. with Dr. Johannes Schöber). Additionally, this represents an important difference to non-glaciated, lower-lying areas, where the majority (up to 90 %) of the annual sediment yield can be exported during short, high-discharge events (Delaney et al., 2018b).

This implies that sediment availability and/or mobilization is higher than in other fluvial systems, i.e. that in the study area, sediment export is more continuous because the transporting agents (i.e. discharge) have more continuous access to sediment supplies in the catchment. For one, these supplies can be constituted of formerly subglacial sediment stores that are exposed as glaciers retreat, and provide large amounts of unconsolidated sediments for fluvial transport from the proglacial area. Additionally, chapter 2 showed that individual precipitation events that had triggered mass movements were associated with up to 26 % of the respective annual sediment yield within just over 24 h (section 2.4.5). Such short events (see also section 2.3.6), mobilize and expose large amounts of sediments – leading to high

sediment yields during the event, but also facilitating transport from the deposits in the longer term. This also illustrates the importance of including antecedent precipitation as a predictor, as heavy precipitation events may lead to pulse-like sediment export in the short-term, as well as elevated sediment export levels in the days and weeks (maybe even months or years) following the event.

5.1.4 RESULTING DECISIONS IN THE MODEL SETUP

Based on these findings of chapter 2, we firstly focused attention on the Vent catchment and its sub-catchment above gauge Vernagt (Figure 3.1), as larger fractions of these catchments are located above 2500 m a.s.l., compared to the catchments above gauges Sölden or Tumpen (Figure 2.1). Secondly, we considered the changing roles of glacier melt and precipitation in Chapters 3 and 4.

Third, we chose the set of predictors for chapters 3 and 4, as outlined in Table 5.1. As Figure 1.1 illustrates, precipitation and temperature are the meteorological drivers that are changing due to climate change, and discharge represents an integrated catchment response to said changes as well as a proxy for transport capacity. We additionally computed ancillary predictors describing the antecedent conditions in non-overlapping time windows (e.g., 24 h, 24–72 h, 72 h to 7 d and 7 to 20 d ahead of each time step; see section 3.3.2 and Zimmermann et al., 2012). This was to capture hysteresis effects, such as increased glacier melt after prolonged warm periods due to widespread removal of the snow covering the glaciers, or potential increases in hillslope instability due to high antecedent moisture conditions. However, since the length of these time windows was optimized in the model training process (section 3.3.2), the considered time periods differed between the gauges. Thus, for simplicity, these predictors are summarized as 'antecedent' conditions in Table 5.1.

Table 5.1. *Overview of the predictors selected for the QRF models and presumably approximated processes. Precipitation, temperature and discharge for every time step are in the resolution of the model (i.e. daily or hourly), while antecedent conditions are calculated for days – weeks ahead of each time step (see also section 3.3.2).*

Predictor	Approximated processes
Precipitation	Hillslope erosion, coupling of hillslopes to channel, overland flow, mass movements, sediment mobilization in river bed, dilution
Antecedent precipitation	Hillslope (in)stability, Hillslope erosion, Mass movements, permafrost thaw
Temperature	Activation of sediment sources, erosive effect of precipitation (rain or snow?), snow and glacier melt
Antecedent temperature	Hillslope (in)stability: permafrost thaw, frost cracking, mass movements, remaining snow cover
Discharge	Glacier melt, snow melt, areal precipitation, sediment transport capacity, sediment mobilization in river bed
Antecedent discharge	Exhaustion of sediment sources (?), antecedent snow and glacier melt
Day of year	Seasonality
Rate of change in discharge	Sediment mobilization in river bed, distinction between glacier melt and snow melt

5.2 RQ 2: QRF TO ESTIMATE SEDIMENT EXPORT FROM HIGH-ALPINE AREAS

The second research question aimed to assess whether quantile regression forest is a suitable approach to estimate past and future sediment export in the study area. In the following, I will detail the identified advantages and limitations of the approach.

5.2.1 ADVANTAGES

Chapter 3 demonstrated that the QRF model was able to meaningfully estimate daily (and hourly) SSC and Q_{sed}, as well as annual yields (Figure 3.3 - Figure 3.5). This was demonstrated in the validation, for which we leveraged the data availability at gauge Vernagt: Here, two 2-year datasets of SSC exist at an interval of almost 20 years, so that we trained separate QRF models on each of the 2-year datasets and compared the resulting estimates against measurements of the remaining two years (Figure 3.4). This showed overall good performance of the models and therefore good ability of temporal extrapolation (sections 3.4.2 and 3.6.1), but also showed that – naturally – the model performance depends on the training data set. For example, the model trained on the years 2019 and 2020 performed better than the model trained on the years 2000 and 2001 (Figure 3.4), which is likely due to a more varied dataset in the later two years (i.e. higher discharge and temperature values, for example). This points at the importance of assessing the representativity of the training data, e.g. through the number and magnitude of out-of-observation-range data points, as suggested in chapter 3.

The final models performed well or very well, as demonstrated by the comparison of out-of-bag estimates (section 1.6.1) to measurements (NSE of 0.6 and 0.82 for daily SSC, at gauge Vent and Vernagt, respectively; section 3.4.4). Days with exceptionally high SSY and Q_{sed} tended to be underestimated, but the underestimation of rare events at daily scale had limited effect on annual estimates.

Chapter 3 also showed that QRF outperformed univariate sediment rating curves by about 20 percentage points of explained variance when considering mean daily SSCs and Q_{sed}, and the difference was even larger for the derived annual SSY (section 3.4.4). This is reasonable against the background of findings from chapter 2, i.e. the importance of temperature and precipitation in addition to discharge. This indicates that discharge-related variables (e.g. transport capacity) alone are not sufficient and that variations in sediment supply need to be approximated as well.

At gauge Vent, we compared SRCs and QRF performances in five-fold cross-validations, which showed that QRF performed much better – especially in the periods that contained the highest sediment export events, induced by heavy precipitation events (Table 3.1 and section 3.4.2). This illustrates that QRF can deal better with threshold effects than SRCs, since it is not bound to linear or monotonous relationships. This constitutes an important advantage

over SRCs, and likely also other linear approaches such as generalized linear models (section 1.4), and implies that – although we face technical limitations in the case of out-of-observation-range data points – QRF appears to perform better with respect to heavy precipitation events.

Advantages compared to other modeling approaches can only be derived to a minor degree from the present work. A key advantage compared to conceptual models is the possibility to derive concrete timings, changes in seasonality and magnitude of sediment yields for individual catchments – given the availability of the required data. This is accompanied by the inherent ability of QRF to assess uncertainty, which was also assessed in chapter 3. While it is out of scope of this thesis, a direct comparison to other machine-learning approaches would be interesting for future studies. For example, it is not straightforward to theoretically infer whether other machine-learning approaches (such as support vector machines or artificial neural networks) would perform better at extrapolating beyond the range of values represented in the training data (see below). However, there is some indication that artificial neural networks do not necessarily perform well in that case (Courtois et al., 2023; Hasson et al., 2019). Such comparative studies are facilitated by the present work, as the necessary data have been gathered and prepared for modeling and are openly available.

5.2.2 LIMITATIONS

A technical limitation of QRF, it that is not possible to extrapolate beyond the range of values represented within the training data set, leading to potential underestimation on days with out-of-observation-range (OOOR) data points. In chapter 3, OOOR days were very few and we concluded that the number or OOOR data points can be leveraged to assess whether the training dataset is sufficiently representative to extrapolate in time. In chapter 4, we used the number of OOOR days and the severity of the respective exceedances to inform a sensitivity analysis (section 4.2.4.2) and estimated the effect of this technical limitation on the annual yield and trend estimates (section 4.3.4.1). This showed that the effect on the annual yield estimates was small ($\leq 3\%$) before 2070 and that the estimated trends were insensitive to a 5-fold inflation of yields on days with OOOR precipitation. We concluded that the estimates after 2070 need to be treated with caution, as the near-completion of deglaciation in more than a few projections (Hanzer et al., 2018) will lead to a major shift in the geomorphological functioning of the catchments, as the direct influence of glaciers, e.g. through subglacial fluvial transport of sediments, diminishes or ceases, while hillslope instability (or, more generally, paraglacial erosion) increases, e.g. due to debuttressing, oversteepened moraines, and/or permafrost melt (see section 1.1). Since this is distinctly different from the conditions the model was trained on, reliability of the model results decreases.

Another characteristic of QRF, which can be seen as both a limitation and an advantage, is its black-box nature. While this approach is well-suited to problems where the input and output data are well-understood, but the processes relating the two are very complex, as in high-alpine sediment dynamics (see section 1.4), it also limits our understanding of what the model has learned. One rather simple way to peek into the black box is to assess feature importance, i.e.

the loss of model performance (or increase in the model's prediction error) if values of a variable are randomly permuted (Boehmke and Greenwell, 2019). This is implemented in QRF, but the interpretation is complicated if variables are (highly) correlated, i.e. if information in one variable is shared by another. For example, we can assume that temperature and discharge share information to some extent, as a large part of discharge originates from snow and glacier melt (Kormann et al. (2016), Schmieder et al. (2018b), Figure 2.6). Thus, even if temperature is permuted, the information is still present to some extent in discharge and thus the loss in model skill is not as pronounced or meaningful as if the two variables were not correlated. As another complication, we can expect that variable importance might change over time: e.g. precipitation might only be very important for sediment export during high-intensity summer rainstorms, but rather unimportant for the rest of the time. Therefore, we abstained from interpreting variable importance.

As another limitation related to the black-box nature of QRF is that it is not possible to comprehend how much of the geomorphological functioning of the catchment has been understood by the model, since no projections or continuous data of geomorphological conditions are available to my knowledge (see also section 5.3.5). As I will point out in the outlook section, future studies could try and include geomorphological changes (e.g. in connectivity, hillslope stability, hillslope-channel coupling or vegetation cover) more explicitly – if such geomorphological projections are feasible and available.

Concluding, the second research question of the present thesis can be answered with 'yes': QRF is a suitable approach with many advantages. It enables meaningfully modeling sediment export from high-alpine areas at the catchment scale in the first place (as compared to process-based models), and in a concrete way for individual catchments (as compared to the generalized predictions of conceptual models). The technical limitations have been clearly illuminated by the present thesis and can sometimes even be taken advantage of. Some inspiration for future studies is provided in the outlook section.

5.3 RQ 3: CHANGES IN PAST AND FUTURE SEDIMENT EXPORT AT DECADAL SCALES

The third research question aimed to assess changes in sediment export in the study area in the past and future, as well as potential reasons for these changes. This was done by analysing the modelled yields for step-like changes, trends and the consequential timing of peak sediment, as well as shifts in the temporal distribution, i.e. with respect to seasonality and the importance of events. I will summarize and discuss the findings in the following.

5.3.1 STEP-LIKE CHANGES

The findings of chapter 3 showed step-like increases in estimated SSY at both gauges at the beginning of the 1980s (Figure 3.6). We concluded that this was attributable to enhanced glacier melt, because high July temperatures in 1982 and 1983 (Figure 3.7) had distinctly altered the accumulation area ratio of the Vernagtferner (which describes how much of the glacier area is melting and how much is covered by snow). This indicates that the firn layer was removed on large parts of the glacier, which affected the albedo of the glacier surface and glacier melt in a lasting way, and – as a consequence – also lead to an increase in sediment-rich glacier meltwater (i.e. accessing sediment supplies from underneath or within the glacier) as well as intensified fluvial erosion (below the glacier or in the glacier forefield) (see also section 3.6.2).

The estimated elevated SSY after 1980 are in accordance with conceptual models, expecting an increase in SSY in response to accelerating glacier retreat (e.g., Antoniazza and Lane, 2021). They also match the findings of chapter 2, that annual glacier mass balance changes correlated with SSY (more so than discharge), which emphasizes the important role of glaciers for sediment dynamics in the study area (Figure 2.5 and Figure 2.6). Adding to this, previous studies analysing decades-long measurements of SSC also reported step-like increases for the upper Rhône basin in Switzerland (Costa et al., 2018), the headwaters of the Yangtze River on the Tibetan Plateau (Li et al., 2020; Zhang et al., 2021), and 28 headwater basins in High Mountain Asia (Li et al., 2021).

5.3.2 TRENDS AND CONSEQUENTIAL TIMING OF PEAK SEDIMENT

To facilitate a clearer overarching analysis with respect to peak sediment (and peak water) in the study area, Figure 5. synthesizes the past and future estimates of chapters 3 and 4, which have been smoothed using a 15-year moving average to gain a clearer picture in the face of high interannual variability.

With respect to the entire estimated time series, i.e. from the 1960s or 1970s to 2100, we detected overall positive trends in the past (chapter 3), i.e. up until 2020, and negative trends in the future, regardless of the emission scenario (chapter 4). This implies that peak sediment is underway or has already passed at both gauges. However, a closer look at Figure 5. and Figure 3.6 reveals that the sub-catchments respond in different ways. Estimated SSY show much more pronounced changes over time at gauge Vernagt (note the different scalings on the y-axis of Figure 5.). This was indicated in the trend analysis of yields after the step-like increases in 1981: at gauge Vent, the trend in mean annual sSSY was (slightly) negative between 1981 and 2020 (Sen's slope of -7.6 t km^{-2} a^{-1}), while the trend at gauge Vernagt was positive (Sen's slope of 23.5 t km^{-2} a^{-1}) (section 3.5.1). Similarly, the decreasing trends in the projections were much stronger at gauge Vernagt (more than -10 t km^{-2} a^{-2} compared to ca. -

5 t km^{-2} a^{-2} at gauge Vent) (Table 4.6). As a result, peak sediment appears to occur earlier at gauge Vent, i.e. between 2000 and 2020, than at gauge Vernagt, where peak sediment appears to occur shortly after 2020. However, this analysis is complicated by the disagreement of past and future estimates in the overlapping years at gauge Vernagt. Firstly, this disagreement is likely due to the nature of the climate and hydrological projections, which cannot reproduce (or forecast) individual days or years, but only the distribution. Secondly, the moving average cannot take into account many years at the beginning of the time series, which leads to the less smooth appearance.

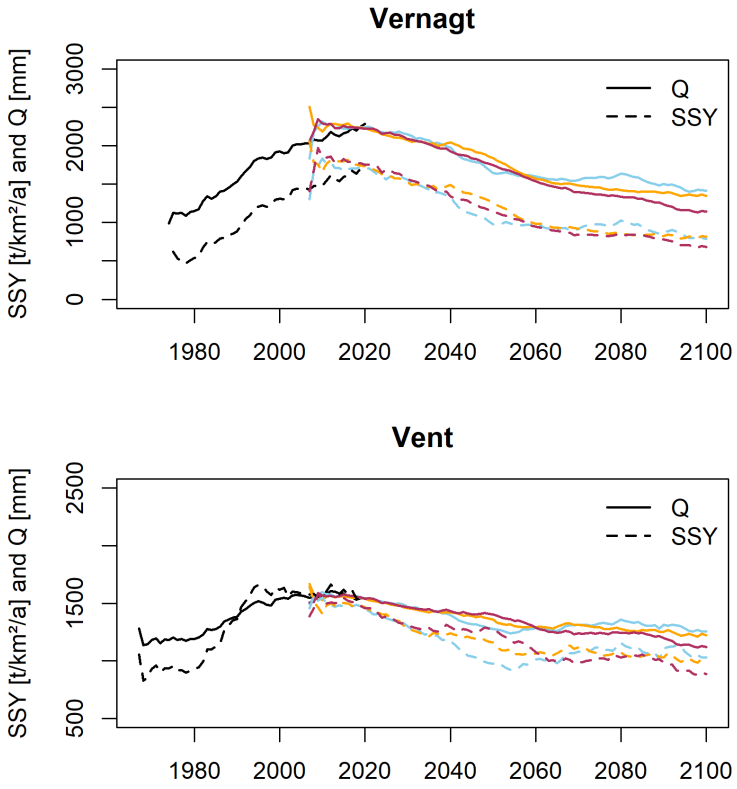

Figure 5.1. *Timings of peak water and peak sediment at gauges Vernagt and Vent. Black lines indicate past mean annual discharge from measurements and mean annual SSY estimates of QRF model; colored lines correspond to different RCPs (compare to Figure 4.10). The annual estimates have been smoothed using a 15-year moving average. Note the different scaling on the y-axes.*

Conceptual models expect that the timing of peak sediment will be 'jointly regulated by changes in meltwater runoff, erosive rainfall and landscape erodibility' and that the location of peak sediment relative to peak water depends on changes in erosive precipitation (Zhang et al., 2022). Thus in the following, I will explore changes in discharge and precipitation over time for the two gauges and discuss their relation to changes in sediment export.

5.3.3 CHANGES IN DISCHARGE AND PEAK WATER

'Peak (melt-)water' describes the turning point between increasing discharge volumes due to increased glacier melt and decreasing discharge volumes once the respective glaciers shrink below a critical size (Zhang et al., 2022). Figure 5. shows that the timing of 'peak meltwater', appears to be different at the two gauges: At gauge Vent, it has likely already passed and occurred between 2000 and 2020, while at gauge Vernagt, it appears to occur shortly after 2020 (although the analysis is difficult due to the disagreement between measurement and projections in the overlap period, as discussed above). This also becomes apparent in the strong positive trends in discharge at gauge Vernagt after 1981 (17.2 mm a^{-1}) compare to no significant trends in discharge at gauge Vent for the same time (see Figure 3.7a) and b) and section 3.5.2).

The different responses in both sediment export and discharge are likely linked to different glacier covers and timings of deglaciation in the subcatchments. As described in section 3.6.2, numerous smaller glaciers in the Vent catchment have practically disappeared, retreated behind rock sills and some developed small proglacial lakes. Such pronounced changes affect both discharge and sediment export, and the Vernagtferner glacier upstream gauge Vernagt, has not changed in such a pronounced way yet.

Interestingly, our results do not indicate a lag between peak meltwater and peak sediment at the two gauges. According to Zhang et al. (2022) this may provide some indication of the role of (erosive) precipitation: peak sediment is thought to occur simultaneously with peak water if erosive precipitation decreases of may lag after peak water if erosive rainfall increases or does not change (see also section 4.1). Thus in the following, I will summarize the findings with respect to changes in precipitation.

5.3.4 CHANGES IN PRECIPITATION

Summer precipitation sums showed an increasing trend at gauge Vernagt in the past, and no significant trend at gauge Vent (Figure 3.7). For future decades, an overall decrease of summer precipitation sums is projected, due to a precipitation shift from summer to winter (Hanzer et al., 2018). However, heavy summer precipitation is projected to become more intense (the 99.5th percentile increases, Figure 4.A2), although the number of heavy precipitation events does not seem to increase to the same extent (section 4.4). Accordingly, sediment export on days with heavy precipitation increases at both gauges (both in absolute terms and relative to respective annual output), indicating that precipitation events do become more important for sediment export in the future.

Nevertheless, the estimated future trends in sediment export are negative, even if yields on days with OOOR precipitation are inflated by a factor of five to account for potential underestimates (section 4.3.4.1). This indicates that the trends in discharge, representing

changes in sediment-rich glacier meltwaters and transport capacity for sediment from the catchment, outweigh changes in precipitation. This appears reasonable, given the substantial reductions of sediment export in the glacier melt period (Figure 4.11). Changes in precipitation might be less important due to the relatively dry climate in the catchment area, owing to its shielded, inner-Alpine location (as described e.g. in section 2.2.1). Additionally, section 2.3.6 showed that precipitation events played a minor role and it was concluded that melt-driven sediment transport was dominant in the present climate (section 2.5). Given these findings, the predominance of changes in discharge over changes in precipitation plausible – assuming the catchment response to precipitation does not change, as I will discuss in the next section.

However, with respect to the trends in precipitation, it has to be kept in mind that the QRF models were trained and applied at daily resolution, which was predetermined by the temporal resolution of the past predictor records as well as the climate projections. This could lead to underestimations in the changes in erosion-relevant precipitation events, that are short in duration and high in intensity, as it is expected that such sub-daily (especially hourly and sub-hourly) convective precipitation events increase faster with increasing temperature than daily-scale precipitation (Westra et al., 2014; Bürger et al., 2019; Fowler et al., 2021).

5.3.5 CHANGES IN ERODIBILITY

Due to the black box nature of the QRF approach, we cannot assess whether (future) changes in erodibility of the catchment area are captured. We attempted to approximate the relevant processes e.g. through antecedent precipitation and temperature conditions, which affect hillslope stability. Additionally, the presence of at least one major mass movement event in 2020 (and probably another one in 2014, section 2.3.6) within the training data provides some opportunity for the model to learn the catchment response under present conditions. However, if the catchment properties in the future should change in such a way that a different response is provoked irrespective of precipitation changes – i.e. through substantial changes in hillslope stability, due to melting permafrost or debuttressed slopes, effectively lowering the threshold triggering mass movements (Huggel et al., 2010, 2012; Savi et al., 2020)– this could change the estimated trends and consequentially also the timing of peak sediment. In contrast, potential negative feedbacks with respect to connectivity would consolidate the negative trends. On a similar note, it is not possible to assess whether changes in transport efficiency are captured, which could occur assuming a transient increase in sediment supply as glaciers vanish. Thus, it is recommended for future studies to attempt to include geomorphological changes more explicitly – if adequate data or modeling results are available at all and at the relevant timescales (section 6.1).

Circling back to the overarching aim of this thesis, which was to estimate sediment export on decadal scales in order to work towards informing e.g. downstream flood hazard management, can the 'all-clear' be given provided the overall negative trends in sediment export?

5.3.6 CHANGES IN TEMPORAL DISTRIBUTION

In chapter 2, we hypothesized that the sediment export season might be extended in the future, due to prolongued snow-free periods. However, Figure 4.11 suggests that this might not be the case. Indeed, the spring increase in sediment export appears to occur slightly earlier in the year towards the end of the century, especially under RCP8.5. However, this is accompanied by earlier and distinct reductions during the glacier melt phase in late summer, resulting in the overall decreasing annual SSYs as described above. Such changes in the temporal distribution of sediment transport can have severe ecological consequences, e.g. on spawning grounds of fish populations such as the brown trout, that depend on a certain sediment supply at a certain time of the year (Junker et al., 2015).

At the same time, Figure 4.A2 shows that very high sediment export in response to heavy precipitation events is possible in the future (which is likely even underestimated due to days with OOOR precipitation, and as increasing trends in heavy precipitation are likely partially masked by the daily resolution of out models, as discussed above). As a result, the fraction of the annual export that is associated with such events increases, which fits with the expectation that sediment transport regimes will eventually shift towards a precipitation-controlled regime in response to a warming climate (Zhang et al., 2022).

Altogether, this implies a two-fold change, i.e. the possibility of very high sediment export during events, despite the overall decrease in annual yields. This has important implications for sediment management, as potentially ecologically challenging reductions of sediment transport need to be considered, while at the same time, events could still transport large amounts of sediment that may increase the damage potential of floods and change river cross-sections in lower reaches.

6 OUTLOOK AND CONCLUSIONS

6.1 OUTLOOK

This thesis has presented past and future estimates of sediment export by exploring quantile regression forest as a modeling tool. Some progress has been made, that future investigations can build upon.

On the one hand, the publicly available pre-processed data facilitate the intercomparison of different (machine-learning) approaches. Alongside the comparison of methodological aspects (such as the ability of different approaches to deal with OOOR values), this could also help to reduce uncertainties and consolidate the projections. On the other hand, the publicly available code facilitates the application of the presented QRF approach to other catchments. Especially, the application to gauges with long SSC measurement time series would be interesting, to explore how well the model estimates perform compared to past measurements. (However, as pointed out in the introduction, there are very few of such long time series, and these are associated with new challenges, such as a very large catchment area and only two measurements per week in the case of the upper Rhône basin (Costa et al., 2018b).) Additionally, the application to a large number of catchments would facilitate comparing sediment export (projections) in space, as well as testing the applicability of the approach for larger catchment areas.

Another methodological aspect would to explore whether the usage of gridded precipitation (and temperature) data instead of the point measurements used in this thesis can improve the results and the process understanding – or if uncertainties within these products prevail. For example, areal precipitation or maximum precipitation intensity could be derived, or precipitation, temperature or snow cover in the areas above 2500 m a.s.l. could be explicitly considered (and separately from the remaining catchment areas). On a similar note, it might be worthwhile to explore additional predictors (if the data allow for it), such as the maximum discharge or precipitation intensity for a given day.

Additionally, as previously indicated, future studies could try to include geomorphologic processes related to changes in erodibility more explicitly, such as changes in connectivity, vegetation cover or hillslope stability. However, one must consider that predictors which increase (or decrease) continuously due to ongoing climate change, such as continuously decreaseing glacier area, will represent a technical problem for QRF, due to the inability to extrapolate.

Beyond that, future works could expand the analyses to beadload, which is even more impactful, e.g. with respect to flood damage costs, but has been very challenging to predict with physically based approaches (Badoux et al., 2014; Ancey, 2020a, b).

With respect to implications for flood hazard, sediment management or riverine ecology, this thesis showed that the presented QRF approach can help to provide more than rough approximations or assumptions derived from conceptual models. Despite remaining uncertainties, delineated tendencies such as the two-fold changes (high-magnitude events despite overall decrease) can provide important information for these fields.

6.1.1 OVERALL CONCLUSIONS

Sediment export from the investigated catchments in the Upper Ötztal in Tyrol, Austria, will likely decrease in the future – unless major changes in erodibility (i.e. hillslope stability due to permafrost thaw etc.) prevail and override the estimated trends.

Consequentially, peak sediment has likely already passed or is underway and occurred more or less simultaneously with peak water at both investigated gauges – unless precipitation changes unfold differently than represented in the projections, or erodibility changes prevail (see above).

Sediment export in the investigated catchments has so far been dominated by thermally induced glacier (and snow) melt. In the future, (precipitation) events will gain in importance in absolute and relative terms (i.e. percent of annual export), yet the trends in discharge, representing changes in sediment-rich glacier meltwaters, appear to outweigh changes in precipitation.

As a consequence, a two-fold development becomes apparent, i.e. very high sediment export rates during events despite the overall negative trend. Along with the projected shifts in seasonal distributions which lead to substantial reductions in sediment transport in late summer, this should be considered in managing sediment, riverine ecology and flood hazard.

Quantile regression forest can be a very useful tool to model sediment export in high-alpine areas and yields reasonable results. Technical limitations and their effects on the resulting estimates (e.g. with respect to out-of-observation-range values) have been illuminated in this thesis. Future studies could e.g. attempt to include geomorphological changes explicitly.

This thesis paves the way for future studies, as the pre-processed data and the model code are publically available. This facilitates testing other (machine-learning) approaches and using our models as a benchmark, or applying the presented approach to different catchments.

7 REFERENCES

Abermann, J., Lambrecht, A., Fischer, A., and Kuhn, M.: Quantifying changes and trends in glacier area and volume in the Austrian Ötztal Alps (1969-1997-2006), The Cryosphere, 3, 205–215, https://doi.org/10.5194/tc-3-205-2009, 2009.

Adnan, M., Kang, S., Zhang, G., Anjum, M. N., Zaman, M., and Zhang, Y.: Evaluation of SWAT Model performance on glaciated and non-glaciated subbasins of Nam Co Lake, Southern Tibetan Plateau, China, J. Mt. Sci., 16, 1075–1097, https://doi.org/10.1007/s11629-018-5070-7, 2019.

Al-Mukhtar, M.: Random forest, support vector machine, and neural networks to modelling suspended sediment in Tigris River-Baghdad, Environ. Monit. Assess., 191, 673, https://doi.org/10.1007/s10661-019-7821-5, 2019.

Altmann, M., Ramskogler, K., Mikolka-Flöry, S., Pfeiffer, M., Haas, F., Heckmann, T., Rom, J., Fleischer, F., Himmelstoß, T., Pfeifer, N., Ressl, C., Tasser, E., and Becht, M.: Quantitative Long-Term Monitoring (1890–2020) of Morphodynamic and Land-Cover Changes of a LIA Lateral Moraine Section, Geosciences, 13, 95, https://doi.org/10.3390/geosciences13040095, 2023.

Ancey, C.: Bedload transport: a walk between randomness and determinism. Part 1. The state of the art, J. Hydraul. Res., 58, 1–17, https://doi.org/10.1080/00221686.2019.1702594, 2020a.

Ancey, C.: Bedload transport: a walk between randomness and determinism. Part 2. Challenges and prospects, J. Hydraul. Res., 58, 18–33, https://doi.org/10.1080/00221686.2019.1702595, 2020b.

Antoniazza, G. and Lane, S. N.: Sediment yield over glacial cycles: A conceptual model, Prog. Phys. Geogr. Earth Environ., 58, 842–865, https://doi.org/10.1177/0309133321997292, 2021.

Badoux, A., Andres, N., and Turowski, J. M.: Damage costs due to bedload transport processes in Switzerland, Nat. Hazards Earth Syst. Sci., 14, 279–294, https://doi.org/10.5194/nhess-14-279-2014, 2014.

Ballantyne, C. K.: Paraglacial geomorphology, Quat. Sci. Rev., 21, 1935–2017, https://doi.org/10.1016/S0277-3791(02)00005-7, 2002.

Bendixen, M., Lønsmann Iversen, L., Anker Bjørk, A., Elberling, B., Westergaard-Nielsen, A., Overeem, I., Barnhart, K. R., Abbas Khan, S., Box, J. E., Abermann, J., Langley, K., and Kroon, A.: Delta progradation in Greenland driven by increasing glacial mass loss, Nature, 550, 101–104, https://doi.org/10.1038/nature23873, 2017a.

Bendixen, M., Lønsmann Iversen, L., Anker Bjørk, A., Elberling, B., Westergaard-Nielsen, A., Overeem, I., Barnhart, K. R., Abbas Khan, S., Box, J. E., Abermann, J., Langley, K., and Kroon, A.: Delta progradation in Greenland driven by increasing glacial mass loss, Nature, 550, 101–104, https://doi.org/10.1038/nature23873, 2017b.

Beniston, M., Farinotti, D., Stoffel, M., Andreassen, L. M., Coppola, E., Eckert, N., Fantini, A., Giacona, F., Hauck, C., Huss, M., Huwald, H., Lehning, M., López-Moreno, J.-I., Magnusson, J., Marty, C., Morán-Tejéda, E., Morin, S., Naaim, M., Provenzale, A., Rabatel, A., Six, D., Stötter, J., Strasser, U., Terzago, S., and Vincent, C.: The European mountain cryosphere: a review of its current state, trends, and future challenges, The Cryosphere, 12, 759–794, https://doi.org/10.5194/tc-12-759-2018, 2018.

Bergmann, H. and Reinwarth, O.: Die Pegelstation Vernagtbach (Ötztaler Alpen) - Planung, Bau und Messergebnisse, Z. Für Gletscherkunde Glazialgeol., 12, 157–180, 1977.

Beylich, A. A., Laute, K., and Storms, J. E. A.: Contemporary suspended sediment dynamics within two partly glacierized mountain drainage basins in western Norway (Erdalen and Bødalen, inner Nordfjord), Geomorphology, 287, 126–143, https://doi.org/10.1016/j.geomorph.2015.12.013, 2017.

Bilotta, G. S. and Brazier, R. E.: Understanding the influence of suspended solids on water quality and aquatic biota, Water Res., 42, 2849–2861, https://doi.org/10.1016/j.watres.2008.03.018, 2008.

Boeckli, L., Brenning, A., Gruber, S., and Noetzli, J.: Permafrost distribution in the European Alps: calculation and evaluation of an index map and summary statistics, The Cryosphere, 6, 807–820, https://doi.org/10.5194/tc-6-807-2012, 2012.

Boehmke, B. and Greenwell, B.: Hands-On Machine Learning with R, Chapman and Hall/CRC, Boca Raton, 488 pp., https://doi.org/10.1201/9780367816377, 2019.

Bogen, J.: The impact of climate change on glacial sediment delivery to rivers. In: Sediment Dynamics in Changing Environments (Proceedings of a symposium held in Christchurch, New Zealand, December 2008), IAHS Publ., 325, 432–439, 2008.

Bolibar, J., Rabatel, A., Gouttevin, I., Zekollari, H., and Galiez, C.: Nonlinear sensitivity of glacier mass balance to future climate change unveiled by deep learning, Nat. Commun., 13, 409, https://doi.org/10.1038/s41467-022-28033-0, 2022.

Braithwaite, R. J. and Raper, S. C. B.: Estimating equilibrium-line altitude (ELA) from glacier inventory data, Ann. Glaciol., 50, 127–132, https://doi.org/10.3189/172756410790595930, 2009.

Braun, L. N., Escher-Vetter, H., Siebers, M., and Weber, M.: Water Balance of the highly Glaciated Vernagt Basin, Ötztal Alps, in: The water balance of the alps: what do we need to protect the water resources of the Alps? Proceedings of the conference held at Innsbruck university, 28–29 September 2006, Univ. Press, Innsbruck, https://diglib.uibk.ac.at/ulbdok/content/pageview/268995 (last access: 8 May 2023), Univ. Press, Innsbruck, 33–42, 2007.

Breiman, L.: Random Forests, Mach. Learn., 45, 5–32, https://doi.org/10.1023/A:1010933404324, 2001.

Breiman, L., Friedman, J. H., Olshen, R. A., and Stone, C. J.: Classification And Regression Trees, Routledge, New York, 368 pp., 1984.

Brils, J.: Sediment monitoring and the European Water Framework Directive, Ann. Dell Ist. Super. Sanità, 44, 218–223, 2008.

Brooke, S., Chadwick, A. J., Silvestre, J., Lamb, M. P., Edmonds, D. A., and Ganti, V.: Where rivers jump course, Science, 376, 987–990, https://doi.org/10.1126/science.abm1215, 2022.

Brunetti, M., Lentini, G., Maugeri, M., Nanni, T., Auer, I., Böhm, R., and Schöner, W.: Climate variability and change in the Greater Alpine Region over the last two centuries based on multi-variable analysis, Int. J. Climatol., 29, 2197–2225, https://doi.org/10.1002/joc.1857, 2009.

Buckel, J. and Otto, J.-C.: The Austrian Glacier Inventory GI 4 (2015) in ArcGis (shapefile) format [data set], https://doi.org/10.1594/PANGAEA.887415, 2018.

Buckel, J., Otto, J. C., Prasicek, G., and Keuschnig, M.: Glacial lakes in Austria - Distribution and formation since the Little Ice Age, Glob. Planet. Change, 164, 39–51, https://doi.org/10.1016/j.gloplacha.2018.03.003, 2018.

Bürger, G., Pfister, A., and Bronstert, A.: Temperature-Driven Rise in Extreme Sub-Hourly Rainfall, J. Clim., 32, 7597–7609, https://doi.org/10.1175/JCLI-D-19-0136.1, 2019.

Campforts, B., Shobe, C. M., Overeem, I., and Tucker, G. E.: The Art of Landslides: How Stochastic Mass Wasting Shapes Topography and Influences Landscape Dynamics, J. Geophys. Res. Earth Surf., 127, e2022JF006745, https://doi.org/10.1029/2022JF006745, 2022.

Carranza, C., Nolet, C., Pezij, M., and van der Ploeg, M.: Root zone soil moisture estimation with Random Forest, J. Hydrol., 593, 125840, https://doi.org/10.1016/j.jhydrol.2020.125840, 2021.

Carrivick, J. L. and Heckmann, T.: Short-term geomorphological evolution of proglacial systems, Geomorphology, 287, 3–28, https://doi.org/10.1016/j.geomorph.2017.01.037, 2017.

Carrivick, J. L. and Tweed, F. S.: Deglaciation controls on sediment yield: Towards capturing spatio-temporal variability, Earth-Sci. Rev., 221, 103809, https://doi.org/10.1016/j.earscirev.2021.103809, 2021.

Cavalli, M., Trevisani, S., Comiti, F., and Marchi, L.: Geomorphometric assessment of spatial sediment connectivity in small Alpine catchments, Geomorphology, 188, 31–41, https://doi.org/10.1016/j.geomorph.2012.05.007, 2013.

Cavalli, M., Heckmann, T., and Marchi, L.: Sediment Connectivity in Proglacial Areas, Geomorphol. Proglacial Syst., 271–287, https://doi.org/10.1007/978-3-319-94184-4_16, 2019.

Chiarle, M., Geertsema, M., Mortara, G., and Clague, J. J.: Relations between climate change and mass movement: Perspectives from the Canadian Cordillera and the European Alps, Glob. Planet. Change, 202, 103499, https://doi.org/10.1016/j.gloplacha.2021.103499, 2021.

Clapuyt, F., Vanacker, V., Christl, M., Van Oost, K., and Schlunegger, F.: Spatio-temporal dynamics of sediment transfer systems in landslide-prone Alpine catchments, Solid Earth, 10, 1489–1503, https://doi.org/10.5194/se-10-1489-2019, 2019.

Cohen, S., Kettner, A. J., Syvitski, J. P. M., and Fekete, B. M.: WBMsed, a distributed global-scale riverine sediment flux model: Model description and validation, Comput. Geosci., 53, 80–93, https://doi.org/10.1016/j.cageo.2011.08.011, 2013.

Collins, D. N.: Seasonal and annual variations of suspended sediment transport in meltwaters draining from an Alpine glacier, in: Hydrological Measurements; the Water Cycle (Proceedings of two Lausanne Symposia), Hydrology in Mountainous Regions I: Hydrological Measurements; the Water Cycle 193, Lausanne, 9, 1990.

Collins, D. N.: A conceptually based model of the interaction between flowing meltwater and subglacial sediment, Ann. Glaciol., 22, 224–232, https://doi.org/10.3189/1996AoG22-1-224-232, 1996.

Costa, A., Anghileri, D., and Molnar, P.: Hydroclimatic control on suspended sediment dynamics of a regulated Alpine catchment: a conceptual approach, Hydrol. Earth Syst. Sci., 22, 3421–3434, https://doi.org/10.5194/hess-22-3421-2018, 2018a.

Costa, A., Molnar, P., Stutenbecker, L., Bakker, M., Silva, T. A., Schlunegger, F., Lane, S. N., Loizeau, J.-L., and Girardclos, S.: Temperature signal in suspended sediment export from an Alpine catchment, Hydrol. Earth Syst. Sci., 22, 509–528, https://doi.org/10.5194/hess-22-509-2018, 2018b.

Courtois, A., Morel, J.-M., and Arias, P.: Can neural networks extrapolate? Discussion of a theorem by Pedro Domingos, Rev. Real Acad. Cienc. Exactas Físicas Nat. Ser. Matemáticas, 117, 79, https://doi.org/10.1007/s13398-023-01411-z, 2023.

Coviello, V., Vignoli, G., Simoni, S., Bertoldi, W., Engel, M., Buter, A., Marchetti, G., Andreoli, A., Savi, S., and Comiti, F.: Bedload Fluxes in a Glacier-Fed River at Multiple Temporal Scales, Water Resour. Res., 58, e2021WR031873, https://doi.org/10.1029/2021WR031873, 2022.

Delaney, I. and Adhikari, S.: Increased Subglacial Sediment Discharge in a Warming Climate: Consideration of Ice Dynamics, Glacial Erosion, and Fluvial Sediment Transport, Geophys. Res. Lett., 47, e2019GL085672, https://doi.org/10.1029/2019GL085672, 2020.

Delaney, I., Bauder, A., Huss, M., and Weidmann, Y.: Proglacial erosion rates and processes in a glacierized catchment in the Swiss Alps, Earth Surf. Process. Landf., 43, 765–778, https://doi.org/10.1002/esp.4239, 2018a.

Delaney, I., Bauder, A., Werder, M., and Farinotti, D.: Regional and annual variability in subglacial sediment transport by water for two glaciers in the Swiss Alps, Front. Earth Sci., 6, 175, https://doi.org/10.3929/ethz-b-000305762, 2018b.

Delaney, I., Werder, M. A., and Farinotti, D.: A Numerical Model for Fluvial Transport of Subglacial Sediment, J. Geophys. Res. Earth Surf., 124, 2197–2223, https://doi.org/10.1029/2019JF005004, 2019.

Delaney, I., Anderson, L. S., and Herman, F.: The spatially distributed nature of subglacial sediment dynamics: using a numerical model to quantify sediment transport and bedrock erosion across a glacier bed in response to glacier behavior and hydrology (preprint), Earth Surf. Dyn. Discuss., 1–37, https://doi.org/10.5194/esurf-2021-88, 2021.

Di Mauro, B. and Fugazza, D.: Pan-Alpine glacier phenology reveals lowering albedo and increase in ablation season length, Remote Sens. Environ., 279, 113119, https://doi.org/10.1016/j.rse.2022.113119, 2022.

eHYD: Hydrographic Service, Austria, Bundesministerium für Landwirtschaft, Regionen und Tourismus [data set], https://ehyd. gv.at/ (last access: 8 May 2023), 2021.

Eichel, J., Draebing, D., and Meyer, N.: From active to stable: Paraglacial transition of Alpine lateral moraine slopes, Land Degrad. Dev., 29, 4158–4172, https://doi.org/10.1002/ldr.3140, 2018.

Embleton-hamann, C. and Slaymaker, O.: The austrian alps and paraglaciation, Geogr. Ann. Ser. Phys. Geogr., 94, 7–16, https://doi.org/10.1111/j.1468-0459.2011.00447.x, 2012.

Environmental Systems Research Institute: (Redlands, CA): ArcGIS Desktop, Release 10.6.1 [code], 2018.

Escher-Vetter, H.: Climate change information as derived from long-term measurements of winter and summer mass balance, in: Extended Abstracts, 29th International Conference on Alpine Meteorology, Chambéry, France, 465–468, 2007.

Escher-Vetter, H. and Siebers, M.: Sensitivity of glacier runoff to summer snowfall events, Ann. Glaciol., 46, 309–315, https://doi.org/10.3189/172756407782871251, 2007.

Escher-Vetter, H., Oerter, H., Reinwarth, O., Braun, L. N., and Weber, M.: Hydrological and meteorological records from the Vernagtferner Basin - Vernagtbach station, for the years 1970 to 2001, [data set], https://doi.org/10.1594/PANGAEA.775113, 2012.

Escher-Vetter, H., Braun, L. N., and Siebers, M.: Hydrological and meteorological records from the Vernagtferner Basin - Vernagtbach station, for the years 2002 to 2012 [data set], https://doi.org/10.1594/PANGAEA.829530, 2014.

Evin, G., Somot, S., and Hingray, B.: Balanced estimate and uncertainty assessment of European climate change using the large EURO-CORDEX regional climate model ensemble, Earth Syst. Dyn., 12, 1543–1569, https://doi.org/10.5194/esd-12-1543-2021, 2021.

Farinotti, D., Usselmann, S., Huss, M., Bauder, A., and Funk, M.: Runoff evolution in the Swiss Alps: projections for selected high-alpine catchments based on ENSEMBLES scenarios, Hydrol. Process., 26, 1909–1924, https://doi.org/10.1002/hyp.8276, 2012.

Felix, D., Albayrak, I., and Boes, R. M.: In-situ investigation on real-time suspended sediment measurement techniques: Turbidimetry, acoustic attenuation, laser diffraction (LISST) and vibrating tube densimetry, Int. J. Sediment Res., 33, 3–17, https://doi.org/10.1016/j.ijsrc.2017.11.003, 2018.

Fischer, A., Seiser, B., Stocker-Waldhuber, M., and Abermann, J.: The Austrian Glacier Inventory GI 3, 2006, in ArcGIS (shapefile) format, https://doi.org/10.1594/PANGAEA.844985, 2015.

Fowler, H. J., Lenderink, G., Prein, A. F., Westra, S., Allan, R. P., Ban, N., Barbero, R., Berg, P., Blenkinsop, S., Do, H. X., Guerreiro, S., Haerter, J. O., Kendon, E. J., Lewis, E., Schaer, C., Sharma, A., Villarini, G., Wasko, C., and Zhang, X.: Anthropogenic intensification of short-duration rainfall extremes, Nat. Rev. Earth Environ., 2, 107–122, https://doi.org/10.1038/s43017-020-00128-6, 2021.

Francke, T.: ssc_prediction - Prediction of sedigraphs and hydrographs from other predictors using RF / QRF, GitHub [code], https://github.com/TillF/ssc_prediction (last access: 8 May 2023), 2017.

Francke, T., López-Tarazón, J. A., and Schröder, B.: Estimation of suspended sediment concentration and yield using linear models, random forests and quantile regression forests, Hydrol. Process., 22, 4892–4904, https://doi.org/10.1002/hyp.7110, 2008a.

Francke, T., López-Tarazón, J. A., Vericat, D., Bronstert, A., and Batalla, R. J.: Flood-based analysis of high-magnitude sediment transport using a non-parametric method, Earth Surf. Process. Landf., 33, 2064–2077, https://doi.org/10.1002/esp.1654, 2008b.

Gabbud, C. and Lane, S. N.: Ecosystem impacts of Alpine water intakes for hydropower: the challenge of sediment management, WIREs Water, 3, 41–61, https://doi.org/10.1002/wat2.1124, 2016.

Gattermayr, W.: Das hydrographische Regime der Ötztaler Ache, in: E.-M. Koch & B. Erschbamer (Hrsg.), Wetter und Klima im Wandel, vol. 3 Klima, Wetter, Gletscher im Wandel, Innsbruck University Press., Innsbruck, 35, 2013.

Geitner, C., Mayr, A., Rutzinger, M., Löbmann, M. T., Tonin, R., Zerbe, S., Wellstein, C., Markart, G., and Kohl, B.: Shallow erosion on grassland slopes in the European Alps – Geomorphological classification, spatio-temporal analysis, and understanding snow and vegetation impacts, Geomorphology, 373, 107446, https://doi.org/10.1016/j.geomorph.2020.107446, 2021.

Giorgi, F., Torma, C., Coppola, E., Ban, N., Schär, C., and Somot, S.: Enhanced summer convective rainfall at Alpine high elevations in response to climate warming, Nat. Geosci., 9, 584–589, https://doi.org/10.1038/ngeo2761, 2016.

Gobiet, A. and Kotlarski, S.: Future Climate Change in the European Alps, vol. A. Gobiet&S. Kotlarski (Eds.), Oxford research encyclopedia of climate science. DOI: 10.1093/acrefore/9780190228620.013.767, Oxford University Press, 2020.

Gobiet, A., Kotlarski, S., Beniston, M., Heinrich, G., Rajczak, J., and Stoffel, M.: 21st century climate change in the European Alps—A review, Sci. Total Environ., 493, 1138–1151, https://doi.org/10.1016/j.scitotenv.2013.07.050, 2014.

Gudmundsson, L.: qmap: Statistical transformations for post-processing climate model output. R package version 1.0-4. [code], https://CRAN.R-project.org/package=qmap (last access: 18 May 2023), 2016.

Gudmundsson, L., Bremnes, J. B., Haugen, J. E., and Engen-Skaugen, T.: Technical Note: Downscaling RCM precipitation to the station scale using statistical transformations; a comparison of methods, Hydrol. Earth Syst. Sci., 16, 3383–3390, https://doi.org/10.5194/hess-16-3383-2012, 2012.

Guillén-Ludeña, S., Manso, P. A., and Schleiss, A. J.: Multidecadal Sediment Balance Modelling of a Cascade of Alpine Reservoirs and Perspectives Based on Climate Warming, Water, 10, 1759, https://doi.org/10.3390/w10121759, 2018.

Guillon, H., Mugnier, J.-L., and Buoncristiani, J.-F.: Proglacial sediment dynamics from daily to seasonal scales in a glaciated Alpine catchment (Bossons glacier, Mont Blanc massif, France), Earth Surf. Process. Landf., 43, 1478–1495, https://doi.org/10.1002/esp.4333, 2018.

Gupta, D., Hazarika, B. B., Berlin, M., Sharma, U. M., and Mishra, K.: Artificial intelligence for suspended sediment load prediction: a review, Environ. Earth Sci., 80, 346, https://doi.org/10.1007/s12665-021-09625-3, 2021.

Hallet, B., Hunter, L., and Bogen, J.: Rates of erosion and sediment evacuation by glaciers: A review of field data and their implications, Glob. Planet. Change, 12, 213–235, https://doi.org/10.1016/0921-8181(95)00021-6, 1996.

Hanus, S., Hrachowitz, M., Zekollari, H., Schoups, G., Vizcaino, M., and Kaitna, R.: Future changes in annual, seasonal and monthly runoff signatures in contrasting Alpine catchments in Austria, Hydrol. Earth Syst. Sci., 25, 3429–3453, https://doi.org/10.5194/hess-25-3429-2021, 2021.

Hanzer, F., Helfricht, K., Marke, T., and Strasser, U.: Multilevel spatiotemporal validation of snow/ice mass balance and runoff modeling in glacierized catchments, The Cryosphere, 10, 1859–1881, https://doi.org/10.5194/tc-10-1859-2016, 2016.

Hanzer, F., Förster, K., Nemec, J., and Strasser, U.: Projected cryospheric and hydrological impacts of 21st century climate change in the Ötztal Alps (Austria) simulated using a physically based approach, Hydrol. Earth Syst. Sci., 22, 1593–1614, https://doi.org/10.5194/hess-22-1593-2018, 2018.

Hartmeyer, I., Delleske, R., Keuschnig, M., Krautblatter, M., Lang, A., Schrott, L., and Otto, J.-C.: Current glacier recession causes significant rockfall increase: the immediate paraglacial response of deglaciating cirque walls, Earth Surf. Dyn., 8, 729–751, https://doi.org/10.5194/esurf-8-729-2020, 2020.

Haselberger, S., Ohler, L.-M., Junker, R. R., Otto, J.-C., Glade, T., and Kraushaar, S.: Quantification of biogeomorphic interactions between small-scale sediment transport and primary vegetation succession on proglacial slopes of the Gepatschferner, Austria, Earth Surf. Process. Landf., 46, 1941–1952, https://doi.org/10.1002/esp.5136, 2021.

Hasson, U., Nastase, S. A., and Goldstein, A.: Direct-fit to nature: an evolutionary perspective on biological (and artificial) neural networks, Neuron, 105, 416–434, https://doi.org/10.1016/j.neuron.2019.12.002, 2019.

Heckmann, T., McColl, S., and Morche, D.: Retreating ice: research in pro-glacial areas matters, Earth Surf. Process. Landf., 41, 271–276, https://doi.org/10.1002/esp.3858, 2016.

Herman, F., De Doncker, F., Delaney, I., Prasicek, G., and Koppes, M.: The impact of glaciers on mountain erosion, Nat. Rev. Earth Environ., 2, 422–435, https://doi.org/10.1038/s43017-021-00165-9, 2021.

Hiebl, J. and Frei, C.: Daily precipitation grids for Austria since 1961—development and evaluation of a spatial dataset for hydroclimatic monitoring and modelling, Theor. Appl. Climatol., 132, 327–345, https://doi.org/10.1007/s00704-017-2093-x, 2018.

Hinderer, M., Kastowski, M., Kamelger, A., Bartolini, C., and Schlunegger, F.: River loads and modern denudation of the Alps — A review, Earth-Sci. Rev., 118, 11–44, https://doi.org/10.1016/j.earscirev.2013.01.001, 2013.

Hirschberg, J., Fatichi, S., Bennett, G. L., McArdell, B. W., Peleg, N., Lane, S. N., Schlunegger, F., and Molnar, P.: Climate Change Impacts on Sediment Yield and Debris-Flow Activity in an Alpine Catchment, J. Geophys. Res. Earth Surf., 126, e2020JF005739, https://doi.org/10.1029/2020JF005739, 2021.

Hock, R.: 4.5 Hydrologische Veränderungen in vergletscherten Einzugsgebieten, in: Warnsignal Klima: Hochgebirge im Wandel., edited by: Lozán, J. L., Breckle, S.-W., and Graßl, H., Österreichischer Wasser- und Abfallwirtschaftsverband ÖWAV, Wien, 5, https://doi.org/10.25592/uhhfdm.9252, 243–252, 2020.

Hock, R., Jansson, P., and Braun, L. N.: Modelling the Response of Mountain Glacier Discharge to Climate Warming, in: Global Change and Mountain Regions: An Overview of Current Knowledge, edited by: Huber, U. M., Bugmann, H. K. M., and Reasoner, M. A., Springer Netherlands, Dordrecht, 243–252, https://doi.org/10.1007/1-4020-3508-X_25, 2005.

Huggel, C., Salzmann, N., Allen, S., Caplan-Auerbach, J., Fischer, L., Haeberli, W., Larsen, C., Schneider, D., and Wessels, R.: Recent and future warm extreme events and high-mountain slope stability, Philos. Trans. R. Soc. Math. Phys. Eng. Sci., 368, 2435–2459, https://doi.org/10.1098/rsta.2010.0078, 2010.

Huggel, C., Clague, J. J., and Korup, O.: Is climate change responsible for changing landslide activity in high mountains?, Earth Surf. Process. Landf., 37, 77–91, https://doi.org/10.1002/esp.2223, 2012.

Huss, M.: Present and future contribution of glacier storage change to runoff from macroscale drainage basins in Europe, Water Resour. Res., 47, W07511, https://doi.org/10.1029/2010WR010299, 2011.

Huss, M. and Hock, R.: Global-scale hydrological response to future glacier mass loss, Nat. Clim. Change, 8, 135–140, https://doi.org/10.1038/s41558-017-0049-x, 2018.

Huss, M., Bookhagen, B., Huggel, C., Jacobsen, D., Bradley, R. S., Clague, J. J., Vuille, M., Buytaert, W., Cayan, D. R., Greenwood, G., Mark, B. G., Milner, A. M., Weingartner, R., and Winder, M.: Toward mountains without permanent snow and ice, Earths Future, 5, 418–435, https://doi.org/10.1002/2016EF000514, 2017.

Hydrographic yearbook of Austria: Hydrographisches Jahrbuch von Österreich, Hydrographischer Dienst in Österreich, Bundesministerium für Land- und Forstwirtschaft, Umwelt und Wasserwirtschaft Abteilung VII/3, https://wasser.umweltbundesamt.at/ hydjb/ (last access: 8 May 2023), 2016.

Institute of Meteorology and Geophysics: Climate Data Vent, Ötztal Alps, 1935-2011 [data set], https://doi.org/10.1594/PANGAEA.806582, 2013.

Iverson, R. M. and George, D. L.: A depth-averaged debris-flow model that includes the effects of evolving dilatancy. I. Physical basis, Proc. R. Soc. Math. Phys. Eng. Sci., 470, 20130819, https://doi.org/10.1098/rspa.2013.0819, 2014.

Jacob, D., Petersen, J., Eggert, B., Alias, A., Christensen, O. B., Bouwer, L. M., Braun, A., Colette, A., Déqué, M., Georgievski, G., Georgopoulou, E., Gobiet, A., Menut, L., Nikulin, G., Haensler, A., Hempelmann, N., Jones, C., Keuler, K., Kovats, S., Kröner, N., Kotlarski, S., Kriegsmann, A., Martin, E., van Meijgaard, E., Moseley, C., Pfeifer, S., Preuschmann, S., Radermacher, C., Radtke, K., Rechid, D., Rounsevell, M., Samuelsson, P., Somot, S., Soussana, J.-F., Teichmann, C., Valentini, R., Vautard, R., Weber, B., and Yiou, P.: EURO-CORDEX: new high-resolution climate change projections for European impact research, Reg. Environ. Change, 14, 563–578, https://doi.org/10.1007/s10113-013-0499-2, 2014.

Jimeno-Sáez, P., Martínez-España, R., Casalí, J., Pérez-Sánchez, J., and Senent-Aparicio, J.: A comparison of performance of SWAT and machine learning models for predicting sediment load in a forested Basin, Northern Spain, CATENA, 212, 105953, https://doi.org/10.1016/j.catena.2021.105953, 2022.

Juen, I. and Kaser, G.: Climate Data Vent, Ötztal Alps, 2012-2016 [data set], https://doi.org/10.1594/PANGAEA.876595, 2017.

Junker, J., Heimann, F. U. M., Hauer, C., Turowski, J. M., Rickenmann, D., Zappa, M., and Peter, A.: Assessing the impact of climate change on brown trout (Salmo trutta fario) recruitment, Hydrobiologia, 751, 1–21, https://doi.org/10.1007/s10750-014-2073-4, 2015.

Kammerlander, J., Achleitner, S., Schöber, J., and Hofer, B.: Geschiebehaushalt in kleinen Hochgebirgsbächen der Nordtiroler Zentralalpen, Österr. Wasser- Abfallwirtsch., 69, 114–124, https://doi.org/10.1007/s00506-017-0378-z, 2017.

Kettner, A. J. and Syvitski, J. P. M.: HydroTrend v.3.0: A climate-driven hydrological transport model that simulates discharge and sediment load leaving a river system, Comput. Geosci., 34, 1170–1183, https://doi.org/10.1016/j.cageo.2008.02.008, 2008.

Klug, C., Rieg, L., Ott, P., Mössinger, M., Sailer, R., and Stötter, J.: A Multi-Methodological Approach to Determine Permafrost Occurrence and Ground Surface Subsidence in Mountain Terrain, Tyrol, Austria, Permafr. Periglac. Process., 28, 249–265, https://doi.org/10.1002/ppp.1896, 2017.

Koppes, M., Hallet, B., and Anderson, J.: Synchronous acceleration of ice loss and glacial erosion, Glaciar Marinelli, Chilean Tierra del Fuego, J. Glaciol., 55, 207–220, https://doi.org/10.3189/002214309788608796, 2009.

Kormann, C., Bronstert, A., Francke, T., Recknagel, T., and Graeff, T.: Model-Based Attribution of High-Resolution Streamflow Trends in Two Alpine Basins of Western Austria, Hydrology, 3, 7, https://doi.org/10.3390/hydrology3010007, 2016.

Kotlarski, S., Gobiet, A., Morin, S., Olefs, M., Rajczak, J., and Samacoïts, R.: 21st Century alpine climate change, Clim. Dyn., 60, 65–86, https://doi.org/10.1007/s00382-022-06303-3, 2023.

Kuhn, M., Nickus, U., and Pellet, F.: Precipitation Patterns in the Inner Ötztal, 17. Internationale Tagung für Alpine Meteorologie, Offenbach am Main, 1982.

Kuhn, M., Helfricht, K., Ortner, M., Landmann, J., and Gurgiser, W.: Liquid water storage in snow and ice in 86 Eastern Alpine basins and its changes from 1970–97 to 1998–2006, Ann. Glaciol., 57, 11–18, https://doi.org/10.1017/aog.2016.24, 2016.

Lalk, P., Haimann, M., and Habersack, H.: Monitoring, Analyse und Interpretation des Schwebstofftransportes an österreichischen Flüssen, Österr. Wasser- Abfallwirtsch., 66, 306–315, https://doi.org/10.1007/s00506-014-0175-x, 2014.

Land Tirol: Digital terrain model of Tyrol, 10m resolution, EPSG 31254 [data set], https://www.data.gv.at/katalog/dataset/land-tirol_tirolgelnde (last access; 8 May 2023), 2016.

Land Tirol: tiris OGD map service "Wasser" [data set], https://www.data.gv.at/katalog/dataset/0b5d6529-d88c-46c0-84f7-b37282e96ce8 (last access: 5 July 2021), 2021.

Landers, M. N. and Sturm, T. W.: Hysteresis in suspended sediment to turbidity relations due to changing particle size distributions: Hysteresis Suspended Sediment-Turbidity With Particle Size, Water Resour. Res., 49, 5487–5500, https://doi.org/10.1002/wrcr.20394, 2013.

Lane, S. N., Bakker, M., Gabbud, C., Micheletti, N., and Saugy, J.-N.: Sediment export, transient landscape response and catchment-scale connectivity following rapid climate warming and Alpine glacier recession, Geomorphology, 277, 210–227, https://doi.org/10.1016/j.geomorph.2016.02.015, 2017.

Lane, S. N., Bakker, M., Costa, A., Girardclos, S., Loizeau, J.-L., Molnar, P., Silva, T., Stutenbecker, L., and Schlunegger, F.: Making stratigraphy in the Anthropocene: climate change impacts and economic conditions controlling the supply of sediment to Lake Geneva, Sci. Rep., 9, 8904, https://doi.org/10.1038/s41598-019-44914-9, 2019.

Lantz, B.: Machine Learning with R: Expert techniques for predictive modeling, 3rd Edition, Packt Publishing Ltd, 459 pp., 2019.

Laser- und Luftbildatlas Tirol: https://lba.tirol.gv.at/public/karte. xhtml (last access: 17 June 2022), last access: 17 June 2022.

Leggat, M. S., Owens, P. N., Stott, T. A., Forrester, B. J., Déry, S. J., and Menounos, B.: Hydrometeorological drivers and sources of suspended sediment flux in the pro-glacial zone of the retreating Castle Creek Glacier, Cariboo Mountains, British Columbia, Canada, Earth Surf. Process. Landf., 40, 1542–1559, https://doi.org/10.1002/esp.3755, 2015.

Li, D., Li, Z., Zhou, Y., and Lu, X. X.: Substantial Increases in the Water and Sediment Fluxes in the Headwater Region of the Tibetan Plateau in Response to Global Warming, Geophys. Res. Lett., 47, e2020GL087745, https://doi.org/10.1029/2020GL087745, 2020.

Li, D., Overeem, I., Kettner, A., Zhou, Y., and Xixi, L.: Air Temperature Regulates Erodible Landscape, Water, and Sediment Fluxes in the Permafrost-Dominated Catchment on the Tibetan Plateau, Water Resour. Res., 57, e2020WR028193, https://doi.org/10.1029/2020WR028193, 2021a.

Li, D., Lu, X., Overeem, I., Walling, D. E., Syvitski, J., Kettner, A. J., Bookhagen, B., Zhou, Y., and Zhang, T.: Exceptional increases in fluvial sediment fluxes in a warmer and wetter High Mountain Asia, Science, 374, 599–603, https://doi.org/10.1126/science.abi9649, 2021b.

Li, D., Lu, X., Walling, D. E., Zhang, T., Steiner, J. F., Wasson, R. J., Harrison, S., Nepal, S., Nie, Y., Immerzeel, W. W., Shugar, D. H., Koppes, M., Lane, S., Zeng, Z., Sun, X., Yegorov, A., and Bolch, T.: High Mountain Asia hydropower systems threatened by climate-driven landscape instability, Nat. Geosci., 15, 520–530, https://doi.org/10.1038/s41561-022-00953-y, 2022.

Lindeløv, J. K.: mcp: An R Package for Regression With Multiple Change Points [code], OSF Preprints, https://doi.org/10.31219/osf.io/fzqxv, 2020.

Madsen, H., Lawrence, D., Lang, M., Martinkova, M., and Kjeldsen, T. R.: Review of trend analysis and climate change projections of extreme precipitation and floods in Europe, J. Hydrol., 519, 3634–3650, https://doi.org/10.1016/j.jhydrol.2014.11.003, 2014.

Mallakpour, I. and Villarini, G.: A simulation study to examine the sensitivity of the Pettitt test to detect abrupt changes in mean, Hydrol. Sci. J., 61, 245–254, https://doi.org/10.1080/02626667.2015.1008482, 2016.

Mao, L., Comiti, F., Carrillo, R., and Penna, D.: Sediment Transport in Proglacial Rivers, in: Geomorphology of Proglacial Systems. Geography of the Physical Environment. Springer, Cham, 199–217, 2019.

Mather, A. L. and Johnson, R. L.: Quantitative characterization of stream turbidity-discharge behavior using event loop shape modeling and power law parameter decorrelation, Water Resour. Res., 50, 7766–7779, https://doi.org/10.1002/2014WR015417, 2014.

Matiu, M., Jacob, A., and Notarnicola, C.: Daily MODIS Snow Cover Maps for the European Alps from 2002 onwards at 250 m Horizontal Resolution Along with a Nearly Cloud-Free Version, Data, 5, 1, https://doi.org/10.3390/data5010001, 2020.

Meinshausen, N.: Quantile Regression Forests, J. Mach. Learn. Res., 7, 983–999, 2006.

Merten, G., Capel, P., and Minella, J. P. G.: Effects of suspended sediment concentration and grain size on three optical turbidity sensors, J. Soils Sediments, 14, 1235–1241, https://doi.org/10.1007/s11368-013-0813-0, 2014.

Micheletti, N. and Lane, S. N.: Water yield and sediment export in small, partially glaciated Alpine watersheds in a warming climate, Water Resour. Res., 52, 4924–4943, https://doi.org/10.1002/2016WR018774, 2016.

Milliman, J. D. and Syvitski, J. P. M.: Geomorphic/Tectonic Control of Sediment Discharge to the Ocean: The Importance of Small Mountainous Rivers, J. Geol., 100, 525–544, https://doi.org/10.1086/629606, 1992.

Milner, A. M., Brown, L. E., and Hannah, D. M.: Hydroecological response of river systems to shrinking glaciers, Hydrol. Process., 23, 62–77, https://doi.org/10.1002/hyp.7197, 2009.

Milner, A. M., Khamis, K., Battin, T. J., Brittain, J. E., Barrand, N. E., Füreder, L., Cauvy-Fraunié, S., Gíslason, G. M., Jacobsen, D., Hannah, D. M., Hodson, A. J., Hood, E., Lencioni, V., Ólafsson, J. S., Robinson, C. T., Tranter, M., and Brown, L. E.: Glacier shrinkage driving global changes in downstream systems, Proc. Natl. Acad. Sci., 114, 9770–9778, https://doi.org/10.1073/pnas.1619807114, 2017.

Moriasi, D. N., Arnold, J. G., Van Liew, M. W., Bingner, R. L., Harmel, R. D., and Veith, T. L.: Model Evaluation Guidelines for Systematic Quantification of Accuracy in Watershed Simulations, Trans. ASABE, 50, 885–900, https://doi.org/10.13031/2013.23153, 2007.

Mueller, E. N., Güntner, A., Francke, T., and Mamede, G.: Modelling sediment export, retention and reservoir sedimentation in drylands with the WASA-SED model, Geosci. Model Dev., 3, 275–291, https://doi.org/10.5194/gmd-3-275-2010, 2010.

Murphy, K. P.: Machine Learning: A Probabilistic Perspective, MIT Press, 1102 pp., ISBN 978-0-262-01802-9, 2012.

Musso, A., Ketterer, M. E., Greinwald, K., Geitner, C., and Egli, M.: Rapid decrease of soil erosion rates with soil formation and vegetation development in periglacial areas, Earth Surf. Process. Landf., 45, 2824–2839, https://doi.org/10.1002/esp.4932, 2020.

Naden, P. S.: The Fine-Sediment Cascade, in: Sediment Cascades, John Wiley & Sons, Ltd, 271–305, https://doi.org/10.1002/9780470682876.ch10, 2010.

Naeser, T.: Schwebstoffuntersuchungen am Gletscherbach des Vernagtferners in den Zentralen Ötztaler Alpen, Diploma thesis, Ludwig-Maximilians-Universität München, München, 92 pp., 2002.

Nash, J. E. and Sutcliffe, J. V.: River flow forecasting through conceptual models part I — A discussion of principles, J. Hydrol., 10, 282–290, https://doi.org/10.1016/0022-1694(70)90255-6, 1970.

Nones, M.: Dealing with sediment transport in flood risk management, Acta Geophys., 67, 677–685, https://doi.org/10.1007/s11600-019-00273-7, 2019.

Orwin, J. F. and Smart, C. C.: Short-term spatial and temporal patterns of suspended sediment transfer in proglacial channels, small River Glacier, Canada, Hydrol. Process., 18, 1521–1542, https://doi.org/10.1002/hyp.1402, 2004.

Pandey, A., Himanshu, S. K., Mishra, S. K., and Singh, V. P.: Physically based soil erosion and sediment yield models revisited, CATENA, 147, 595–620, https://doi.org/10.1016/j.catena.2016.08.002, 2016.

Pettitt, A. N.: A Non-Parametric Approach to the Change-Point Problem, J. R. Stat. Soc. Ser. C Appl. Stat., 28, 126–135, https://doi.org/10.2307/2346729, 1979.

Pilla, R. M. and Williamson, C. E.: Earlier ice breakup induces changepoint responses in duration and variability of spring mixing and summer stratification in dimictic lakes, Limnol. Oceanogr., 67, S173–S183, https://doi.org/10.1002/lno.11888, 2022.

Pilz, T., Delgado, J. M., Voss, S., Vormoor, K., Francke, T., Costa, A. C., Martins, E., and Bronstert, A.: Seasonal drought prediction for semiarid northeast Brazil: what is the added value of a process-based hydrological model?, Hydrol. Earth Syst. Sci., 23, 1951–1971, https://doi.org/10.5194/hess-23-1951-2019, 2019.

Pohlert, T.: trend: Non-Parametric Trend Tests and Change-Point Detection. R package version 1.1.2. CRAN [code], https:// CRAN.R-project.org/package=trend (last access: 10 May 2023), 2020.

R Core Team: R: A language and environment for statistical computing [code], https://www.R-project.org/ (last access: 10 May 2023), 2018.

Rahman, K. U., Pham, Q. B., Jadoon, K. Z., Shahid, M., Kushwaha, D. P., Duan, Z., Mohammadi, B., Khedher, K. M., and Anh, D. T.: Comparison of machine learning and process-based SWAT model in simulating streamflow in the Upper Indus Basin, Appl. Water Sci., 12, 178, https://doi.org/10.1007/s13201-022-01692-6, 2022.

Reichstein, M., Camps-Valls, G., Stevens, B., Jung, M., Denzler, J., Carvalhais, N., and Prabhat: Deep learning and process understanding for data-driven Earth system science, Nature, 566, 195–204, https://doi.org/10.1038/s41586-019-0912-1, 2019.

Rickenmann, D., Badoux, A., and Hunzinger, L.: Significance of sediment transport processes during piedmont floods: the 2005 flood events in Switzerland, Earth Surf. Process. Landf., 41, 224–230, https://doi.org/10.1002/esp.3835, 2016.

Rottler, E., Francke, T., Bürger, G., and Bronstert, A.: Long-term changes in central European river discharge for 1869–2016: impact of changing snow covers, reservoir constructions and an intensified hydrological cycle, Hydrol. Earth Syst. Sci., 24, 1721–1740, https://doi.org/10.5194/hess-24-1721-2020, 2020.

Rottler, E., Vormoor, K., Francke, T., Warscher, M., Strasser, U., and Bronstert, A.: Elevation-dependent compensation effects in snowmelt in the Rhine River Basin upstream gauge Basel, Hydrol. Res., 52, 536–557, https://doi.org/10.2166/nh.2021.092, 2021.

Sailer, R., Rutzinger, M., Rieg, L., and Wichmann, V.: Digital elevation models derived from airborne laser scanning point clouds: appropriate spatial resolutions for multi-temporal characterization and quantification of geomorphological processes, Earth Surf. Process. Landf., 39, 272–284, https://doi.org/10.1002/esp.3490, 2014.

Santander Meteorology Group: fume: FUME package. R package version 1.0. [code], https://CRAN.R-project.org/ package=fume (last access: 10 May 2023), 2012.

Savi, S., Comiti, F., and Strecker, M. R.: Pronounced increase in slope instability linked to global warming: A case study from the eastern European Alps, Earth Surf. Process. Landf., 46, 1328–1347, https://doi.org/10.1002/esp.5100, 2020.

Schaefli, B. and Gupta, H. V.: Do Nash values have value?, Hydrol. Process., 21, 2075–2080, https://doi.org/10.1002/hyp.6825, 2007.

Schäuble, H.: Sedimentfrachtprognosen mit GIS, phd, Technische Universität, Darmstadt, https://doi.org/10/Anhang_1.pdf, 2006.

Scherrer, S. C., Fischer, E. M., Posselt, R., Liniger, M. A., Croci-Maspoli, M., and Knutti, R.: Emerging trends in heavy precipitation and hot temperature extremes in Switzerland, J. Geophys. Res. Atmospheres, 121, 2626–2637, https://doi.org/10.1002/2015JD024634, 2016.

Schmidt, L. K. and Hydrographic Service of Tyrol, Austria: Discharge and suspended sediment time series of 2006–2020 of gauges Vent Rofenache and Tumpen in the glacierized high alpine Ötztal, Tyrol, Austria, B2SHARE [data set], DOI: https://b2share.eudat.eu/records/be13f43ce9bb46d8a7eedb7b56df3140, 2021.

Schmidt, L. K., Grosse, P. M., and Francke, T.: A Quantile Regression Forests approach for sedigraph-reconstruction and sediment yield calculation B2SHARE [data set], DOI: https://b2share.eudat.eu/records/5f706863fc5041c49cb8d1a8cd55f613, 2022a.

Schmidt, L. K., Francke, T., Rottler, E., Blume, T., Schöber, J., and Bronstert, A.: Suspended sediment and discharge dynamics in a glaciated alpine environment: identifying crucial areas and time periods on several spatial and temporal scales in the Ötztal, Austria, Earth Surf. Dyn., 10, 653–669, https://doi.org/10.5194/esurf-10-653-2022, 2022b.

Schmidt, L. K., Francke, T., Grosse, P. M., Mayer, C., and Bronstert, A.: Reconstructing five decades of sediment export from two glacierized high-alpine catchments in Tyrol, Austria, using nonparametric regression, Hydrol. Earth Syst. Sci., 27, 1841–1863, https://doi.org/10.5194/hess-27-1841-2023, 2023.

Schmieder, J., Hanzer, F., Marke, T., Garvelmann, J., Warscher, M., Kunstmann, H., and Strasser, U.: The importance of snowmelt spatiotemporal variability for isotope-based hydrograph separation in a high-elevation catchment, Hydrol. Earth Syst. Sci., 20, 5015–5033, https://doi.org/10.5194/hess-20-5015-2016, 2016.

Schmieder, J., Garvelmann, J., Marke, T., and Strasser, U.: Spatio-temporal tracer variability in the glacier melt end-member — How does it affect hydrograph separation results?, Hydrol. Process., 32, 1828–1843, https://doi.org/10.1002/hyp.11628, 2018a.

Schmieder, J., Marke, T., and Strasser, U.: Wo kommt das Wasser her? Tracerbasierte Analysen im Rofental (Ötztaler Alpen, Österreich), Österr. Wasser- Abfallwirtsch., 70, 507–514, https://doi.org/10.1007/s00506-018-0502-8, 2018b.

Schöber, J. and Hofer, B.: The sediment budget of the glacial streams in the catchment area of the Gepatsch reservoir in the Ötztal Alps in the period 1965-2015, in: ICOLD (International Comission on Large Dam Systems) Proceedings, TwentySixth International Congress on Large Dams, Vienna, Austria, ISBN 9780429465086, 1–21, 2018.

Schöber, J., Schneider, K., Helfricht, K., Schattan, P., Achleitner, S., Schöberl, F., and Kirnbauer, R.: Snow cover characteristics in a glacierized catchment in the Tyrolean Alps - Improved spatially distributed modelling by usage of Lidar data, J. Hydrol., 519, 3492–3510, https://doi.org/10.1016/j.jhydrol.2013.12.054, 2014.

Sen, P. K.: Estimates of the Regression Coefficient Based on Kendall's Tau, J. Am. Stat. Assoc., 63, 1379–1389, https://doi.org/10.1080/01621459.1968.10480934, 1968.

Singh, A. T., Sharma, P., Sharma, C., Laluraj, C. M., Patel, L., Pratap, B., Oulkar, S., and Thamban, M.: Water discharge and suspended sediment dynamics in the Chandra River, Western Himalaya, J. Earth Syst. Sci., 129, 206, https://doi.org/10.1007/s12040-020-01455-4, 2020.

Slater, L. J., Singer, M. B., and Kirchner, J. W.: Hydrologic versus geomorphic drivers of trends in flood hazard, Geophys. Res. Lett., 42, 370–376, https://doi.org/10.1002/2014GL062482, 2015.

Sommer, C., Malz, P., Seehaus, T. C., Lippl, S., Zemp, M., and Braun, M. H.: Rapid glacier retreat and downwasting throughout the European Alps in the early 21 st century, Nat. Commun., 11, 3209, https://doi.org/10.1038/s41467-020-16818-0, 2020.

Stoll, E., Hanzer, F., Oesterle, F., Nemec, J., Schöber, J., Huttenlau, M., and Förster, K.: What Can We Learn from Comparing Glacio-Hydrological Models?, Atmosphere, 11, 981, https://doi.org/10.3390/atmos11090981, 2020.

Stott, T. and Convey, P.: Seasonal hydrological and suspended sediment transport dynamics and their future modelling in the Orwell Glacier proglacial stream, Signy Island, Antarctica, Antarct. Sci., 33, 192–212, https://doi.org/10.1017/S0954102020000607, 2021.

Stott, T. and Mount, N.: Alpine proglacial suspended sediment dynamics in warm and cool ablation seasons: Implications for global warming, J. Hydrol., 332, 259–270, https://doi.org/10.1016/j.jhydrol.2006.07.001, 2007.

Strasser, U., Marke, T., Braun, L., Escher-Vetter, H., Juen, I., Kuhn, M., Maussion, F., Mayer, C., Nicholson, L., Niedertscheider, K., Sailer, R., Stötter, J., Weber, M., and Kaser, G.: The Rofental: a high Alpine research basin (1890–3770 m a.s.l.) in the Ötztal Alps (Austria) with over 150 years of hydrometeorological and glaciological observations, Earth Syst. Sci. Data, 10, 151–171, https://doi.org/10.5194/essd-10-151-2018, 2018.

Swift, D. A., Nienow, P. W., and Hoey, T. B.: Basal sediment evacuation by subglacial meltwater: suspended sediment transport from Haut Glacier d'Arolla, Switzerland, Earth Surf. Process. Landf., 30, 867–883, https://doi.org/10.1002/esp.1197, 2005.

Syvitski, J., Ángel, J. R., Saito, Y., Overeem, I., Vörösmarty, C. J., Wang, H., and Olago, D.: Earth's sediment cycle during the Anthropocene, Nat. Rev. Earth Environ., 3, 179–196, https://doi.org/10.1038/s43017-021-00253-w, 2022.

Syvitski, J. P. M. and Milliman, J. D.: Geology, Geography, and Humans Battle for Dominance over the Delivery of Fluvial Sediment to the Coastal Ocean, J. Geol., 115, 1–19, https://doi.org/10.1086/509246, 2007.

Tahmasebi, P., Kamrava, S., Bai, T., and Sahimi, M.: Machine learning in geo- and environmental sciences: From small to large scale, Adv. Water Resour., 142, 103619, https://doi.org/10.1016/j.advwatres.2020.103619, 2020.

Talebi, A., Mahjoobi, J., Dastorani, M. T., and Moosavi, V.: Estimation of suspended sediment load using regression trees and model trees approaches (Case study: Hyderabad drainage basin in Iran), ISH J. Hydraul. Eng., 23, 212–219, https://doi.org/10.1080/09715010.2016.1264894, 2017.

Tan, Z., Leung, L. R., Li, H., Tesfa, T., Vanmaercke, M., Poesen, J., Zhang, X., Lu, H., and Hartmann, J.: A Global Data Analysis for Representing Sediment and Particulate Organic Carbon Yield in Earth System Models, Water Resour. Res., 53, 10674–10700, https://doi.org/10.1002/2017WR020806, 2017.

Tecklenburg, C., Francke, T., Kormann, C., and Bronstert, A.: Modeling of water balance response to an extreme future scenario in the Ötztal catchment, Austria, in: Advances in Geosciences, Proceedings of the 15th Workshop on Large-scale Hydrological Modelling, Innsbruck, Austria, 2011, 63–68, https://doi.org/10.5194/adgeo-32-63-2012, 2012.

van Tiel, M., Kohn, I., Loon, A. F. V., and Stahl, K.: The compensating effect of glaciers: Characterizing the relation between interannual streamflow variability and glacier cover, Hydrol. Process., 34, 553–568, https://doi.org/10.1002/hyp.13603, 2019.

Tschada, H. and Hofer, B.: Total solids load from the catchment area of the Kaunertal hydroelectric power station: the results of 25 years of operation, in: Hydrology in Mountain Regions. II – Artificial Reservoirs; Waters and Slopes (Proceedings of two Lausanne Symposia), Lausanne, 8, 1990.

Tsyplenkov, A., Vanmaercke, M., Golosov, V., and Chalov, S.: Suspended sediment budget and intra-event sediment dynamics of a small glaciated mountainous catchment in the Northern Caucasus, J. Soils Sediments, 20, 3266–3281, https://doi.org/10.1007/s11368-020-02633-z, 2020.

Turowski, J. M., Rickenmann, D., and Dadson, S. J.: The partitioning of the total sediment load of a river into suspended load and bedload: a review of empirical data, Sedimentology, 57, 1126–1146, https://doi.org/10.1111/j.1365-3091.2009.01140.x, 2010.

Umweltbundesamt: CORINE Landcover 2018 [data set], https://www.data.gv.at/katalog/dataset/clc2018 (last access: 13 September 2018), 2018.

Vautard, R., Kadygrov, N., Iles, C., Boberg, F., Buonomo, E., Bülow, K., Coppola, E., Corre, L., van Meijgaard, E., Nogherotto, R., Sandstad, M., Schwingshackl, C., Somot, S., Aalbers, E., Christensen, O. B., Ciarlo, J. M., Demory, M.-E., Giorgi, F., Jacob, D., Jones, R. G., Keuler, K., Kjellström, E., Lenderink, G., Levavasseur, G., Nikulin, G., Sillmann, J., Solidoro, C., Sørland, S. L., Steger, C., Teichmann, C., Warrach-Sagi, K., and Wulfmeyer, V.: Evaluation of the Large EURO-CORDEX Regional Climate Model Ensemble, J. Geophys. Res. Atmospheres, 126, e2019JD032344, https://doi.org/10.1029/2019JD032344, 2021.

Veh, G., Lützow, N., Kharlamova, V., Petrakov, D., Hugonnet, R., and Korup, O.: Trends, Breaks, and Biases in the Frequency of Reported Glacier Lake Outburst Floods, Earths Future, 10, e2021EF002426, https://doi.org/10.1029/2021EF002426, 2022.

de Vente, J., Poesen, J., Verstraeten, G., Govers, G., Vanmaercke, M., Van Rompaey, A., Arabkhedri, M., and Boix-Fayos, C.: Predicting soil erosion and sediment yield at regional scales: Where do we stand?, Earth-Sci. Rev., 127, 16–29, https://doi.org/10.1016/j.earscirev.2013.08.014, 2013.

Vercruysse, K., Grabowski, R. C., and Rickson, R. J.: Suspended sediment transport dynamics in rivers: Multi-scale drivers of temporal variation, Earth-Sci. Rev., 166, 38–52, https://doi.org/10.1016/j.earscirev.2016.12.016, 2017.

Vergara, I., Garreaud, R., and Ayala, Á.: Sharp Increase of Extreme Turbidity Events Due To Deglaciation in the Subtropical Andes, J. Geophys. Res. Earth Surf., 127, e2021JF006584, https://doi.org/10.1029/2021JF006584, 2022.

Vigiak, O., Malagó, A., Bouraoui, F., Vanmaercke, M., Obreja, F., Poesen, J., Habersack, H., Fehér, J., and Grošelj, S.: Modelling sediment fluxes in the Danube River Basin with SWAT, Sci. Total Environ., 599–600, 992–1012, https://doi.org/10.1016/j.scitotenv.2017.04.236, 2017.

Vormoor, K., Lawrence, D., Heistermann, M., and Bronstert, A.: Climate change impacts on the seasonality and generation processes of floods - projections and uncertainties for catchments with mixed snowmelt/rainfall regimes, Hydrol. Earth Syst. Sci., 19, 913–931, https://doi.org/10.5194/hess-19-913-2015, 2015.

Walling, D. E.: Tracing suspended sediment sources in catchments and river systems, Sci. Total Environ., 344, 159–184, https://doi.org/10.1016/j.scitotenv.2005.02.011, 2005.

Weber, M. and Prasch, M.: Influence of the Glaciers on Runoff Regime and Its Change, in: Regional Assessment of Global Change Impacts, edited by: Mauser, W. and Prasch, M., Springer International Publishing, Cham, 493–509, https://doi.org/10.1007/978-3-319-16751-0_56, 2016a.

Weber, M. and Prasch, M.: Influence of the Glaciers on Runoff Regime and Its Change, Reg. Assess. Glob. Change Impacts, 493–509, https://doi.org/10.1007/978-3-319-16751-0_56, 2016b.

Westra, S., Fowler, H. J., Evans, J. P., Alexander, L. V., Berg, P., Johnson, F., Kendon, E. J., Lenderink, G., and Roberts, N. M.: Future changes to the intensity and frequency of short-duration extreme rainfall, Rev. Geophys., 52, 522–555, https://doi.org/10.1002/2014RG000464, 2014.

Wijngaard, R. R., Helfricht, K., Schneeberger, K., Huttenlau, M., Schneider, K., and Bierkens, M. F. P.: Hydrological response of the Ötztal glacierized catchments to climate change, Hydrol. Res., 47, 979–995, https://doi.org/10.2166/nh.2015.093, 2016.

World Glacier Monitoring Service: Fluctuations of Glaciers Database, WGMS [data set], https://doi.org/10.5904/wgms-fog-2021-05, 2021.

Wulf, H., Bookhagen, B., and Scherler, D.: Climatic and geologic controls on suspended sediment flux in the Sutlej River Valley, western Himalaya, Hydrol. Earth Syst. Sci., 16, 2193–2217, https://doi.org/10.5194/hess-16-2193-2012, 2012.

Yadav, V., Ghosh, S., Mueller, K., Karion, A., Roest, G., Gourdji, S. M., Lopez-Coto, I., Gurney, K. R., Parazoo, N., Verhulst, K. R., Kim, J., Prinzivalli, S., Fain, C., Nehrkorn, T., Mountain, M., Keeling, R. F., Weiss, R. F., Duren, R., Miller, C. E., and Whetstone, J.: The Impact of COVID-19 on CO2 Emissions in the Los Angeles and Washington DC/Baltimore Metropolitan Areas, Geophys. Res. Lett., 48, e2021GL092744, https://doi.org/10.1029/2021GL092744, 2021.

Yue, S. and Wang, C.: The Mann-Kendall Test Modified by Effective Sample Size to Detect Trend in Serially Correlated Hydrological Series, Water Resour. Manag., 18, 201–218, https://doi.org/10.1023/B:WARM.0000043140.61082.60, 2004.

Yue, S., Kundzewicz, Z. W., and Wang, L.: Detection of Changes, in: Changes in Flood Risk in Europe, edited by: Kundzewicz, Z. W., IAHS Press, Wallingford, 387–408, ISBN 9780203098097, 2012.

Zentralanstalt für Meteorologie und Geodynamik (ZAMG): Climate Data of Austria 1971–2000, http://www.zamg.ac.at/fix/klim/oe71-00/klima2000/klimadaten_oesterreich_1971_ frame1.htm (last access: 15 October 2021), 2013.

Zhang, T., Li, D., Kettner, A. J., Zhou, Y., and Lu, X.: Constraining Dynamic Sediment-Discharge Relationships in Cold Environments: The Sediment-Availability-Transport (SAT) Model, Water Resour. Res., 57, e2021WR030690, https://doi.org/10.1029/2021WR030690, 2021.

Zhang, T., Li, D., East, A. E., Walling, D. E., Lane, S., Overeem, I., Beylich, A. A., Koppes, M., and Lu, X.: Warming-driven erosion and sediment transport in cold regions, Nat. Rev. Earth Environ., 3, 832–851, https://doi.org/10.1038/s43017-022-00362-0, 2022.

Zimmermann, A., Francke, T., and Elsenbeer, H.: Forests and erosion: Insights from a study of suspended-sediment dynamics in an overland flow-prone rainforest catchment, J. Hydrol., 428–429, 170–181, https://doi.org/10.1016/j.jhydrol.2012.01.039, 2012.